KAUNAS UNIVERSITY OF TECHNOLOGY

RASA KERUCKIENĖ

SYNTHESIS AND PROPERTIES OF INDOLE-BASED ELECTROACTIVE COMPOUNDS

Doctoral Dissertation
Technological Sciences, Materials Engineering (08T)

2017, Kaunas

This doctoral dissertation was prepared at Kaunas University of Technology, Faculty of Chemical Technology, Department of Polymer Chemistry and Technology during the period of 2013–2017. The studies were supported by Research Council of Lithuania.

Scientific Supervisor:

Prof. Dr. Habil . Juozas Vidas Gražulevičius (Kaunas University of Technology, Technological Sciences, Materials Engineering – 08T).

Doctoral dissertation has been published in:
http://ktu.edu

Editor:
Armandas Rumšas (Publishing Office “Technologija”)

ISBN 978-609-02-1348-3

The bibliographic information about the publication is available in the National Bibliographic Data Bank (NBDB) of the Martynas Mažvydas National Library of Lithuania.

KAUNO TECHNOLOGIJOS UNIVERSITETAS

RASA KERUCKIENĖ

INDOLO FRAGMENTUS TURINČIŲ ELEKTROAKTYVIŲ JUNGINIŲ SINTEZĖ IR SAVYBĖS

Daktaro disertacija
Technologijos mokslai, Medžiagų inžinerija (08T)

2017, Kaunas

Disertacija parengta 2013–2017 metais Kauno technologijos universiteto Cheminės technologijos fakulteto Polimerų chemijos ir technologijos katedroje. Mokslinius tyrimus rėmė Lietuvos mokslo taryba.

Mokslinis vadovas:
Prof. habil. Dr. Juozas Vidas GRAŽULEVIČIUS (Kauno technologijos universitetas, technologijos mokslai, medžiagų inžinerija – 08T).

Interneto svetainės, kurioje skelbiama disertacija, adresas:
http://ktu.edu

Redagavo:
Armandas Rumšas (leidykla „Technologija“)

ISBN 978-609-02-1348-3

Leidinio bibliografinė informacija pateikiama Lietuvos nacionalinės Martyno Mažvydo bibliotekos Nacionalinės bibliografijos duomenų banke (NBDB)

TABLE OF CONTENTS

List of Abbreviations

AFM – atomic force microscopy;

Alq_3–tris(8-hydroxyquinolinato) aluminum;

Ar – aromatic;

ATR-IR – attenuated total reflectance infrared spectroscopy;

CDCl – deuterated chloroform;

CIE – chromaticity coordinates;

CV – cyclic voltammetry;

^{13}C NMR– carbon ^{13}C nuclear magnetic resonance;

d – dublet;

DFT – density functional theory;

DSC – differential scanning calorimetry;

DCM – dichloromethane;

EA_{CV}–electron affinity estimated by CV;

E_g^{opt}–optical bandgap determined from UV-vis spectra;

EQE–external quantum efficiency;

EL – electroluminescence;

E_T – triplet energy;

^1H NMR – proton nuclear magnetic resonance;

HOMO – highest occupied molecular orbital;

IP_{CV} – ionisation potential estimated by CV;

IQE – internal quantum efficiency;

IP_{PE} – ionisation potential estimated by electron photoemission in air method;

ITO – indium tin oxide;

λ_{Abs} – wavelength of absorption maxima;

λ^{PL}_{max} – wavelength of emission maxima;

λ^{PH}_{max} – wavelength of phosphorescence maxima;

LUMO – lowest unoccupied molecular orbital;

m – multiplet;

m/m – mass-to-mass ratio;

m/z – mass-to-charge ratio;

μ – charge drift mobility;

MS – mass spectrometry;

M.p. – melting point;

m-MTDATA – 4,4′,4″-tris[3-methylphenyl(phenyl)amino]triphenylamine);

MW – molar mass;
NPB–N,N′-di(1-naphthyl)-N,N′-diphenyl-(1,1′-biphenyl)-4,4′-diamine;
η_c – maximum current efficiency;
η_p – maximum power efficiency;
Nd:YAG – neodymium-doped yttrium aluminum garnet;
OFET – organic field effect transistor;
OLED – Organic light emitting diode;
PBD – 2-(4-biphenylyl)-5-(t-butylphenyl)1,3,4-oxidiazole;
PEDOT:PSS – poly(3,4-ethylenedioxythiophene)-poly(styrenesulfonate);
PhOLED – phosphorescent light emitting diode;
q – quadruplet;
rISC – reverse intersystem crossing;
s – singlet;
S_0 – ground state;
S_1 – excited state;
δ – chemical shift;
T_1 – triplet level;
TADF – thermally activated delayed fluorescence;
T_{CR} – crystallization temperature;
TCTA – tris(4-carbazoyl-9-ylphenyl)amine;
TCz1 – 3,6-di(9-carbazolyl)-9-(2-ethylhexyl) carbazole;
T_G – glass transition temperature;
TGA – thermogravimetric analysis;
THF – tetrahydrofuran;
T_{ID} – initial weight loss temperature;
TMS – tetramethylsilane;
TPBi – 2,2′,2″-(1,3,5-Benzinetriyl)-tris(1-phenyl-1-H-benzimidazole);
TOF – time of flight;
UV-Vis – ultraviolet-visible light;
V_{on} – turn-on voltage;
XRD – X-ray diffraction.

1. Introduction

Organic light emitting diodes (OLEDs) are being commercialized as components of high resolution full-scale large screens and information displays [1]. In addition, employment of OLEDs enhances opportunities not only for the application as solid-state lighting sources [2] but also for such more innovative opportunities as flexible wearable electronic devices [3]. The wide application opportunities come with easily adjustable properties of OLEDs: high colour purity, ease of fabrication, low power consumption and relatively low cost [4]. On the other hand, some major drawbacks still do not allow to boost the production scale at present. A few of the major issues are the short operational lifetime and the degradation issues as well as the insufficient efficiency of devices [5].

OLEDs have multiple functional layers such as charge injection, charge transport, exciton blocking, and emitting layers. The types of materials used for the formation of the active layers can be divided into two groups, i.e low-molar-mass compounds and polymers. The demanding requirements for the organic light emitting diodes force researchers to seek the most effective materials. The most widely investigated candidates for OLEDs are derivatives of carbazole, triphenylamine, anthracene, and acridane [6–9]. The applicability of other classes of organic electroactive materials in OLEDs is much less explored. In this work, the attention is focused on indole moiety as the main chromophore in the design and synthesis of electroactive materials. Indole-derived compounds exhibit good luminescent and hole-transporting properties [10] which make them interesting candidates for the application in OLEDs. However, indole moiety is still rarely used for the design and synthesis of luminescent and charge-transporting materials.

Efficient OLEDs can be obtained only by building multilayer structures. Multilayer devices can be prepared either by vacuum evaporation or by spin coating. The main difficulty in the preparation of such devices by spin-coating is the solubility of the material which forms the bottom layer onto which the top layer has to be cast, because most organic semiconductors are soluble in the same solvents. One approach that can be employed to circumvent this problem is the application of electroactive derivatives with reactive functional groups which allow to convert materials into insoluble networks or polymers with decreased solubility. There still are few reports on the synthesis and studies of indole derivatives with reactive functional groups. Therefore, particular attention has to be paid to the synthesis and studies of derivatives of indole with reactive functional groups. It can open up new possibilities in the fabrication of stable OLEDs. The main subject of this work will be design, synthesis and investigation of new electroactive organic materials for organic light emitting diodes.

The aim of this work was the synthesis and investigation of new indole moiety-based charge-transporting and luminescent derivatives for OLEDs.

The main objectives for the achievement of the aim are as follows**:**

- Synthesis of 2-phenylindole twin derivatives with vinylene and single bond linkages between the chromophores.
- Synthesis of 2-phenylindole and carbazole hybrid derivatives with reactive functional groups.
- Synthesis of methyl- or naphthyl-substituted indole and benzo[b]carbazole derivatives.
- Synthesis of benzophenone derivatives bearing phenylindole and other donor moieties.
- Investigation of the properties of the newly synthesized derivatives by experimental and computational methods.
- Estimation of the performance of the synthesized derivatives in OLEDs.

The scientific novelty of the work is that new series of the indole-based electroactive organic derivatives were designed. New materials were synthesised and their thermal, optical, photophysical, electrochemical and photoelectrical properties were investigated. Computational methods were employed to compare the structure-properties relationship.

The practical value of the work. The extended properties investigation of the newly designed and synthesized indole-based derivatives confirmed their applicability in organic (opto)electronic devices. 2-Phenylindole- and carbazole-based derivatives were used as host materials in phosphorescent organic light-emitting diodes. Indole and benzo[b]carbazole derivatives were used as emissive layers in blue light-emitting diodes.

Personal input of the author. The author has designed, synthesized, and characterized all the new compounds described in Chapter 4. The author has performed infrared spectroscopy, UV-vis absorption spectrometry, cyclic voltammetry measurements, as well as thermally and photochemically induced cross-linking experiments employing the attenuated total reflectance infrared spectroscopy. Spectroelectrochemical measurements were also performed by the author under supervision of dr. Paula Wagner at *Intelligent Polymer Research Institute*, University of Wollongong (Australia). Structure analysis of the obtained materials as well as their thermal characteristics, charge drift mobility and ionization potential measurements were performed in collaboration with the colleagues from *Department of Polymer Chemistry and Technology* and *Department of Organic Chemistry*, Kaunas University of Technology (KTU). The analysis of electroactive layers of compounds employing X-ray diffraction and atomic force microscopy was performed by Algirdas Lazauskas at the Institute of Materials Science, KTU. Computational calculations were carried out with the help of dr. Viktorija Mimaitė. Design, fabrication and investigation of phosphorescent light emitting diodes was performed in collaboration with Dmytro Volyniuk at the Department of Polymer Chemistry and Technology, KTU. Non-doped organic light emitting diodes were fabricated and investigated by dr. Khrystyna Ivaniuk at Lviv Polytechnic National University (Ukraine).

2. Literature Review

2.1.Organic Light Emitting Diodes

A breakthrough in the research of organic light emitting diodes (OLEDs) came after the publication of the article by Tang and Van Slyke on the first functioning device in 1987 [11]. The emitter tris(8-hydroxyquinolinato) aluminum (Alq_3) was sandwiched between the anode, the hole transporting layer and the cathode by vacuum deposition process, and green emission was obtained when applying voltage to the device. Since then, the materials [12, 13], device structures [14–18] and fabrication processes [19–22] have been developed thus allowing to reach efficient production scale.

OLEDs are being commercialized as high resolution full-scale large screens and information displays. Their employment also promises great future prospects for flexible wearable electronics, such as the recently reported e-skin devices [23] and solid-state lighting sources [24, 25]. The wide application opportunities come with the easily adjustable properties of OLEDs: high colour purity, ease of fabrication, low power consumption and relatively low cost [14, 26]. On the other hand, the short operational lifetime and degradation issues as well as the lack of efficiency of the devices make them a highly relevant research topic.

One of the main challenges, the lifetime of OLEDs, is due to several internal and external degradation sources. OLEDs based on both inorganic and organic semiconducting materials suffer from internal energy losses, and these losses convert into heat [27]. The generated heat can then act by itself as a cause of degradation resulting in the decrease of the lifetime of OLED devices [28].

Another concerning issue is the relevant fabrication method of the devices as their structures have become more complicated. OLEDs have multiple functional layers acting as charge injection, charge transport, exciton blocking, and emitting layers. The types of materials used for the formation of these layers can be divided into two groups: small molecule-based devices and polymeric ones. The appropriate fabrication method is often different in terms of the used materials. Polymeric devices cannot be fabricated by vacuum evaporation. Most of the devices based on low-molar-mass compounds are prepared by vacuum deposition, and commercial OLEDs are currently made by using this process [29, 30]. Although vacuum thermal evaporation is generally preferred as the fabrication process of OLEDs, the vacuum deposition method poses a number of problems, among which, the inefficient use of material, the poor scalability, the high equipment costs, and the complicated colour patterning processes can be mentioned [31–32].

Solution processing provides a low-cost approach to the fabrication of OLEDs. The early production solution-processed OLEDs were based on a simple architecture with an emitting polymer layer and a hole injection polymer layer [33, 34]. Since then, attempts have been dedicated to developing solution-processed small-molecule OLEDs with mixed emission layers [35, 36]. As the general spin coating method is not entirely compatible with high scale production, it is highly desirable to improve the solution process that can be continuously performed in the course of

manufacturing. One of the most challenging tasks in the fabrication of multilayer light-emitting diodes by solution processes is to avoid the interfacial mixing between different layers since most of the commercially available emissive and charge-transporting materials are soluble in common organic solvents. A good solution allowing to circumvent this problem is to introduce cross-linkable electroactive materials which can form insoluble and solvent-resistable functional layers [37, 38]. However, in the case of single-layer devices, the performance of solution-processed OLEDs is still inferior with respect to OLEDs fabricated by vacuum evaporation [39, 40].

The OLEDs evolved from a single layer device structure with only one emitting layer into multilayer structures with charge transport layers and an emitting layer thus bringing improvement to the device performance of the OLEDs [41–43].

At first, fluorescent materials were used as emitting materials of OLEDs, but the intrinsic low internal quantum efficiency of 25% of the fluorescent emitting materials limited the application of fluorescent OLEDs [44]. It is known that the ratio of singlet excitons to triplet excitons is 1:3 from spin statistics, and the use of triplet excitons for light emission enables to achieve 100% internal quantum efficiency (IQE) [43, 45]. The triplet excitons cannot be utilized for light emission in common organic materials because of non-radiative decay of triplet excitons via the internal conversion process [46, 47]. The radiative transition from the triplet excited state to the singlet ground state is a spin-forbidden transition, but the transition can be allowed in organometallic complexes with heavy metals such as Ir, Pt and Os due to spin-orbit coupling [48–50].

The triplet excitons can be used for light emission, and internal quantum efficiency of 100% can be obtained in phosphorescent OLEDs. Currently, almost 100% IQE has already been reported in red, green, and blue phosphorescent OLEDs by several research groups. Organic complexes (Figure 2.1) for the emitting layers were used in these devices [51, 52]. A wide array of examples of the most commonly used organic complexes for emissive layers can be presented:

- bis(2-methyldibenzo[f,h]quinoxaline)(acetylacetonate)iridium(III) ($Ir(MDQ)_2(acac)$) – a red emitter;
- tris[2-phenylpyridinato-C2,N]iridium(III) (Ir(ppy)3) – a green emitter;
- bis[2-(4,6-difluorophenyl)pyridinato-C2,N](picolinato)iridium(III) (FIrpic) – a blue emitter;
- bis[2-(5-cyano-4,6-difluorophenyl)pyridinato-C2,N](picolinato)iridium(III) (FCNIrpic) – a blue emitter.

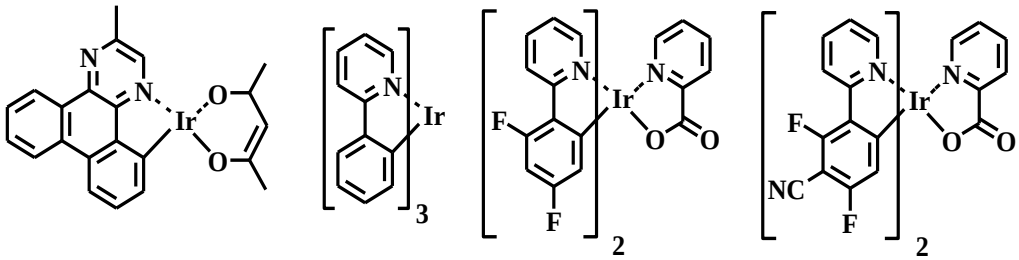

Figure 2.1. Organic complexes

The research on high efficiency OLEDs has focused on developing organic materials and device structures for phosphorescent OLEDs. Thus the design and synthesis of new phosphorescent emitters and their host materials represent two research focuses in the PhOLED field to improve the device performance [13].

The challenging object for the design of the suitable materials is that both the phosphorescent emitters and host materials are very critical for the PhOLEDs for modulating the charge carrier injection/transporting and emission processes. In order to guarantee high electroluminescence efficiencies, all the excitons in the emission layer should be harnessed effectively by the radiative triplet states of the guest phosphorescent emitters during the period of operation of PhOLEDs [53, 54]. In addition, one of the critical roles played by the host materials is to have them excited by the recombination of holes and electrons migrating from the charge transporting layers and then effectively transferring the energies to the guest emitters. Therefore, the condition that a good host material must satisfy is that the triplet energy (E_T) of the host material should be higher than that of the guest emitter in order to avoid the undesired reverse energy transfer from the guests to the host materials and to effectively confine triplet excitons on the guest molecules [55]. E_T is regarded as a critical parameter for the host materials, especially for those used in combination with blue phosphorescent emitters. In order to block the reverse energy transfer, the PhOLEDs involving blue phosphorescent emitters require the use of host materials with a very large band gap (E_g) and a high E_T level. Host materials for blue phosphorescent emitters often possess poor charge injection/transporting features due to their large E_g. The development of high performance host materials, especially those for blue or even deep-blue phosphorescent emitters, with enhanced charge injection/transporting ability is highly desired. Furthermore, the balance between electrons and holes in the emissive layer is also one of the most important factors allowing to obtain higher quantum efficiency of the devices [56–60].

One of the latest trends in the design of efficient emitting materials for OLEDs is the employment of thermally activated delayed fluorescence (TADF). Although TADF has been known since 1960 [61], the use of TADF emitters in optoelectronic devices was proposed independently and quite recently [62–71].

TADF occurs via the up-conversion mechanism which converts triplet excitons into singlet-excited states [72]. By preparing molecules with a small

difference between the singlet and triple energy levels ($\Delta E_{(S-T)}$), reverse intersystem crossing (rISC) can be realized by harvesting the environmental thermal energy. This eventuates in delayed fluorescence, which could lead to total electroluminescent efficiency if the conversion efficiency is 100%. TADF molecules have a low $\Delta E_{(S-T)}$, usually of an order of 10^{-2} meV [73]. Although direct transitions between T_1 and S_0 are still forbidden, it is possible to go from T_1 back to S_1 by means of rISC if the thermal energy (k_bT) is sufficient. Compared with the regular fluorescence where the excited-state lifetime is in the order of nanoseconds, the lifetime of TADF is longer, often in the order of microseconds or more [74, 75]. TADF is a promising mechanism for the implementation of efficient OLEDs with the maximum efficiency. It can equally compete with the phosphorescence mechanism which is now the go-to solution for efficient OLEDs [76–78]. The basic concept of the three described mechanisms is shown in Figure 2.2.

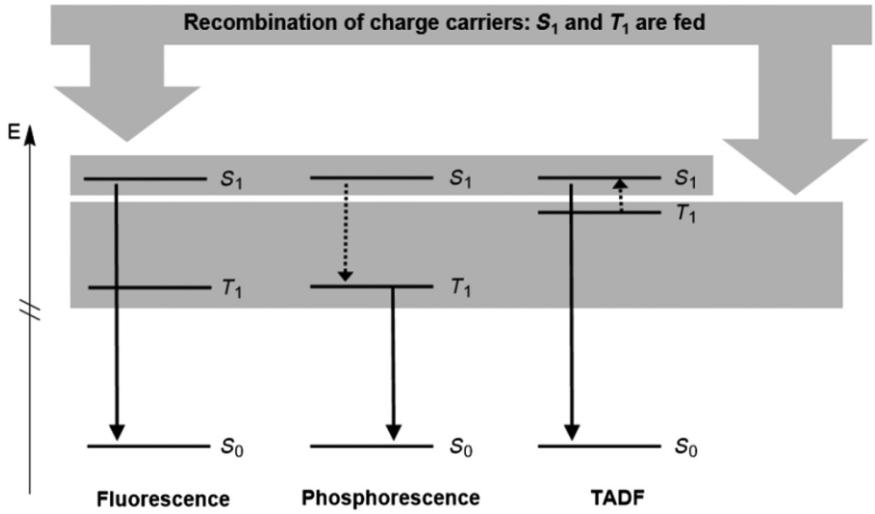

Figure 2.2. A schematic comparison of fluorescence, phosphorescence, and TADF. Straight arrows represent emissive transitions whereas dotted arrows indicate up- or down-conversion processes (ISC and rISC) [79]

Efficient emission also relies on efficient electron and hole injection/transport from the cathodes and anodes [80, 81]. This requires that the ideal electroluminescent materials should possess not only good luminescence properties but also have good electron and hole-transporting capacity, which is difficult to achieve with most of the current electroluminescent organic materials. One of the approaches to overcome this problem is to fabricate multilayer OLEDs by using a hole-transporting (or injecting) layer or an electron-transporting (or injecting) layer in the device fabrication. The utilisation of phosphorescent and TADF materials as organic emitters boosted the IQE of OLEDs from 25% to nearly 100% thus indicating that the carriers can be thoroughly liberated to generate photons [82, 83].

The demanding requirements for the devices force to search for the most prominent materials. Materials design, synthesis and investigation is still an ongoing process where researchers are in constant search for perfection.

In the following chapter, both vacuum-deposited and solution-proccessed devices will be discussed with an emphasis on the indole moiety as the main chromophore in their electroactive layers.

2.2. Indole-Based Electroactive Materials

Indole is an aromatic heterocyclic organic compound with a bicyclic structure consisting of a benzene ring and a pyrrole ring which occurs predominantly in natural materials such as various plants alkaloids and fungal metabolites [84, 85].

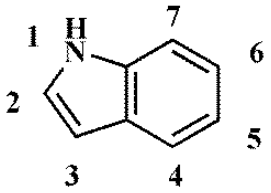

indole

Figure 2.3. The structure of indole

Indole has a privileged structure because of its ubiquity in natural products and a wide span of biological activity. In addition, indole is unsaturated, electron rich compound capable to display its unique electrical, chemical, optical and physical properties with a great potential for many different applications [86, 87]. There are multiple reactive sites in the indole group, and the most active ones are N-1, C-2, C-3 and C-5 positions (see Figure 2.3) which can be used to design numerous significant materials and chemical intermediates through C–N [88] or C–C [89, 90] bond-forming reactions. Attachment of appropriate substituents at C-2, C-3, and C-5 positions of the indole moiety may allow to fine-tune its properties. The presence of reactive sites and the relatively easy chemical modification of the indole nucleus make it a good candidate to be used as a basic chromophore for the development of new OLED materials. Indole derivatives usually posses both planar-fused aromatic geometry and proficient electron donating characteristics [91]. They exhibit photoluminescence (PL) emission in the blue–UV region with high quantum efficiency [92–94].

However, vulnerable resistance to the oxidation of indole in many cases hampered the direct substitution of protons with functional groups, especially at C-2 or C-3 positions [95]. Since five-membered aromatic/heteroaromatic rings provide reduced intra-chain steric hindrance resulting in better planar back-bond conformation in conjugated molecules rather than in the comparable six-membered rings, devising an effective way of extending π-conjugation through the five-membered ring of indole or its derivatives could be helpful when seeking to provide promising electroactive materials [96].

Taking into account all the pros and cons of this building block, the indole moiety is still not widely investigated as a possible candidate for the design of OLED materials as its counterparts such as carbazole [97, 98], triphenylamine [99], fluorene [100] or acridane [64, 101]. Reported indole-based electroluminescent materials are still very scarce.

2.2.1. Indole Moiety Containing Materials as Hosts of Emitting Layers of Organic Light Emitting Diodes

The derivatives of indole seem to have a good potential as host materials because of their high triplet energy values. Tri(1*H*-indol-3-yl)methane moiety was taken as a building block in the synthesis of high triplet energy materials [102]. In this moiety, three indolyl fragments are linked to the sp^3 hybridized carbon atom which serves as a spacer to prevent π-conjugation (Figure 2.4). One of the compounds contains the reactive epoxypropyl- functional group which could be (photo)cross-linked for solution-processed device production. The characteristics of the materials are outlined in Table 2.1.

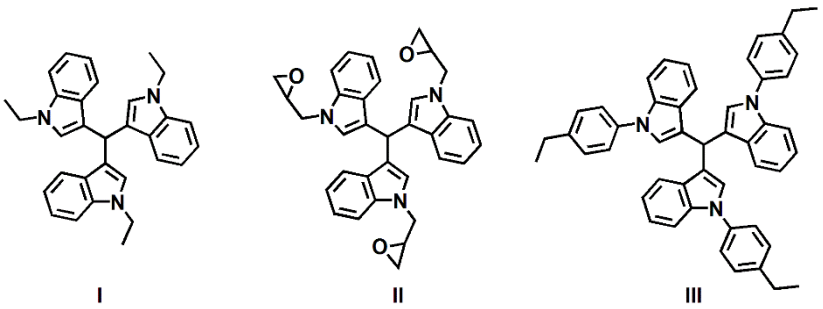

Figure 2.4. Tri(1H-indol-3-yl)methane derivatives

Table 2.1. Characteristics of the indolo-carbazole derivatives **I**–**VII**

	T_{ID}, °C	T_G, °C	E_T, eV	IP_{PE}, eV
I	245	123	2.97 (2.81)	5.72
II	306	75	2.99 (2.78)	5.80
III	310	–	2.99 (2.82)	5.67
IV	290	89	2.97	5.68
V	296	105	2.62	5.60
VI	308	96	2.99	5.80
VII	281	143	2.97	5.60

T_{ID} – the initial weight loss temperature obtained from TGA curves; T_G – the glass transition temperature from the second DSC heating scan; E_T – the triplet energy estimated as $1240/\lambda_{PH}$; IP_{PE} – the ionization potential estimated by the electron photoemission in air method.

The alkylated tri(1*H*-indol-3-yl)methane derivative (**I**) has the lowest initial decomposition temperature (T_{ID}=245 °C) while oxetanyl-and aryl-substituted derivatives start to decompose at 306 °C and 310 °C, respectively. Although these materials were obtained as crystals, they could still be transformed into the glassy state, except for material **III**, as detected during differential scanning calorimetry (DSC) measurements.

As the triplet energy value (E_T) is one of the determent characteristics in terms of choosing the suitable host for OLED, these values were obtained from the phosphorescence spectra of substituted tri(1*H*-indol-3-yl)methane toluene solutions and spin-coated films (the values shown in parentheses in Table 2.1.). The triplet

energy values established from the highest energy phosphorescence peaks of these compounds in the solid state are slightly lower than those of dilute solutions as it is also typically observed for various phosphorescent host materials [103]. This can be explained by an enhanced intermolecular interaction in the solid state, e.g. the formation of triplet excimers takes place in the solid samples of tri(1*H*-indol-3-yl)methane derivatives. Nevertheless, E_T values range from 2.78 to 2.82 eV in solid state samples thus making derivatives **I**–**III** good candidates as host materials for blue PhOLEDS.

IP values for the thin films of the compounds were established by employing the electron photoemission technique. It is evident that the replacement of alkyl groups by the aryl group results in the ionization potentials shifting to lower energy.

Indole-carbazole hybrid derivatives (Figure 2.5) were synthesized by replacing one of the indole moieties with a carbazole fragment [104]. This change in the structure improved the thermal stability of the materials. The initial thermal decomposition temperatures range around 300 °C degrees. The characteristics of the discussed materials are presented in Table 2.1.

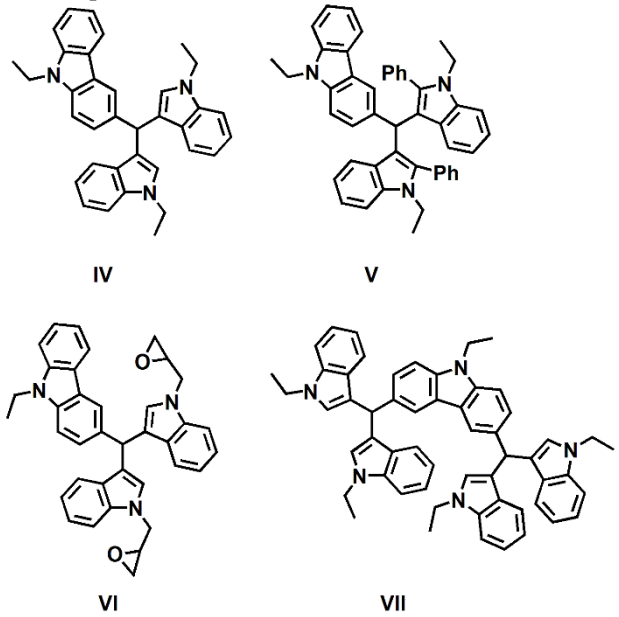

Figure 2.5. The indole-carbazole hybrid derivatives

Materials **IV**, **VI** and **VII** exhibit relatively high triplet energy values of 2.97–2.99 eV. Such values are sufficiently high to function as host materials for deep blue phosphorescent dopants. The lower triplet energy value of compound **V** is apparently due to the possession of the 2-phenylindole moiety since the latter has a lower triplet energy than the carbazole moiety [105, 106].

Energy level positions are important for the proper host–guest system combination in efficient electroluminescent devices. The authors determined the IP energy values from the electron photoemission technique. The values were found to range from 5.60 to 5.80 eV. Such values are close compared to those of common

carbazole-based materials [105–108], which suggests that the energy levels are mainly determined by the carbazole unit.

These compounds exhibited similar electrochemical behaviour and displayed irreversible oxidation and reduction. The irreversible electrochemical oxidation is even found in the compounds with blocked electroactive sites such as C-3 and C-6 of the carbazole moiety in compound **VII**, and C-2 of the indole species in compound **V**. The irreversible oxidation behaviour can be possibly ascribed to the triaryl-substituted carbon center which can easily deliver a proton and quench the radical cation upon electrochemical oxidation.

3,6-Bis(indol-1-yl)-9-phenylcarbazole derivatives **VIII**–**XI** (Figure 2.6) were tested as hosts and emitters in blue-green phosphorescent devices and single-layer blue light emitting devices [109]. Their characteristics are presented in Table 2.2.

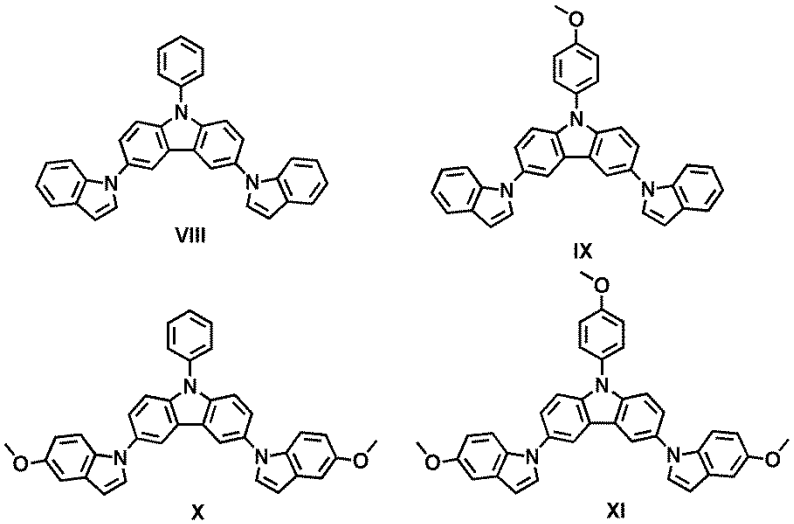

Figure 2.6. 3,6-Bis(indol-1-yl)-9-phenylcarbazole derivatives

The thermal stability of these compounds is superior in comparison with that of the previously described compounds. The different decomposition as well as the glass transition temperatures of the similar materials **VIII**–**XI** are explained by the influence of the methoxy groups. The introduction of the latter group to the C-5 position of the indole moiety increases both T_{ID} and T_G as a result of the elongation of the indole moiety in the direction across the spinning axis (the C–N bond), and the rotation in this moiety becomes slightly hindered.

The fluorescence spectra of the 3,6-bis(indol-1-yl)-9-phenylcarbazole derivatives **VIII**–**XI** are characterized by two vibrational peaks. Since carbazole and indole fragments exhibit emission below 360 nm [110,102], the observed fluorescence band at 390 nm can be attributed to the excitation of the whole molecules. The triplet energy values obtained from the phosphorescence spectra of the materials solutions at 77 °K range from 2.72 eV to 2.81 eV. These values provide a possibility to use these materials as hosts in blue PhOLEDs [105]. The values of IP obtained by photoelectron emission spectrometry are given in Table 2.2.

The effect of methoxy-substitution at the phenyl ring on the energy levels of the derivatives seems to be negligible as the IP values of derivatives **VIII** and **IX** are the same. The values of IP of derivatives **X** and **XI** are also close; however, they are somewhat lower than those of derivatives **VIII** and **IX** because of methoxy-substitution at indole moieties.

Table 2.2. Thermal, photophysical and photoelectrical characteristics of the 3,6-bis(indol-1-yl)-9-phenylcarbazole derivatives **VIII**–**XI**

	T_{ID}, °C	$T_{G,}$ °C	λ^{PL}_{max}, nm		E_T, eV	IP, eV
VIII	309	89	387, 404		2.81	5.68
VIX	385	77	391, 406		2.73	5.66
X	402	95	394, 408		2.72	5.52
XI	410	92	396, 409		2.73	5.45
Device	ITO/CuI (12 nm)/**VIII**–**XI** (30 nm)/Ca (40 nm)/Al (200 nm)					
	V_{on}, V	EL maxima, nm	η_c, Cd/A	Brightness, $\times 10^{-3}$ cd/m^2	CIE (x, y)	EQE, %
VIII–**XI**	4.0–6.2	393–442	3.7–4.1	0.7–1.2	–	2.1–5.5
Device	ITO/CuI/ **VIII**–**XI**:$Ir(Fppy)_3$ (50 nm)/TCz1 (10 nm)/ Ca (40 nm)/Al (200 nm)					
VIII–**XI**	6.8–7.9	476, 500	10.8–12.3	15.9–19.4	0.19, 0.05	3.9–4.4
Device	ITO/CuI/**XI**:DMAC(27/36) (40 nm)/TCz1 (7 nm)/ Ca (7 nm)/Al (100 nm)					
XI:DMAC27	3.4	412	5.3	3.5	0.19, 0.05	10.1
XI:DMAC36	3.4	444	13.5	12.5	0.14, 0.06	16.7

Because of the favourable optical and electroluminescent properties of 3,6-bis(indol-1-yl)-9-phenylcarbazole derivatives **VIII**–**XI**, these materials were used as emitters for single-layer electroluminescent devices. The structure and characteristics of the devices are presented in Table 2.2. These devices exhibited emission in the blue region, and the external quantum afficiencies ranged from 2.1 to 5.5%. These materials were also used as hosts for PHOLEDs with the commercial $Ir(ppy)_3$ as the emitter. The triplet energy of 3,6-bis(indol-1-yl)-9-phenylcarbazoles **VIII**–**XI** is more than 0.1 eV higher than that of $Ir(Fppy)_3$ [111]. Thus the efficient Förster energy transfer is possible from the host to $Ir(Fppy)_3$ [111]. Even though the emitting colour of the device was not deep-blue, it can still be useful in blue-green displays and lighting [112]. The low current efficiency observed for the devices based on derivatives **X** and **XI** corresponds to the higher current density caused by non-radiative recombination [113].

It is desirable to avoid the use of phosphorescent dyes containing heavy-metal (such as iridium, platinum, osmium, etc. [114]) ions in order to reduce the fabrication costs of OLEDs. The doped fluorescent host-emitter systems in simple device structures with the balanced charge carrier transport may also be effectively

employed for light emission [115]. Compound **XI** was chosen as a host for OLEDs based on the phenomenon of delayed fluorescence [116]. 2,7-diphenylamino-carbazole and 3,6-diphenylamino-carbazole derivatives were used as emitters because of their efficient blue-light emission [117, 118]. Highly efficient violet and blue organic electroluminescent devices were produced. They exhibited high current efficiency of 5.3 and 13.5 cd/A, high brightness of 3458 and 12535 cd/m^2 and high external quantum efficiency up to 17%. Such high efficiency of the manufactured devices is due to the efficient spin up-conversion from non-radiative triplet states T_1 of the host to radiative singlet states S_1 of the guests.

The advantages of spirofluorene-, carbazole- and indole- moieties were combined in the design and synthesis of three host materials **XII**–**XIV** with a different linkage between spiroluorene- and indole fragments (Figure 2.7) [119]. The thermal and photophysical properties of derivatives **XII**–**XIV** are presented in Table 2.3.

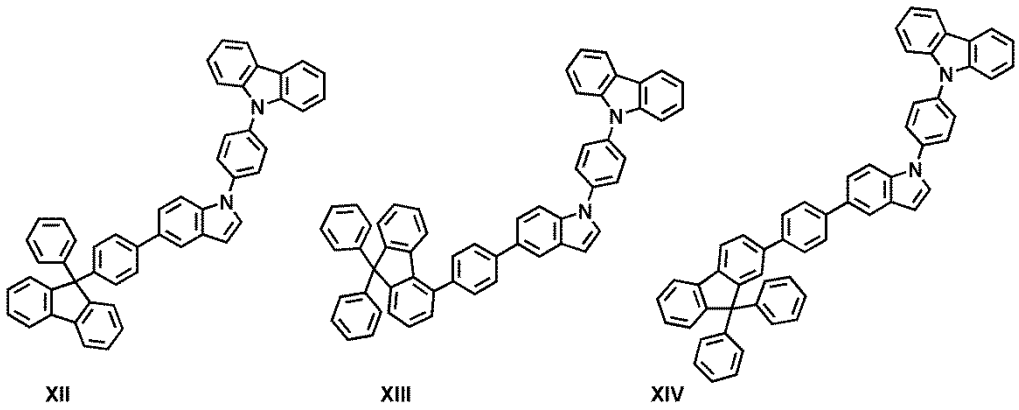

Figure 2.7. Derivatives of spirofluorene, indole and carbazole

The onset decomposition temperatures of the three materials were higher than 400 °C thus implying that they are highly thermally stable. The glass transition temperature (T_G) for derivative **XIV** was determined to be 165 °C. High T_G is desirable for stable high-performance OLEDs. Derivative **XIV** showed high T_G and T_{ID} values, apparently due to its sterically hindered molecular structure.

The IP_{CV} values for derivatives **XII**–**XIV** established by cyclic voltammetry measurements were found to be ca. 5.45 eV. The EA_{CV} values of derivatives **XII**–**XIV** were determined to be around 1.80 eV.

In the view of the different linkage ways of spirofluorene and indole units, the conjugation of compounds **XIII** and **XIV** was found to be more efficient than that of compound **XII**. The maximum emission peaks of compounds **XIII** and **XIV** were red-shifted if compared with the emission peak of **XII** [120]. From the phosphorescence spectra of the solutions in THF at 77 °K, the triplet energies (E_T) of compounds **XII**–**XIV** were determined to be higher than 3 eV. These photophysical properties of compounds **XII–XIV** render them suitable for the fabrication of blue PhOLEDs [121].

Table 2.3. Thermal and photophysical characteristics of compounds **XII**–**XIV**

	T_{ID}, °C	$T_{G,}$ °C	λ^{PL}_{max}, nm	E_T, eV	IP_{CV}, eV	EA_{CV}, eV
XII	407	–	350	3.204	5.42	1.74
XIII	405	–	364	3.018	5.49	1.86
XIV	412	165	364	3.204	5.43	1.80
Device	ITO/MoO_3 (5 nm)/TCTA (50 nm)/**XII**–**XIV**: $Ir(ppy)_3$ (35 nm, 8 wt%)/TPBi (35 nm)/LiF (1 nm)/Al (200 nm)					
	V_{on}, V	η_c, Cd/A		η_p, lm/W	CIE (x, y)	EL maxima, nm
XII	4.2	29.6		13.5	0.31, 0.61	510
XIII	4.7	30.8		17.2	0.30, 0.62	510
XIV	4.5	45.2		23.3	0.30, 0.62	510

IP_{CV} – ionization potential estimated by CV as $IP_{CV}=E_{onset\ ox\ vs.Fc}+5.1$ eV [122, 123]; *EA_{CV}* – electron affinity estimated as $EA_{CV}=IP_{CV}-E_g^{opt}$; TCTA – tris(4-carbazoyl-9-ylphenyl)amine; TPBi–2,2′,2″-(1,3,5-benzinetriyl)-tris(1-phenyl-1-H-benzimidazole); η_p – the maximum power efficiency.

In order to investigate the electroluminescent performance of compounds **XII**–**XIV** as host materials, green electroluminescent devices based on compounds **XII**–**XIV** were produced. The emitting layer was composed of 8 wt% $Ir(ppy)_3$ doped into host materials (**XII**–**XIV**). Compounds **XII**–**XIV** appeared to be excellent host materials. Green OLED based on compound **XIV** exhibited the best performance. The turn-on voltage of the device was 4.5 V. The maximum current efficiency was 45.2 Cd/A, whereas the maximum power efficiency was 23.3 lm/W. The high triplet energy level of compound **XIV** can contribute to the effective energy transfer from the host to the emitter which subsequently contribuutes to the improvement of the device's performance. Therefore, combining spirofluorene, indole and carbazole derivatives is a good method to enhance the performances of OLED devices, which also broadens the category of organic host materials [124].

Similar host materials were synthesized by Chen *et al.* [125]. Fluorene moiety was replaced with a triazine-based species, and the properties of the resulting compounds (**XV** and **XVI**) were investigated. The characteristics of these compounds are presented in Table 2.4.

Both materials started decomposing above 450 °C, and the T_G of compound **XVI** was 124 °C. However, the T_G of compound **XV** was not observed even during the second DSC scan.

The maximum emission peaks of the solutions of compounds **XV** and **XVI** were 409 nm and 407 nm, whereas their maximum emission peaks in the solid state (as shown in Table 1.4 in parentheses) were red-shifted to 428 nm and 425 nm, respectively, owing to the intermolecular π-stacking in the solid state. Meanwhile, compound **XV** exhibited a very small red-shift compared to compound **XVI** both in toluene and in the solid state thus indicating that the *para*- substituent on the triazine unit would be beneficial for the delocalization of the π electron clouds. The triplet energy levels evaluated from the highest-energy vibronic sub-bands of the low

temperature phosphorescent spectra were 2.47 eV for compound **XV** and 2.66 eV for compound **XVI**, which qualifies them to be potential hosts for red or green PhOLEDs. Compared to compound **XVI** having a *para*-substituted phenyl group, compound **XV** possessing a *meta*-substituted benzene moiety exhibited a dramatically higher E_T and a larger band gap, which indicates that the *meta*-linking design strategy could partially reduce the π-conjugation between the electron-withdrawing and electron-donating groups [126]. The IP_{CV} values obtained by conducting cyclic voltammetry measurements [127] were estimated to be around 5.50 eV. Meanwhile, the EA_{CV} was 2.36 eV for compound **XV** and 2.00 eV for compound **XVI**.

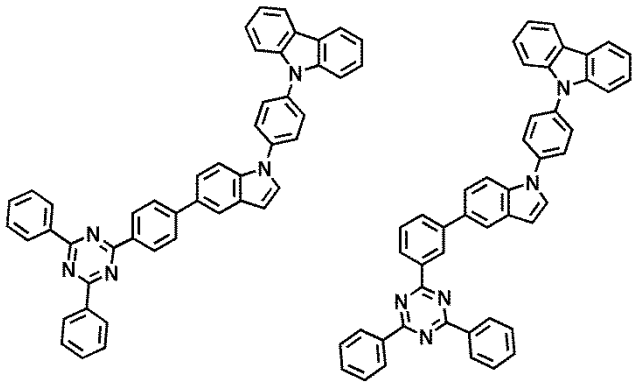

Figure 2.8. Triazine, indole and carbazole derivatives

A comparison of the properties of these compounds with those of compounds **XII**–**XIV** shows that the change of the fluorene moiety to the strong acceptor triazine-based moiety results in the bathochromic shift of the fluorescence and phosphorescence spectra as well as in the increased EA_{CV}.

Table 2.4. Thermal, photophysical and photoelectrical characteristics of compounds **XV**–**XVI**

	T_{ID}, °C	$T_{G,}$ °C	λ^{PL}_{max}, nm	E_T, eV	IP_{CV}, eV	EA_{CV}, eV
XV	452	–	409 (428)	2.47	5.56	2.36
XVI	460	124	407 (425)	2.66	5.50	2.00
Device	ITO /2-TNATA (60 nm) / TCTA (10 nm) / **XV**–**XVI**: Ir(MDQ)$_2$acac (8%, 25 nm)/ TPBi (10 nm) / BPhen (30 nm) / LiF (1 nm) / Al (80 nm)					
	V_{on}, V	η_c, Cd/A	η_p, lm/W	CIE (x, y)		EQE, %
XV	–	17.33	11.17	0.65, 0.34		17.53
XVI	–	14.15	8.64	0.65, 0.34		14.53

2-TNATA–4,4′,4″-tris[2-naphthyl(phenyl)amino]triphenylamine; BPhen–bathophenanthroline

Compounds **XV**–**XVI** were used as host materials in red PhOLEDs. The device structure and characteristics are shown in Table 2.4. The red emissive

Ir(MDQ)2acac [128] was doped in compounds **XV** and **XVI** with the doping concentration of 8 wt % so that to form the emitting layers. The device containing *para*-substituted derivative **XV** delivered superior performance even though the *meta*-substituted compound **XVI**-based device showed more balanced bipolar carrier-transporting ability than the device based on compound **XV**. The maximum current efficiency reached 17.33 Cd/A, and the maximum power efficiency was 11.17 lm/W for the **XV**-based device. The carrier-transport ability of the host produced a greater effect on the device's performance. In addition, both devices exhibited pure red emission and showed no residual emission from the host or other layer materials, which highlighted that the electroluminescence solely originated from the complete energy transfer from the host to the dopant.

In conclusion, indole-moiety containing materials show promising properties to be considered for efficient light-emitting diodes.

2.2.2. Indole-Moiety Containing Materials as Emitters and Hole Transporting Materials

In contrast to indole-based hosts, only a few examples of indole derivatives as emitters were reported. Hwu *et al.* [129] designed and synthesized indole derivative **XVII** as a potential emitter.

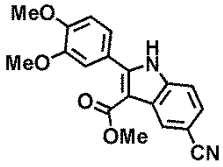

XVII

Figure 2.9. Luminescent indole derivative

Attachment of the appropriate substituents at C-2, C-3, and C-5 positions of indole allowed to tune its emission. The steric congestion between the esther group at C-3 position and the hydrogen atoms on the dimethoxyphenyl moiety at C-2 position may generate a dihedral angle between these two planes. This possible non-planarity, however, gives an advantage for compound **XVII** to become a promising OLED material.

This derivative possesses fairly good thermal stability (T_{ID}=289 °C) and is denoted by the possibility to form a solid amorphous film (T_G=136 °C). The solution of derivative **XVII** in dichloromethane emitted violet light (397–404 nm) with the quantum efficiency of 59.2%. The emission of the solid thin film was bathochromically shifted to blue light (439 nm). The bathochromic shift caused by the electron-withdrawing moiety (CN–) was due to the intermolecular interactions between this auxochrome and the main indole chromophore in the excited state [130]. A pure blue light-emitting diode employing this material was produced. The obtained device including compound **XVII** exhibited the turn-on voltage of 6.0 V. Its brightness reached 184 cd/m^2 at 20 mA and 8.3 V as well as 783 cd/m^2 at 100 mA and 10.2 V. The observed maximum brightness of this device was at 2417 cd/m^2 at 551 mA and 15.0 V. The external maximum quantum and power

efficiencies of the device were 0.87% and 0.45 lm/W recorded at 7.6 V (4.1 mA/cm^2, 46 cd/m). The electroluminescence spectrum of a compound **XVII**-based device showed the emission maximum at 443 nm. The colour of the device was blue (x=0.18, y=0.12) in the *Commission Internationale de L'Éclairage* (CIE) chromaticity coordinates. The EQE of the device is rather low (0.87%) compared to that of a similar device based on the different blue emitter (9,10-bis(4-(2,2-diphenylvinyl))phenylanthracene). The eficiency of the latter device was 3% [131], but it exhibited a greener colour with the CIE chromaticity coordinates of x=0.14, y=0.17.

Compounds having an indole moiety can not only contribute to the active emission layers of electroluminescent devices but can also be useful for the preparation of charge-transporting layers. Generally, hole-transporting layers in OLEDs play the role of facilitating the hole injection from the anode into the organic layer, accepting holes, and transporting the injected holes to the emitting layer. The hole-transporting layer can also block electrons [132, 133]. High triplet energy charge transport materials play a role of confining the charges and the excitons inside the emitting layer thus improving the quantum efficiency of PhOLEDs. Park *et al*. [134] designed, synthesized and investigated compounds with a fused indole rigid core structure (Figure 2.10).

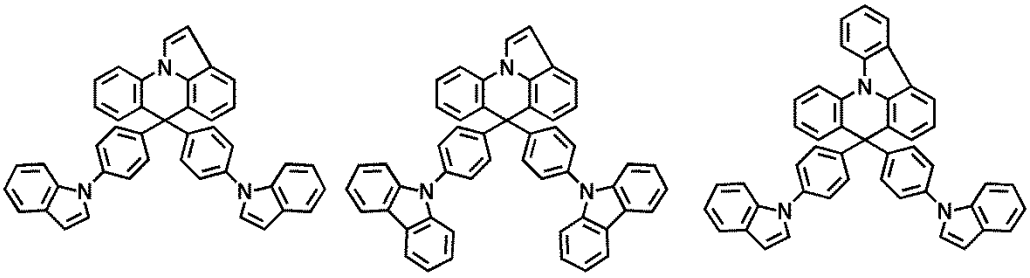

XVIII XIX XX

Figure 2.10. Structures of the derivatives of fused indole and carbazole

Derivatives **XVIII** and **XIX** showed a high T_G of 123 °C to 125 °C due to the rigid molecular backbone structure. The thermal stability data was, unfortunately, not provided in the publication.

The phenyl unit in the N-phenylindole moiety can freely rotate through the chemical bond between the indole and the phenyl unit, but the rotation of the phenyl group is hindered in fused indole compounds due to the structure of the fused ring through the sp^3 carbon atom. In addition, the fused indole core is connected to the carbazole and indole units through the sp^3 carbon, which does not extend the conjugation of the fused indole core and maintains the high triplet energy (2.70 eV for compound **XVIII** and 2.80 eV for compound **XIX**). Due to the high triplet energy of these compounds, the triplet exciton quenching can be blocked by hole transport layers in deep blue PHOLEDs [135, 136].

Table 2.5. Thermal, photophysical and photoelectrical characteristics of triazine-indole-carbazole derivatives **XVIII**–**XX**

	T_{ID}, °C	T_G, °C	λ^{PL}_{max}, nm	E_g^{opt}, eV	IP_{CV}, eV	EA_{CV}, eV
XVIII	–	123	336	3.83	5.90	2.09
XIX	–	125	350	3.57	6.04	2.24
XX	–	142	367	3.40	5.86	2.57
Device	ITO (150 nm)/PEDOT:PSS(60 nm)/ NPB (5 nm)/**XVIII**–**XX** (10 nm)/ mCPPO1:FCNIrpic(30 nm, 3%)/ TSPO1(25 nm)/LiF(1 nm)/Al(200 nm)					
	V_{on}, V	η_c, Cd/A	η_p, lm/W	CIE (x, y)		EQE, %
XVIII	3.5	30.7	30.0	0.137, 0.182		24.7
XIX	3.5	29.9	29.3	0.137, 0.185		23.9
XX	–	–	14.2	0.14, 0.17		19.3

E_g^{opt} – the optical bandgap determined from UV-vis spectra; PEDOT:PSS – poly(3,4-ethylenedioxythiophene)-poly(styrenesulfonate); NPB – N,N′-di(1-naphthyl)-N,N′-diphenyl-(1,1′-biphenyl)-4,4′-diamine

Hole-only devices of derivatives **XVIII** and **XIX** were produced in order to compare the hole injection and transport properties. The hole current density of a compound **XIX**-based device was higher than that of a compound **XIX**-based device. In general, the hole current density is determined by the energy barrier for hole injection and hole transport properties. The energy barrier for hole injection between NPB (IP=5.50 eV) and compound **XVIII** (IP_{CV}=5.90 eV) was 0.40 eV, whereas between NPB (IP=5.50 eV) and compound **XIX** (IP_{CV}=6.04 eV) it was 0.54 eV. Therefore, the low energy barrier for hole injection enhanced the hole current density of the device based on compound **XVIII**. In addition to the low energy barrier for hole injection, hole transport properties of compounds **XVIII** and **XIX** also contributed to the high hole current density.

Deep blue PHOLEDs were fabricated by using compounds **XVIII** and **XIX** for the preparation of hole transport layers. Organic complex FCNIrpic [137] was used as an emitter. A device based on compound **XVIII** showed a higher current density than a compound **XIX**-based one. The turn-on voltage of the deep blue PHOLEDs was 3.5 V whereas the driving voltages at 1000 cd/m^2 were 6.9 V and 7.4 V for compound **XVIII**- and **XIX**-based devices, respectively. Both devices showed high quantum efficiency although the quantum efficiency of a compound **XIX**-based device was a little lower compared with that of a compound **XVIII**-based device. The maximum external quantum efficiencies of the devices were 24.7% and 23.9%, whereas the quantum efficiencies at 1000 cd/m^2 were 22.3% and 21.7%. The prominently high quantum efficiency can be explained by the efficient hole injection, exciton blocking and electron blocking properties of compounds **XVIII** and **XIX**. The triplet energy of the triplet emitter was 2.75 eV, and the triplet exciton quenching could be suppressed by the hole transport layer due to the high triplet energy of the hole transport materials. Both devices exhibited similar emission spectra with the maximum emission peak at 458 nm and the shoulder at 486 nm. The colour coordinates of compound **XVIII**- and **XIX**-based devices at 1000 cd/m^2 were

(x=0.137, y=0.182) and (x=0.137, y=0.185), which corresponds to the real deep blue colour.

The same research group [138] suggested compound **XX** with the fused indole and indoloacridine structure as a high triplet energy hole transport material (Figure 2.10). The design concept of compound **XX** was to obtain high triplet energy and thermal stability by using the indoloacridine core. The indoloacridine core has an indole unit fused to the acridine moiety which keeps the high triplet energy of the indole unit and provides rigidity to the molecule. High triplet energy (2.95 eV) of compound **XX** is explained by the separation of conjugation between the indoloacridine core and 1-phenylindole through the sp^3 carbon linkage [138]. The triplet energy of compound **XX** was high enough for triplet exciton blocking of deep blue PhOLEDs since common deep blue triplet emitters have a triplet energy of 2.70–3.05 eV [139]. Derivative **XX** exhibited T_G of 142 °C. The rigid indoloacridine core and the bulky 1-phenylindole unit induced the high T_G of compound **XX**. The hole mobility of the material was measured by the space charge-limited current curve of the hole-only device, and the obtained value was 10^{-4} cm^2/Vs.

This material was used for the preparation of the hole transporting layer of a blue PhOLED. The current density and luminance of the blue PhOLED were high, which indicates high hole current density in the emitting layer. The high hole current density was explained by the efficient hole injection and the high hole mobility of material **XX** [138]. The energy barrier for hole injection from NPB [140] to the material **XX** hole transport layer was 0.36 eV. The other factor which can be used for the explanation of the high hole current density is high hole mobility of material **XX**. This deep blue device exhibited a high external quantum efficiency of 19.3%. The high triplet energy of material **XX** suppressed triplet exciton quenching of the FCNIrpic deep blue emitter and confined the triplet excitons of FCNIrpic, which led to the high quantum efficiency. The colour coordinates of the blue PhOLED were (x=0.14, y=0.17).

More extended heteroaromatic structures containing an indole moiety are also used in the preparation of materials for OLEDs. Among the most widely studied compounds of this sort are derivatives of indolo[3,2-b]carbazole [141, 142]. Such a chromophore is more rigid and planar compared to sole indole or carbazole moieties. Thus condensation of more aromatic rings could improve thermal, charge transport and luminescence properties [143, 144].

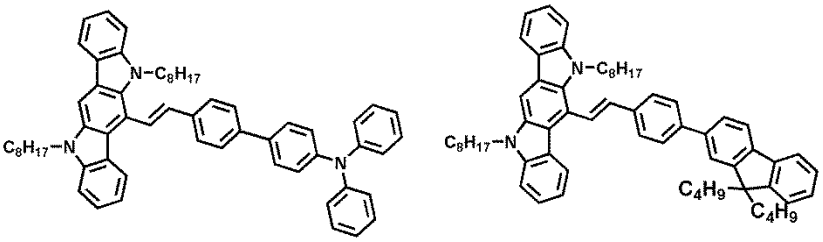

XXI XXII

Figure 2.11. Indolo[3,2-b]carbazole derivatives

Zhao *et al*. [145] designed and investigated luminescent derivatives of indolo[3,2-b]carbazole with triphenylamino (**XXI**) or fluorenyl (**XXII**) substituents at C-6 position (Figure 2.11).

Compounds **XXI** and **XXII** exhibited high thermal stbility with the temperatures of the onset of thermal degradation exceeding 400 °C. However, no obvious glass transitions were observed for the two compounds by DSC.

These two compounds were highly fluorescent both in toluene solution and in the solid state. The fluorescent quantum yields of the solutions of compounds **XXI** and **XXII** were 0.40 and 0.45, respectively. Their solutions in toluene exhibit narrow emission peaks at 499 nm. It could be presumed that the emission wavelengths are mostly controlled by the indolo[3,2-b]carbazole unit according to their very similar optical properties. Moreover, the two compounds exhibited similar λ_{max} of emission both in the solution and in the thin films, which indicates that there were minimal intermolecular interactions in the films [146].

Table 2.6. Thermal, photophysical and photoelectrical characteristics of indolo[3,2-b]carbazole derivatives **XXI**–**XXIV**

	T_{ID}, ℃	$T_{G,}$℃	λ^{PL}_{max}, nm (toluene solution)	E_g^{opt}, eV	IP_{CV}, eV	EA_{CV}, eV
XXI	420	–	499	2.62	5.10	2.48
XXII	408	–	499	2.63	5.10	2.47
XXIII	–	–	435	3.48	5.04	1.56
XXIV	–	–	444	3.22	4.99	1.77
Device	ITO/NPB (30 nm)/**XXI**–**XXII** (40 nm)/TPBI (40 nm)/LiF (1 nm)/Al (80 nm)					
	V_{on}, V	η_c, Cd/A	η_p, lm/W	Brightness, $\times10^{-3}$cd/m^2	CIE (x, y)	EL maxima, nm	EQE, %
XXI	2.99	6.90	6.74	66	0.224, 0.562	502	2.39
XXII	2.65	7.06	7.92	69	0.214, 0.568	503	2.79
Device	ITO/**XXIII**–**XXIV**(50 nm)/Alq_3(50 nm)/ Mg:Ag (10:1,150 nm)/Ag (10 nm)						
XXIII	3.7	2.156	1.45	13.3	0.295, 0.552	524	0.816
XXIV	4.1	1.161	0.74	19.5	0.313, 0.554	526	0.383

The ionization potential values estimated by CV were 5.10 eV for both compounds whereas the electrochemically estimated electron affinity values were 2.48 for derivative **XXI** and 2.47 eV for derivative **XXII**.

Both indolo[3,2-b]carbazole derivatives **XXI** and **XXII** were used as emitters in electroluminescent (EL) devices. The devices exhibited low turn-on voltage of 2.65 V. The EL devices showed similar peaks with those of PL spectra of the thin films. This observation indicates that both PL and EL originate from the same radiative decay process of the singlet excitons [147, 148]. The devices showed almost identical characteristics of current, power efficiency and brightness

signifying the lack of substituent influence on C-6 position of the materials. The luminescence efficiency of indolo[3,2-b]carbazole-derived materials is quite promising in the actual use of light-emitting devices.

Similar compounds bearing triphenylamine (TPA) moieties at different positions of the indolo[3,2-b]carbazole fragment were synthesised and studied [149] (Figure 2.12). The characteristics of the compounds and devices are presented in Table 2.6.

The large Stokes shifts of the dilute solutions (89 nm for compound **XXIII** and 147 nm for compound **XXIV**) could be attributed to the conformational changes of the molecules upon excitation. Theorical quantum chemical calculations proved that the introduction of triphenylamine moieties in different positions of the indolo[3,2-b]carbazole backbone influenced the conjugation length of the molecules, which resulted in such differences of their optical properties [149].

If compared with the common electron-blocking materials, the relatively high EA values of these compounds may make them useful as effective electron-blocking layers blocking electrons from escaping from the emitting layer to the anode and thus contributing to the improvement of the efficiency of the devices [150].

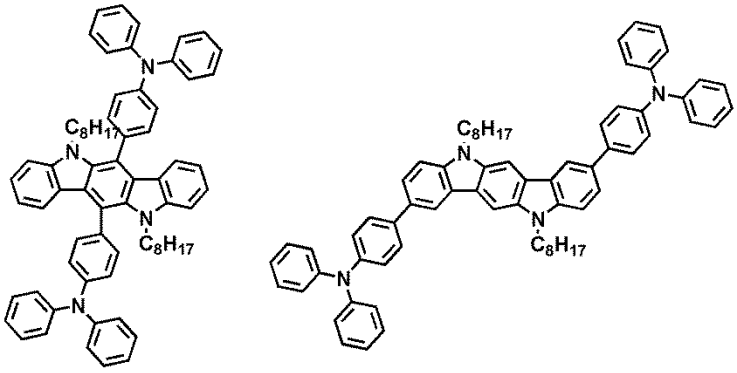

XXIII XXIV

Figure 2.12. Derivatives of indolo[3,2-b]carbazole featuring triphenylamino moieties

The double-layer EL devices were produced by using compounds **XXIII** and **XXIV** for the preparation of hole-transporting layers and Alq_3 as the emitting and electron-transporting material. The structure of the devices is shown in Table 2.6. Green emission from Alq_3 was obtained, which suggests that the charge recombination was localised in the Alq_3 layer and that the indolo[3,2-b]carbazole derivatives acted primarily as hole transporters and also that there was no exciplex formation at the interface with Alq_3. All the devices exhibited low activating voltage (recorded at 1 cd/m^2). The lower activating voltage of the device containing compound **XXIV** might suggest that TPA groups atttached at C-6 and C-12 positions were more helpful in enhancing the hole-injection performance than those attached at C-2 or C-8 positions. The device produced by using compound **XXIII** for the hole-injection layer showed better current and luminance efficiency. These results indicate that disubstituted at C-6 and C-12 positions indolo[3,2-b]carbazole derivatives demonstrate superior hole-transporting performance.

Indole-derived compounds possess good luminescent and hole-transporting properties which make them interesting candidates for the application in OLEDs.

2.3.Cross-Linkable Electroactive Materials

2.3.1.Thermally Activated Cross-Linking

Thermaly initiated or photoinitiated cross-linking is the most commonly applied in manufacturing insoluble polymeric films. The major advantage of such polymeric cross-linked films is that they do not deteriorate after the deposition of the subsequent layers when using the spin-coating or any other solution processing technique [151, 152]. The thermal induced self-polymerisation offers several advantages over other methods of the preparation of polymers. For example, it often enables avoiding purification which, comparatively, is a time consuming procedure. The charge transporting layers obtained by self-polymerisation of electroactive monomers are free from the residual initiator which can act as traps for charge carriers. Moreover, thermally cured polymers reveal very good solvent resistance and are electrochemically stable [153–156].

Vinyl groups are well-known for their capacity to undergo polymerization through radical as well as anionic mechanisms. In particular, radical polymerization can be thermally initiated [157, 108]. Thus polymerisation of vinyl groups can potentially serve as a method for thermally cross-linkable OLED materials [158]. A small molecule functionalised with a single reactive functional group after polymerisation results in yielding a soluble linear polymer [159, 160]. Therefore, candidates for cross-linking are typically functionalised with at least two reactive functional groups [161–163].

Attractive features of styrene chemistry involve the aspect that no additional reagents are required and that no side products are anticipated besides those associated with chain terminations [164–166]. However, functional organic materials must be stable at the temperatures required for cross-linking and relatively unreactive towards the propagating polymer chain [167–169].

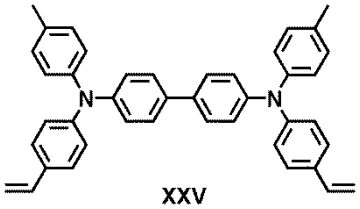

XXV

Figure 2.13. Cross-linkable hole-transporting compound

Cheng *et al*. [170] demonstrated a white emitting OLED with novel cross-linkable hole transporting material **XXV**. The structure of the device was ITO/PEDOT:PSS/ **XXV**/PF doped with BFBT (0.04 wt %)/CsF/Al. Polyfluorene (PF) was used as the blue host. 4,7-bis(9,9-dihexylfluoren-2-yl)-2,1,3-benzothiadiazole (BFBT) was used as a guest. The layer of monomer **XXV** was deposited by spin-casting and annealed at 180 °C in a nitrogen glove for 30 min. The white colour was obtained by manipulating three-colour emission. The blue region

was a characteristic emission of the PF host, whereas the green emission came from the guest BFBT, while the red emission came from the exciplex formed at the interface between the cross-linked compound **XXV**-based layer and the fluorenone species. Fluorenone was detected as an impurity in PF. The device showed its maximum luminous efficiency of 5.28 cd/A with the chromaticity coordinates of 0.33, 0.42 (the ideal white point is 0.33, 0.33). This example indicates that cross-linkable electroactive monomers look promising for solution-processed white OLEDs.

Sun *et al*. [171] designed and investigated two cross-linkable monomers with vinylbenzyl groups. The product of cross-linking of compound **XXVI** was chosen to act as the host for blue OLEDs due to its high triplet energy of 2.95 eV. Compound **XXVII** showed the property of thermally activated delayed fluorescence, which enabled efficient exciton-harvesting via the spin up-conversion from T_1 states to S_1 states. In order to investigate the characters of OLEDs, devices were produced, and thermally cross-linked films of both monomers were employed as the emissive layers. The mixed solution of different ratios of both monomers was spin-coated onto the PEDOT:PSS layer from a chlorobenzene solution and heated at 200 °C for 30 minutes. Other active layers were thermally deposited onto the insoluble films. By employing such polymers as the emitters in OLEDs, the blue device showed the maximum EQE of 2.0% with the peak electroluminescence wavelength of 444 nm.

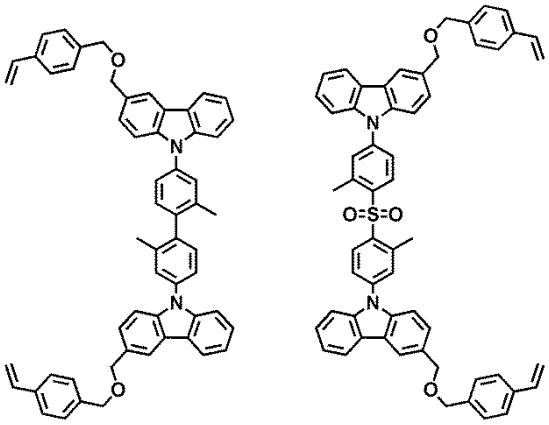

Figure 2.14. Cross-linkable monomers for the emitting layer

2.3.2.Photochemically Activated Cross-Linking

The thermal cross-linking technique requires a high annealing temperature (above 180 °C) and long processing times ranging from 30 min to several hours in order to obtain fully insoluble films. The long annealing time may lead to the thermal degradation of the electroactive materials in OLEDs [172, 173]. These requirements of extensive thermal treatment may cause difficulty in and inefficiency of the mass production of large-area devices.

The other approach towards the fabrication of solution-processed, multi-layer structured OLEDs involves materials that contain photo-crosslinkable groups such

as oxetanyl [174–177], or epoxy groups [166–179]. Photocross-linking can be conducted under much milder conditions of room temperature rather than thermal annealing. However, so far, little success has been achieved in applying the photo cross-linking approach for the solution processing of multilayer OLEDs [180, 181]. Since the processes of photo-crosslinking of the currently available materials usually require a relatively long exposure towards high-power UV irradiation, additional side reactions can occur during the crosslinking process, and they can have adverse effects on the efficiency and lifetime of the devices. Also, photocrosslinking approaches can deteriorate the molecular packing, which would affect not only the charge transport but also the device's performance as the functional groups may interfere with molecular diffusion and packing [182, 183].

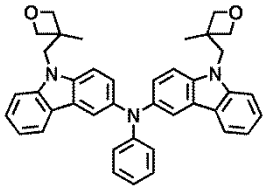

XXVIII

Figure 2.15. Carbazolyl-containing arylamine with oxetanyl-functional groups

Carbazolyl-containing arylamine with oxetanyl-functional groups **XXVIII** was employed as the hole transporting material in green OLEDs in two different ways: as a monomer and for photopolymerization in order to obtain a cross-linked material [184]. Alq_3 was used as an emitter. The polymeric hole-transporting layer was made by spin-coating of a 30–40 nm layer of derivative **XXVIII** with 5 wt % of {4-[(2-hydroxytetradecyl)-oxyl]-phenyl}-phenyliodonium hexafluorantimonate as a cationic photoinitiator from a solution and irradiating it with an UV lamp for 90 seconds at room temperature. When positive voltage was applied to the device, the bright green electroluminescence of Alq_3 was observed with the emission maximum at around 520 nm which was the same for the device containing derivative **XXVIII** as a monomeric hole-transporting layer. This confirms that the insoluble polymer of derivative **XXVIII** functions well as the hole-transporting layer and its hole mobility is sufficient for the charge carrier recombination occurring within the Alq_3 layer. Comparative low turn-on voltage of 5 V and the operation voltage (100 cd/m^2 at ~8V) of this device suggest that the cross-linked layer of derivative **XXVIII** could function well as the hole-transporting layer. The maximum electroluminescence efficiency of the device exceeded 0.8 cd/A.

Cross-linkable derivatives of indolo[3,2-b]carbazole bearing oxetanyl functional groups (**XXIX–XXXI**) were synthesised and tested as hole-transporting prepolymers for OLEDS [174]. The formation procedure of the insoluble polymeric layer was the same as the previously described one. Alq_3 was used as the emitter. When positive voltage was applied, the bright green electroluminescence of Alq_3 was observed with the emission maximum at around 520 nm. No exciplex formation at the interface between the polymeric hole transporting layer and the Alq3 layer was observed. The devices with phenyl-substituted indolo[3,2-b]carbazole derivative

XXXI exhibited the best overall performance (showing the turn-on voltage of 5 V, the maximum luminance efficiency of 3.64 cd/A, and the maximum brightness of ca. 5700 cd/m^2).

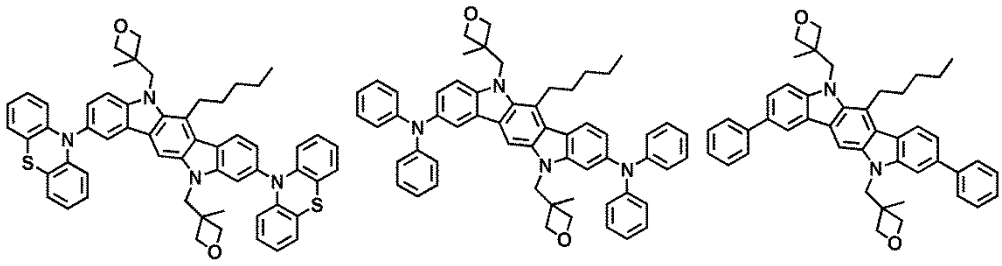

Figure 2.16. Oxetanyl-substituted indolo[3,2-b]carbazole cross-linkable compounds

Cross-linked layers of these derivatives were also tested as hole transporting structures in multilayer OLEDs. Poly[(9,9-dioctylfluorene-2,7-diyl)-co-2,5-di(phenyl-4-yl)-2,1,3-benzothiadiazole] was used as the green emitter [185]. The device containing a cross-linked layer of phenyl-substituted indolo[3,2-b]carbazole derivative **XXXI** demonstrated the maximum photometric efficiency of 2.8 cd/A and the maximum brightness of 7790 cd/m^2.

Although the photo-crosslinking concept is simple, the development of cross-linkable materials with a high cross-linking rate and the minimal disturbance in the electrical properties after cross-linking remains a major challenge.

2.4.Conclusions of the Literature Review

The above discussed indole moiety-containing materials show high triplet energy values of up to 3 eV, sufficient charge transport properties and controllable ionisation potential values. They also possess the capacity to form molecular glasses. The high reactivity of several positions of the indole moiety allows modifying its structure and tuning its thermal, optical and photophysical properties according to the requirements of organic light-emitting devices. Therefore, it is important to evaluate the influence of different substituents and of the linking topology of chromophores on the thermal stability, ability to form glasses, photophysical properties, ionization potential values, electrochemical stability as well as charge-transporting properties of the newly synthesised derivatives of the indole.

There are still relatively few reports on the synthesis and studies of indole derivatives with reactive functional groups. Therefore, particular attention has to be paid to the synthesis and studies of cross-linkable derivatives. It may open up new possibilities in the fabrication of stable OLEDs.

3. Experimental Part

3.1. Instrumentation

Nuclear magnetic resonance (NMR) spectroscopy. ^{1}H and ^{13}C NMR spectra were recorded by using a *Bruker Avance III* apparatus (400 MHz). The samples were prapered by dissolving around 20 mg of the material in 1 ml of deuterated chloroform (CDCl) with an inner standard, tetramethylsilane (TMS). Hydrogen nuclei ^{1}H were excited by using the frequency of 400 MHz, and carbon nuclei ^{13}C were excited by using the frequency of 101 MHz. The data is presented as chemical shifts (δ) in ppm against tetramethylsilane (in parentheses: multiplicity, integration, coupling constant).

Attenuated total reflectance infrared spectroscopy (ATR-IR). IR spectra were recorded by using a *Vertex 70 Bruker* spectrometer equipped with an ATR attachment with a diamond crystal over frequencies of 600–3500 cm^{-1} with a resolution of 5 cm^{-1} over 32 scans. IR spectra are presented as a function of transparency (T) expressed in percent (%) against the wavenumber (ν) expressed in cm^{-1}.

Mass spectrometry. Mass spectra were obtained on a *Waters ZQ 2000* mass spectrometer. The introduction of the sample into the ion source occurs by coupling a gas chromatograph and a HPLC (High pressure liquid chromatograph) device. The samples were prepared as diluted solutions of the materials and were ionized by using electrospray ionization. Mass spectra are presented as an abundance of the ion versus the mass-to-charge ratio (*m/z*).

UV-VIS absorption spectroscopy. The absorption spectra of the dilute solutions (10^{-4}–10^{-5} mol/l) and thin films of the synthesized materials were recorded with a *Perkin Elmer Lambda 25* spectrophotometer. The spectra were recorded under ambient conditions. The spectra are plotted as a function of absorbance (A) against the wavelength (λ) expressed in nm. In most cases, the spectra are normalized where the intensities of bands are equalized at certain wavelengths.

Photoluminescence spectroscopy (PL). Fluorescence spectra of the thin films and the dilute solutions (10^{-4}–10^{-5} mol/l) of the synthesized materials were recorded at room temperature with a luminescence spectrometer *Edinburgh Instruments FLS980*. The fluorescence quantum yields of the solutions and thin films of the materials were measured by using an integrating sphere. The phosphorescence spectra were recorded at a low temperature (77 °K). The samples were prepared in the same way as for UV-VIS absorption measurements. The spectra are presented as normalized PL intensity (I) against the wavelength, nm.

Differential scanning calorimetry (DSC) measurements were carried out by using a *TA Instruments Q2000* thermosystem. The samples were examined at a heating/cooling rate of 10 °C/min under nitrogen atmosphere. The sample (approximately 2–3 mg) was placed in a closed aluminum pan. An empty pan was used as a reference.

The **melting points** of the compounds were determined by using an Electrothermal MEL-TEMP apparatus.

Thermogravimetric analysis (TGA) was performed on a *TA Instruments Q50* analyser. The heating rate was 20 °C/min under nitrogen atmosphere. The sample of ca. 2–3 mg was placed in an open alumina (Al_2O_3) pan.

Electron photoemission spectrometry was used to determine the ionization potentials (IP) of the layers of the synthesized compounds. For the recording of the photoelectron emission spectra, the layers were prepared by drop-casting chloroform solutions of the materials on cleaned indium tin oxide (ITO)-coated glass substrates. The negative voltage of 300 V was applied to the sample substrate. The deep UV deuterium light source ASBN-D130-CM and CM110 1/8 m monochromator were used for the illumination of the samples with the monochromatic light. A *6517B Keithley* electrometer was connected to the counter-electrode for the measurement of the photocurrent which was flowing in the circuit under illumination. Energy scan of the incident photons was performed while increasing the photon energy. The photocurrent (which is attributed to d*U*/d*t*) is dependent on the incident light photon energy (*hv*). The *Ip* was estimated as the intersection points of the extrapolated linear part of the dependence (d*U*/d*t*)1/2=*f*(*hv*) and the *hv* axis (i.e. the *hv* value at zero photocurrent) [186].

Cyclic voltammetry measurements were performed by using a glassy carbon working electrode (a disk with the diameter of 2 mm) in a three-electrode cell while using an Autolab Type potentiostat – galvanostat. The measurements were carried out for the solutions in dry dichloromethane containing 0.1 M tetrabutylammonium hexafluorophosphate at 25 °C; the scan rate was 50 mV/s while the sample concentration was 10^{-3} M. The potentials were measured against silver as a reference electrode. Platinum wire was used as a counter electrode. The potentials were calibrated with the standard ferrocene/ferrocenium (Fc/Fc^+) redox system [187].

Spectroelectrochemistry measurements were performed *in situ* by using an *EDAQ* potentiostat and monitoring the UV-VIS spectra on a *Shimadzu UV–1800* spectrometer. The electrochemical cell was comprised of a platinum wire counter electrode, a silver wire reference electrode and ITO quartz glass as the working electrode. The measurements were made in 0.01 M concentrations of all the materials in 0.1 M tetrabutylammonium perchlorate solution in dry dichloromethane.

Computational methods. In order to estimate the frontier molecular orbitals, density functional theory (DFT) calculations were performed. The ground-state geometries were optimized by using the B3LYP (Becke three parameters hybrid functional with Lee-Yang-Perdew correlation) [188] functional at 6-31G (d, p) level in vacuum with the Spartan'14[189] or Gaussian [190] programs.

Firstly, while using Spartan'14, the equilibrium conformer search at the ground state was performed by using the MMFF (Molecular mechanics force fields) method, and then this geometry was used for further optimisation. The vertical triplet energy values were calculated by using the energy difference between the neutral and deprotonated species at the neutral state geometry.

The time-dependent DFT (TD-DFT) calculations were carried out with the *Gaussian 09* software package. Molecular orbitals were visualized by using *Gaussview or Spartan'14*.

Charge-drift mobility measurements were performed by employing two methods: time-of-flight or space-charge-limited current. The time-of-flight (TOF) method was used in order to test charge drift mobility of vacuum-deposited layers of the compounds. Diode-like samples were prepared for being measured with ITO bottom and aluminum top electrodes. The thickness of the layers ranged from 1 to 3.5 μm. The sample area was of 2×3 mm^2. The experimental setup included an *Nd:YAG* laser *EKSPLA NL300*, a *Tektronix TDS 3032C* oscilloscope, and a *6517B Keithley* electrometer. For the calculation of the charge drift mobility, the following formula was used:

$$\mu = d^2(U \times t_{tr})^{-1},$$

where d is the layer thickness, U is the voltage applied to the samples, and t_{tr} is the transit time [191].

Hole-only devices were fabricated for the space-charge-limited current (SCLC) experiments [192]. The indium tin oxide (ITO)-coated glass substrates with the sheet resistance of 15 Ω/sq were cleaned in acetone and isopropyl alcohol ultrasonic baths for ca. 5 min before depositing functional layers. The hole-only devices with the following architectures were fabricated: ITO/m-MTDATA(20 nm)/the studied compound (80 nm)/m-MTDATA(20 nm)/Al(60 nm). The layer of m-MTDATA (4,4′,4″-tris[3-methylphenyl(phenyl)amino]triphenylamine) was used as the hole-injecting and electron-blocking layer. The values of hole mobility were estimated by employing the Mott-Gurney Law [193]:

$$J_{SCLC} = \mu_{SCLC} \frac{9}{8} \varepsilon \varepsilon_0 \frac{V^2}{d^3} \quad (3.1)$$

where J_{SCLC} is the steady-state current density (SCLC), μ_{SCLC} is the SCLC mobility; V is the applied voltage; d is the film thickness, ε is the permittivity of the film (~3); ε_0 is the absolute permittivity of the free space. Organic and metal layers were vacuum-deposited under vacuum higher than $3 \cdot 10^{-6}$ mBar. The deposition rate of the guest was of 0.1 Å/s, while the deposition rate of hosts was set at 1.0 Å/s. The thickness of thin films was monitored during the deposition process by using a quartz crystal microbalance. The sample area was 6 mm^2 with 7 devices per substrate. A *Keithley source meter 2400-C* was utilised for recording the current density–voltage characteristics of the devices.

Device fabrication and characterization. Phosphorescent OLEDs (PhOLEDs) described in Chapter 4.2 were fabricated by thermal vacuum deposition under vacuum conditions higher than $3 \cdot 10^{-6}$ mBar. The host:guest emission layers were deposited by the co-deposition of host (m/m 90%), the investigated compound and the dopant (m/m 10%) (tris[2-phenylpyridinato-C2,N]iridium(III) ($Ir(ppy)_3$)) from two different sources. The deposition rate of the guest was of 0.1 Å/s, while the deposition rate of the host was set at 1.0 Å/s. A *Keithley* source meter *2400-C* was employed for recording the current density–voltage characteristics of the devices.

The current density–luminance characteristics were estimated by using a calibrated silicon photodiode with a *6517B Keithley* electrometer. Electroluminescence (EL) spectra were recorded by an *Avantes AvaSpec-2048XL* spectrometer. The current, power and external quantum efficiencies were estimated using the current density, luminance, and EL spectra as reported earlier [194].

The electroluminescent devices described in Chapter 4.3 were fabricated by means of vacuum deposition of organic semiconductor layers and metal electrodes onto pre-cleaned ITO coated glass substrate under vacuum of 10−6 Torr. The devices were produced by step-by-step deposition of different organic layers. The active area of the obtained devices was 3x6 mm^2. The density current-voltage and luminance-voltage characteristics were measured by using a semiconductor parameter analyser (HP 4145A) in the air without passivation immediately after the formation of the device. The brightness measurements were performed by using a calibrated photodiode. The electroluminescence spectra were recorded with an *Ocean Optics USB2000* spectrometer.

Atomic force microscopy (AFM) experiments were carried out in air at room temperature by using a *NanoWizardIII* atomic force microscope (JPK Instruments), while the data was analysed by using *SurfaceXplorer* and *JPKSPM Data Processing* software. The AFM images were collected by using a V-shaped silicon cantilever (the spring constant of 3 N/m, the tip curvature radius of 10.0 nm and the cone angle of 20º) operating in the contact mode.

X-ray diffraction measurements at grazing incidence (**XRD**) were performed by using a *D8 Discover* diffractometer (Bruker) with Cu K_α (λ=1.54 Å) X-ray source. Parallel beam geometry while employing a 60 mm Göbel mirror (an X-ray mirror on a high precision parabolic surface) was used in order to obtain the relevant data. This configuration enables transforming the divergent incident X-ray beam from the line focus of the X-ray tube into a parallel beam that is free of K_β radiation. The primary side also had a Soller slit with an axial divergence of 2.5º. The secondary side had a *LYNXEYE* (1D mode) detector with the opening angle of 2.16º and the slit opening of 6.0 mm. The sample stage was a Centric Eulerian cradle mounted onto a horizontal *D8 Discover* device with a vacuum chuck (sample holder) fixed onto the top of the stage. The X-ray generator's voltage and current were 40.0kV and 40mA, respectively. The XRD scans of the emitting layers were performed in the range of 3–134.0º with a step size of 0.065º, the time per step set at 19.2 s, and the auto-repeat function being enabled. The XRD scans were performed at the incidence angle of 1.0º. The processing of the resultant diffractograms was performed with DIFFRAC.EVA software.

3.2. Materials

Aluminum trichloride (99.9%), benzyltrimethylammonium chloride (BTMAC) (97%), azobisisobutyronitrile (98%), benzyl chloride (99%), boron trifluoride diethyl etherate (46.5%), bromoethane (98%), 2-chloro-2-methylpropane (99%), cyclopentadienyl(fluorene)iron(II) hexafluorophosphate (98%), 4,4'-difluorobenzophenone (99%), 9-ethylcarbazole (97%), epichlorohydrin (99%), iron

(III) chloride (99.9%), 1-methylindole (97%), *o*-phthaldialdehyde (97%), *p*-toluenesulfonic acid monohydrate (98%), 2-phenylindole (95%), 2-phenylindole-3-carbaldehyde (97%), phosphorus (V) oxychloride ($POCl_3$) (99%), potassium *tert*-butoxide (99%), sodium borohydride (96%), sodium carbonate (99%), 1,2,3,4-tetrahydrocarbazole (99%), tetrabutylammonium hexafluorophosphate (98%), tetrabutylammonium perchlorate (98%), titanium tetrachloride, 4-vinylbenzyl chloride (90%), zinc (99.9%) (all the materials sourced from Aldrich), phenoxazine (97%) (purchased from Acros Organics), 3-bromomethyl-3-methyloxetane (95%), concentrated hydrochloric acid (36%), sodium sulphate (99%) (by Chemada Fine Chemicals), 2-methylpropyl iodide (97%) (produced by Fluka), 9*H*-carbazole (chemical grade) and $NaHCO_3$ (99.5%) (purchased from Reakhim) were used as received. Thin layer chromatography was performed by using TLC plates covered with a silica gel matrix on aluminum backing (purchased fromAldrich).

Alkylation procedure. The addition of reactive functional groups or alkyl chains was performed by using a procedure similar to that described elsewhere [195]. To a mechanically stirred mixture of the intermediate aromatic amine (1.125 mmol), either 1,2-bis(2-phenyl-1*H*-indol-3-yl)ethene (0.5 g), 2-phenyl-3-(2-phenyl-1H-indol-3-yl)-1H-indole (0.4 g), 3-((9*H*-carbazol-3-yl)(2-phenyl-1*H*-indol-3-yl)methyl)-9*H*-carbazole (0.25 g) or 11-(3-indolyl)benzo[b]carbazole (0.2 g), dimethyl sulphoxide (DMSO) (10 ml), potassium *tert*-butoxide (0.375 g, 3.375 mmol), BTMAC (0.01 mmol) and the respective aliphatic halide (4.5 mmol) were added. The resulting mixture was stirred at room temperature for 24 h under nitrogen atmosphere. The reaction was stopped by adding water and neutralized with 10% HCl (5 ml) to pH 6–7. The crude product was extracted with chloroform several times (50 ml×3). The chloroform solution was washed with water, dried with anhydrous sodium sulphate, filtered, and the solvent was subsequently evaporated.

Polymerization. Photopolymerization of monomers was performed by using an UV lamp *OmniCure® S2000* (manufactured by Lumen Dynamics). Thermally initiated cross-linking of the monomers was performed by using a *West 6100+* process and temperature controller. In both cases, the solution of a monomer containing 3 mol % of photoinitiator cyclopentadienyl(fluorene)iron(II)hexafluorophosphate or radical initiator azobisizobutyronitrile was drop-cast onto the surface of the ATR crystal of an *ATR-IR* spectrometer (by Vertex 70 Bruker), and the decrease of the intensity of a signal of the reactive functional group under exposure to the UV radiation source or temperature was monitored on IR spectra.

The polymerization of monomer **12** was carried out in the solution of dry dichloromethane **(**0.5 mol/l) under the argon blanket. After dissolving the monomer, initiator $BF_3{\cdot}(C_2H_5)_2O$ (0.15 mol/l) was added. The reaction was being carried out for 3 days and monitored by TLC (eluent: dichloromethane). The initiator was neutralised with $NH_{3\,(aq)}$, and the reaction product was precipitated in methanol. The precipitate was washed with methanol several times and dried. The molecular weights of the products of polymerisation were determined by gel chromatography by using the Waters SEC system with a *Waters 501* UV detector and polystyrene standards.

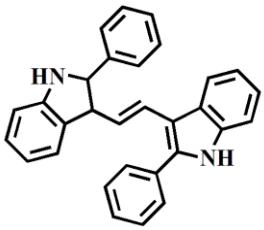

1,2-Bis(2-phenyl-1*H*-indol-3-yl)ethene was synthesized by employing the McMurry reaction according to the reported procedure [196]. Zinc (2.35 g, 36 mmol) was added to dry tetrahydrofuran (THF, 35 ml), and the mixture was cooled down to 0 °C. Titanium tetrachloride (2.17 ml, 19 mmol) was added dropwise, and then the reaction mixture was slowly brought to room temperature. 2-Phenylindole-3-carbaldehyde (4 g, 18 mmol) was added dropwise, and then the reaction mixture was refluxed for 1h. The reaction was monitored by TLC while using hexane:ethylacetate 1:1 as an eluent. The solution of sodium carbonate was poured in and stirred for 14 h. After the extraction with chloroform, the organic layer was washed with water, dried with anhydrous sodium sulphate and filtered. The solvent was evaporated, and the product was crystallized from methanol. The yield of greenish crystals was 75%. MW=412.0 g/mol. $C_{30}H_{24}N_2$. M.p. 167–168 ºC. ^{1}H NMR (400 MHz, $CDCl_3$) δ ppm 7.72 (s, 2H, N–H), 7.43 (d, 8H, Ar., *J*=8.9 Hz), 7.38–7.34 (m, 12H, Ar.), 6.93 (s, 2H). ^{13}C NMR (101 MHz, $CDCl_3$) δ ppm 135, 134, 133, 129, 128, 127, 122, 119, 113, 110, 26. MS: *m*/*z* 413 [$(M+H)^+$].

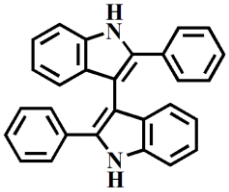

2-Phenyl-3-(2-phenyl-1*H*-indol-3-yl)-1*H*-indole was synthesized according to the described procedure [197].

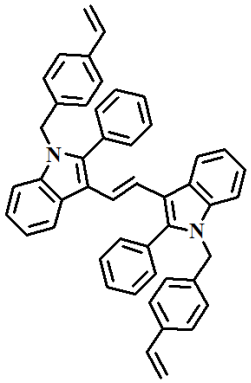

1

1,2-Bis(1-(4-vinylbenzyl)-2-phenylindol-3-yl)ethene (1) was obtained by employing the alkylation procedure while using 1,2-bis(2-phenyl-1H-indol-3-

yl)ethene as the starting compound. The product was purified by silica gel column chromatography using hexane as an eluent. The yield of yellow crystals was 59%. MW=558.62 g/mol. $C_{48}H_{38}N_2$. M.p. 201–203 °C. ^{1}H NMR (400 MHz, $CDCl_3$) δ ppm 7.43 (d, 8H, Ar., *J*=8.9 Hz), 7.31–7.25 (m, 10H, Ar.), 7.22–7.11 (m, 8H, Ar.), 6.95 (s, 2H, C<u>H</u>=C<u>H</u>), 6.73–6.64 (m, 2H, AMX system <u>CH</u>=CH_2 proton H^A), 5.72 (dd, 2H, AMX system –CH=<u>CH_2</u> proton H^M trans J_{AM}=5.75 Hz and gem J_{MX}=5.80 Hz), 5.27–5.22 (m, 2H, AMX system of –CH=<u>CH_2</u> proton H^X cis J_{AX}=14.1 Hz), 5.20 (s, 4H, C<u>H_2</u>). ^{13}C NMR (101 MHz, $CDCl_3$) δ ppm 137, 136, 130, 128, 126, 122, 120, 119, 113, 110, 47. ATR-IR (solid state on ATR, cm^{-1}): 3047 (*ν* C–H Ar), 2922, 2853 (*ν* C–H aliph.), 1463 (*ν* C=C Ar), 1366 (*ν* C–N Ar), 986, 899 (C–H of the vinyl group), 831, 735 (*γ* C–H Ar). MS: *m/z* 559 [$(M+H)^+$].

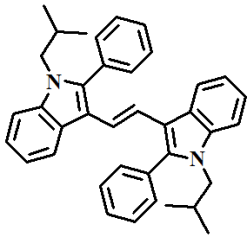

2

1,2-Bis(1-isopropyl-2-phenylindol-3-yl)ethene (2) was obtained by employing the alkylation procedure while using 1,2-bis(2-phenyl-1H-indol-3-yl)ethene as the starting compound. The product was purified by silica gel column chromatography using hexane as an eluent. The yield of a yellowish powder was 89%. MW=498.60 g/mol. $C_{36}H_{34}N_2$. ^{1}H NMR (400 MHz, $CDCl_3$) δ ppm 7.36–7.27 (m, 10H, Ar.), 7.19–7.13 (d, 8H, Ar. *J*=27.5 Hz), 6.97 (s, 2H, C<u>H</u>=C<u>H</u>), 4.66–4.39 (m, 2H, C<u>H</u>), 1.28 (s, 12H, C<u>H_3</u>). ^{13}C NMR (101 MHz, $CDCl_3$) δ ppm 139, 138, 137, 136, 130, 128, 126, 122, 113, 110, 47. ATR-IR (solid state on ATR, cm^{-1}): 3048 (*ν* C–H Ar), 2922, 2853 (*ν* C–H aliph.), 1493, 1462 (*ν* C=C Ar), 1363 (*ν* C–N Ar), 831, 807, 767 (*γ* C–H Ar). MS: *m/z* 522 [$(M+Na)^+$].

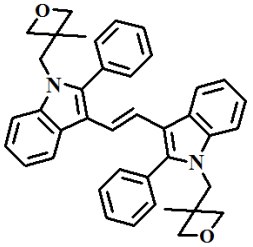

3

1,2-Bis(1-((3-methyloxetan-3-yl)methyl)-2-phenylindol-3-yl)ethene (3) was obtained by employing the alkylation procedure while using 1,2-bis(2-phenyl-1H-indol-3-yl)ethene as the starting compound. The product was purified by performing silica gel column chromatography using hexane as an eluent. The yield of yellow crystals was 97%. MW=512.57 g/mol. $C_{40}H_{38}N_2O_2$. M.p. 184–186 °C. ^{1}H NMR (400 MHz, $CDCl_3$) δ ppm 7.53–7.43 (m, 10H, Ar.), 7.36–7.25 (m, 8H, Ar.), 7.13 (s, 2H, C<u>H</u>=C<u>H</u>), 4.40 (s, 4H, <u>CH_2</u>), 4.15 (d, 4H, <u>CH_2</u>, *J*=6.0 Hz), 3.97 (d, 4H, <u>CH_2</u>, *J*=6.0 Hz), 1.28 (s, 6H, C<u>H_3</u>). ^{13}C NMR (101 MHz, $CDCl_3$) δ ppm 138, 131, 128, 125, 122, 121, 118, 114, 110, 81, 41, 22. ATR-IR (solid state on ATR, cm^{-1}): 3056 (*ν* C–H

Ar), 2923, 2853 (*ν* C–H aliph.), 1489, 1457 (*ν* C=C Ar), 1346 (*ν* C–N Ar), 1235, 1181 (*ν* C–O–C), 822, 759 (*γ* C–H Ar). MS: *m*/*z* 536 [(M+Na)$^+$].

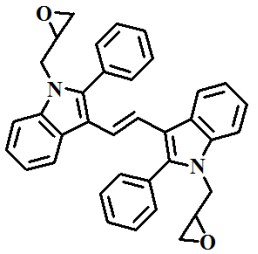

4

1,2-Bis(1-((oxiran-2-yl)methyl)-2-phenylindol-3-yl)ethene (4). A solution of 1,2-bis(2-phenyl-1*H*-indol-3-yl)ethene (0.2 g, 0.45 mmol), potassium *tert*-butoxide (0.52 g, 4.6 mmol) in epichlorohydrin (4 ml, 51 mmol) was stirred at 120 °C for 24 h under argon atmosphere. Then epichlorhydrin was removed by distillation. The product was purified by employing silica gel column chromatography using hexane as an eluent. The yield of yellow crystals was 42.5%. MW=498.52 g/mol. $C_{36}H_{30}N_2O_2$. M.p. 185–187 °C. ^{1}H NMR (400 MHz, $CDCl_3$) δ ppm 7.64–7.49 (m, 8H, Ar.), 7.38–7.33 (m, 10H, Ar.), 7.18 (s, 2H, C<u>H</u>=C<u>H</u>), 4.34–4.30 (m, 4H, <u>CH$_2$</u>), 4.28 (d, 4H, <u>CH$_2$</u>, *J* = 4.1 Hz), 3.20 (m, 1H, <u>CH</u>), 2.73 (t, 1H, <u>CH</u>, *J*=4.4 Hz). ^{13}C NMR (101 MHz, $CDCl_3$) δ ppm 138, 137, 131, 128, 125, 122, 121, 119, 114, 110, 45. ATR-IR (solid state on ATR, cm^{-1}): 3051 (*ν* C–H Ar), 2923, 2854 (*ν* C–H aliph.), 1460 (*ν* C=C Ar), 1362 (*ν* C–N Ar), 1226, 1195 (*ν* C–O–C), 840, 741 (*γ* C–H Ar). MS: *m*/*z* 522 [(M+Na)$^+$].

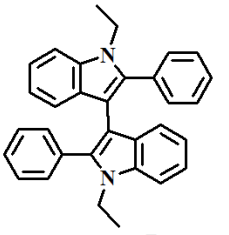

5

1-Ethyl-3-(1-ethyl-2-phenylindol-3-yl)-2-phenylindole (**5**) was obtained by employing the alkylation procedure while using 2-phenyl-3-(2-phenyl-1*H*-indol-3-yl)-1*H*-indole as the starting compound. The product was purified by performing silica gel column chromatography while using hexane as an eluent. The yield of greenish crystals was 31%. MW=440.58 g/mol. $C_{32}H_{28}N_2$. M.p. 143 °C. ^{1}H NMR (400 MHz, $CDCl_3$) δ ppm 7.61–7.42 (m, 10H, Ar.), 7.47–7.36 (m, 8H, Ar.) 4.26 (q, 4H, <u>CH$_2$</u>, *J*=7.2 Hz), 1.38 (t, 6H, C<u>H</u>$_3$, *J*=7.2 Hz). ^{13}C NMR (101 MHz, $CDCl_3$) δ ppm 137, 133, 130, 126, 125, 123, 117, 110, 38, 15. ATR-IR (solid state on ATR, cm^{-1}): 3049 (*ν* C–H Ar), 2989 (*ν* C–H aliph.), 1479, 1457, 1446 (*ν* C=C Ar), 1350 (*ν* C–N Ar), 847, 797 (*γ* C–H Ar). Elemental analysis for $C_{32}H_{28}N_2$. % Calc.: C 87.24%; H 6.41%; N 6.36%; % found: C 87.24%; H 6.41%; N 6.36%. MS: *m*/*z* 441 [(M+H)$^+$].

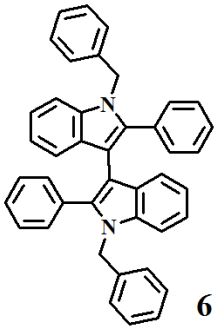

6

1-Benzyl-3-(1-benzyl-2-phenylindol-3-yl)-2-phenylindole (**6**) was obtained by employing the alkylation procedure while using 2-phenyl-3-(2-phenyl-1*H*-indol-3-yl)-1*H*-indole as the starting compound. The product was purified by performing silica gel column chromatography using hexane as an eluent. The yield of yellowish crystals was 71%. MW=564.72 g/mol. $C_{42}H_{32}N_2$. M.p. 132 °C. ^{1}H NMR (400 MHz, $CDCl_3$) δ ppm 7.71–7.62 (m, 4H, Ar.), 7.50–7.31 (m, 10H, Ar.), 7.30–7.11 (m, 10H, Ar.), 5.38 (s, 4H, $\underline{CH_2}$). ^{13}C NMR (101 MHz, $CDCl_3$) δ ppm 132, 127, 124, 122, 120, 110, 47. ATR-IR (solid state on ATR, cm^{-1}): 3049 (*ν* C–H Ar), 2924, 2854 (*ν* C–H aliph.), 1493, 1480, 1457, 1446 (*ν* C=C Ar), 1350 (*ν* C–N Ar), 848, 797 (*γ* C–H Ar). Elemental analysis for $C_{42}H_{32}N_2$. % Calc.: C 89.33%; H 5.71%; N 4.96%; % Found: C 89.33%; H 5.71%; N 4.96%. MS: *m*/*z* 565[$(M+H)^+$].

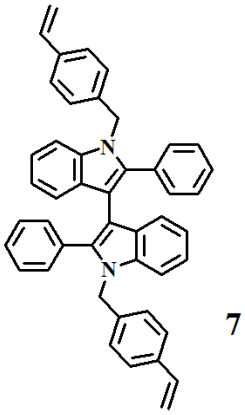

7

1-(4-Vinylbenzyl)-3-(1-(4-vinylbenzyl)-2-phenylindol-3-yl)-2-phenylindole (**7**) was obtained by employing the alkylation procedure while using 2-phenyl-3-(2-phenyl-1*H*-indol-3-yl)-1*H*-indole as the starting compound. The product was purified by performing silica gel column chromatography using hexane as an eluent. The yield of a greenish powder was 20%. MW=616.79 g/mol. $C_{46}H_{36}N_2$. ^{1}H NMR (400 MHz, $CDCl_3$) δ ppm 8.20–7.78 (m, 8H, Ar.), 7.47–7.32 (m, 10H, Ar.), 7.23–7.18 (m, 8H, Ar.), 6.72 (m, 2H, AMX system $\underline{CH}$=CH_2 proton H^A), 5.77 (d, 2H, AMX system –CH=$\underline{CH_2}$ proton H^M trans J_{AM}=5.75 Hz and gem J_{MX}=5.80 Hz), 5.28 (d, 2H, AMX system of –CH=$\underline{CH_2}$ proton H^X cis J_{AX}=10.6 Hz), 5.17 (d, 4H, $\underline{CH_2}$, *J*=13.1 Hz). ^{13}C NMR (101 MHz, $CDCl_3$) δ ppm 136, 134, 132, 128, 126, 121, 117, 112, 110, 49. ATR-IR (solid state on ATR, cm^{-1}): 3056 (*ν* C–H Ar), 2925, 2855 (*ν*

C–H aliph.), 1492, 1460, 1446 (*ν* C=C Ar), 1342 (*ν* C–N Ar), 988, 918, 896 (C–H of the vinyl group), 825, 765 (*γ* C–H Ar). Elemental analysis for $C_{46}H_{36}N_2$. % Calc.: C 89.58%; H 5.88%; N 4.54%; % Found: C 89.53%; H 5.83%; N 4.59%. MS: *m*/*z* 617 [M^+].

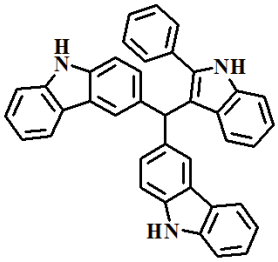

3-((9*H*-Carbazol-3-yl)(2-phenyl-1*H*-indol-3-yl)methyl)-9*H*-carbazole. To a mixture of 9*H*-carbazole (5 g, 30 mmol) and 2-phenylindole-3-carbaldehyde (3.3 g, 15 mmol) in chloroform (40mL), hydrochloric acid (conc., 5 ml) was added dropwise, and the reaction mixture was being stirred at room temperature for 8 h. Then, water (10 mL) was added to quench the reaction, and the mixture was stirred vigorously for an additional 10 min. The crude product was extracted with chloroform several times. The chloroform solution was washed with water, dried with anhydrous sodium sulphate, filtered, and the solvent was evaporated. The product was purified by performing silica gel column chromatography using hexane:ethylacetate (1:6) as an eluent. The yield of a reddish powder was 4.5 g (56%). MW=537 g/mol. $C_{39}H_{27}N_3$. ^{1}H NMR (400 MHz, $CDCl_3$) δ 8.34 (s, 3H, NH), 8.23–7.72 (m, 9H, Ar.), 7.60–7.48 (m, 14H, Ar.), 5.41 (s, 1H, Ar–CH). ^{13}C NMR (101 MHz, $CDCl_3$) δ 139, 126, 124, 119, 50.

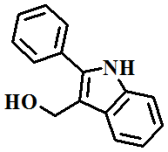

3-Hydroxymethyl-2-phenylindole was synthesized as described before[198].

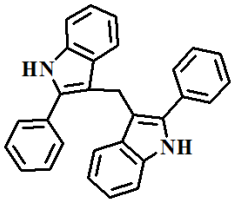

2-Phenyl-3-[(2-phenyl-1*H*-indol-3-yl)methyl]-1*H*-indole. To a mechanically stirred solution of 3-hydroxymethyl-2-phenylindole (1.3 g 5.8 mmol) and 2-phenylindole (1.12 g, 5.8 mmol) in dry dichloromethane (40 ml), boron trifluoride diethyl etherate (3.2 ml) was added dropwise, and the reaction mixture was stirred at room temperature for 3 h. The crude product was extracted with dichloromethane several times. The dichloromethane solution was washed with water, dried with anhydrous sodium sulphate, filtered, and the solvent was evaporated. The product was purified by performing silica gel column chromatography using

hexane:ethylacetate (1:9) as an eluent. The yield of a greenish powder was 1.1 g (62%). MW=398 g/mol. $C_{29}H_{22}N_2$. ^{1}H NMR (400 MHz, $CDCl_3$) δ 8.33 (s, 2H, NH), 8.00–7.74 (m, 18H, Ar.), 5.41 (s, 2H, Ar–CH). ^{13}C NMR (101 MHz, $CDCl_3$) δ 141, 137, 129, 127, 126, 123, 121, 119, 22.

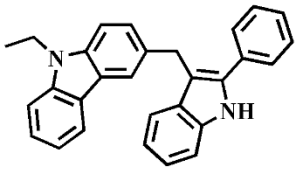

3-[(2-Phenyl-1*H*-indol-3-yl)methyl]-9*H*-carbazole. To a mechanically stirred solution of 3-hydroxymethyl-2-phenylindole (1.3 g 5.8 mmol) and 9-ethylcarbazole (1.5 g, 5.8 mmol) in dry dichloromethane (40 ml), boron trifluoride diethyl etherate (3.2 ml) was added dropwise, and the reaction mixture was stirred at room temperature for 3 h. The crude product was extracted with dichloromethane 3×50 ml. The dichloromethane solution was washed with water, dried with anhydrous sodium sulphate, filtered, and the solvent was evaporated. The product was purified by performing silica gel column chromatography while using hexane:ethylacetate (1:9) as an eluent. The yield of greenish powder was 1.3 g (58%). MW=400 g/mol. $C_{29}H_{24}N_2$. ^{1}H NMR (400 MHz, $CDCl_3$) δ 10.01 (s, 1H, NH), 8.00–7.74 (m, 9H), 7.43–7.15 (m, 7H), 5.69 (s, 2H, Ar–CH), 4.04 (q, 2H, *J*=7.1 Hz, CH_2), 1.32 (t, 3H, *J*=7.1 Hz, CH_3). ^{13}C NMR (101 MHz, CDCl3) δ 141, 137, 133, 128, 121, 118, 112, 111, 108, 37, 30, 14.

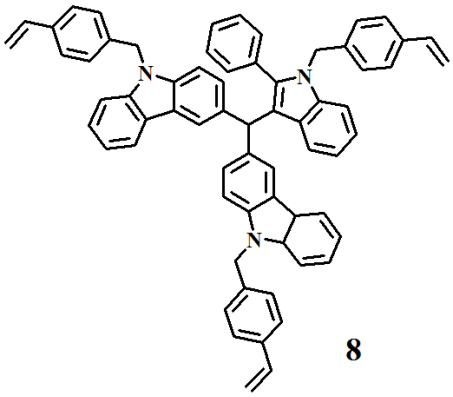

8

9-(4-vinylbenzyl)-3-((1-(4-vinylbenzyl)-2-phenyl-1H-indol-3-yl)(9-(4-vinylbenzyl)-9H-carbazol-3-yl)methyl)-9H-carbazole (**8**) was obtained by performing the alkylation procedure while using 3-((9*H*-carbazol-3-yl)(2-phenyl-1*H*-indol-3-yl)methyl)-9*H*-carbazole as the starting compound. The product was purified by performing silica gel column chromatography while using hexane as an eluent. The yield of a reddish powder was 0.86 g (75%). MW=886 g/mol. $C_{66}H_{51}N_3$. ^{1}H NMR (400 MHz, $CDCl_3$) δ 8.23–7.72 (m, 9H, Ar.), 7.60–7.48 (m, 14H, Ar.), 7.21–7.07 (m, 12H), 6.62 (m, 3H, AMX system CH=CH_2 proton H^A), 5.67 (dd, 3H, AMX system –CH=CH_2 proton H^M trans J_{AM}=5.75 Hz and gem J_{MX}=5.80 Hz), 5.41 (s, 1H, Ar–CH), 5.18 (d, 3H, AMX system of –CH=CH_2 proton H^X cis J_{AX}=11 Hz),

3.39 (s, 6H, C<u>H</u>$_2$). ^{13}C NMR (101 MHz, $CDCl_3$) δ 139, 125, 123, 119, 110, 50, 45. ATR-IR (solid state on ATR, cm^{-1}): 3050 (*ν* C–H Ar), 2919 (*ν* C–H aliph.), 1450 (*ν* C=C Ar), 1363 (*ν* C–N Ar), 995, 928 (C–H of vinyl group), 841, 820, 745 (*γ* C–H Ar). MS: *m*/*z* 886 [M$^+$].

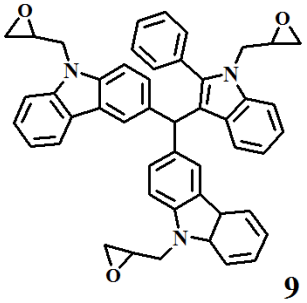

9

9-[(Oxiran-2-yl)methyl]-3-[[1-{(oxiran-2-yl)methyl}-2-phenyl-indol-3-yl][9-{(oxiran-2-yl)methyl}-carbazol-3-yl]methyl]-carbazole (**9**)**.** A solution of 3-[(9*H*-carbazol-3-yl)(2-phenyl-1*H*-indol-3-yl)methyl]-9*H*-carbazole (0.7 g, 1.3 mmol) potassium *tert*-butoxide (0.52 g, 4.6 mmol) in epichlorohydrin (4 ml, 51 mmol) was stirred at 120 °C for 24 h under argon atmosphere. Then, epichlorhydrin was removed by distillation. The obtained product was purified by performing silica gel column chromatography using hexane as an eluent. It was recrystallized from methanol. The yield of reddish crystals was 0.74 g (81%). M.p. 110 °C (DSC). MW=705 g/mol. $C_{48}H_{39}N_3O_3$. ^{1}H NMR (400 MHz, $CDCl_3$) δ 7.88 (d, 9H, *J*=7.8 Hz, Ar.), 7.28–7.22 (m, 7H, Ar.), 7.1–7.0 (m, 7H, Ar.), 5.07 (s, 1H, Ar–C<u>H</u>), 4.40 (dd, 6H, *J*=15.8, *J*=3.4 Hz, C<u>H</u>$_2$), 4.18 (dd, 4H, *J*=15.8, *J*=8.1 Hz, C<u>H</u>$_2$), 3.12 (d, 2H, *J*=6.4Hz, C<u>H</u>$_2$), 2.57 (t, 3H, *J*=4.1 Hz, C<u>H</u>).^{13}C NMR (101 MHz, $CDCl_3$) δ 140, 125, 123, 119, 109, 50, 45. ATR-IR (solid state on ATR, cm^{-1}): 3052 (*ν* C–H Ar), 2920 (*ν* C–H aliph.), 1453 (*ν* C=C Ar), 1351 (*ν* C–N Ar), 1220 (*ν* C–O–C), 841, 779 (*γ* C–H Ar). MS: *m*/*z* 706 [(M+H)$^+$].

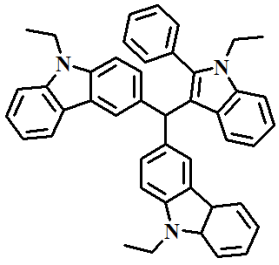

10

9-Ethyl-3-[(1-ethyl-2-phenyl-1H-indol-3-yl)(9-ethyl-9H-carbazol-3-yl)methyl]-9H-carbazole (**10**) was obtained by performing the alkylation procedure while using 3-((9*H*-carbazol-3-yl)(2-phenyl-1*H*-indol-3-yl)methyl)-9*H*-carbazole as the starting compound. The product was purified by performing silica gel column chromatography while using hexane as an eluent. The yield of a reddish powder was 0.53 g (66%). MW=621 g/mol. $C_{45}H_{39}N_3$. ^{1}H NMR (400 MHz, $CDCl_3$) δ 7.89 (d, 9H, *J*=7.8 Hz, Ar.), 7.38–7.29 (m, 7H, Ar.), 7.2–7.11 (m, 7H, Ar.), 5.20 (s, 1H, Ar–

C<u>H</u>), 4.02 (q, 6H, *J*=7.3 Hz, C<u>H</u>$_2$), 1.32 (t, 9H, *J*=7.1 Hz, C<u>H</u>$_3$). ^{13}C NMR (101 MHz, $CDCl_3$) δ 139, 125, 123, 119, 110, 50, 45. ATR-IR (solid state on ATR, cm^{-1}): 3052 (*ν* C–H Ar), 2925 (*ν* C–H aliph.), 1492, 1450 (*ν* C=C Ar), 1358 (*ν* C–N Ar), 842, 745 (*γ* C–H Ar). MS: *m*/*z* 635 [(M+Na)$^+$].

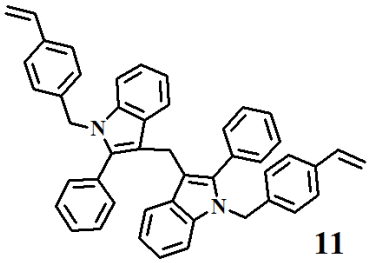

11

1-(4-Vinylbenzyl)-3-{[1-(4-vinylbenzyl)-2-phenyl-1H-indol-3-yl]methyl}-2-phenyl-1H-indole (**11**) was obtained by employing the alkylation procedure while using 2-phenyl-3-[(2-phenyl-1*H*-indol-3-yl)methyl]-1*H*-indole as the starting compound. The product was purified by performing silica gel column chromatography using hexane as an eluent. The yield of greenish crystals was 1.7 g (74%). MW=632 g/mol. $C_{47}H_{40}N_2$. M.p. 120 ºC (DSC). ^{1}H NMR (400 MHz, $CDCl_3$) δ 8.05 (d, 8H, *J*=7.8, Ar.), 8.00–7.74 (m, 18H, Ar.), 6.62 (m, 2H, AMX system C<u>H</u>=CH$_2$ proton H^A), 5.61 (dd, 2H AMX system –CH=C<u>H</u>$_2$ proton H^M trans J_{AM}=16.2 Hz and gem J_{MX}=8.40), 5.41 (s, 2H, Ar–C<u>H</u>), 5.26 (d, 2H, AMX system of –CH=C<u>H</u>$_2$ proton H^X cis J_{AX}=12.7 Hz), 5.14–5.07 (m, 2H, AMX system of –CH=C<u>H</u>$_2$ proton H^X), 3.38 (s, 4H, C<u>H</u>$_2$). ^{13}C NMR (101 MHz, $CDCl_3$) δ 140, 137, 128, 127, 125, 123, 121, 116, 46, 41, 23. ATR-IR (solid state on ATR, cm^{-1}): 3052 (*ν* C–H Ar), 2927 (*ν* C–H aliph.), 1485, 1450 (*ν* C=C Ar), 1381 (*ν* C–N Ar), 994, 969, 927 (C–H of the vinyl group), 842, 785, 746 (*γ* C–H Ar). MS: *m*/*z* 633 [(M+H)$^+$].

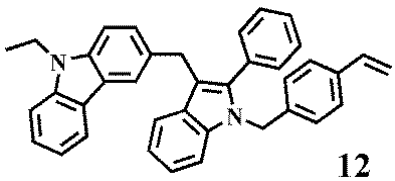

12

3-{[1-(4-Vinylbenzyl)-2-phenyl-1H-indol-3-yl]methyl}-9-ethyl-9H-carbazole (**12**) was obtained by employing the alkylation procedure while using 3-[(2-phenyl-1*H*-indol-3-yl)methyl]-9*H*-carbazole as the starting compound. The product was purified by performing silica gel column chromatography using hexane as an eluent. The yield of a greenish powder was 1.7 g (68%). MW=516 g/mol. $C_{38}H_{32}N_2$. ^{1}H NMR (400 MHz, $CDCl_3$) δ 8.13–8.01 (m, 2H), 8.00–7.74 (m, 9H), 7.43–7.15 (m, 7H), 6.69–6.51 (m, 1H, AMX system C<u>H</u>=CH$_2$ proton H^A), 5.69 (s, 2H, Ar–C<u>H</u>), 5.66–5.54 (m, 1H, AMX system of –CH=C<u>H</u>$_2$ proton H^X cis), 5.22–5.05 (m, 1H, AMX system of –CH=C<u>H</u>$_2$ proton H^X), 4.04 (q, 2H, *J*=7.1 Hz, C<u>H</u>$_2$), 3.40 (s, 2H), 1.32 (t, 3H, *J*=7.1 Hz, C<u>H</u>$_3$). ^{13}C NMR (101 MHz, $CDCl_3$) δ 141, 137, 130, 129, 125, 121, 120, 116, 111, 38, 22. ATR-IR (solid state on ATR, cm^{-1}): 3052 (*ν* C–H Ar),

2925 (*ν* C–H aliph.), 1480, 1452 (*ν* C=C Ar), 1359 (*ν* C–N Ar), 993, 969, 926 (C–H of the vinyl group), 842, 745 (*γ* C–H Ar). MS: *m*/*z* 540 [$(M+Na)^+$].

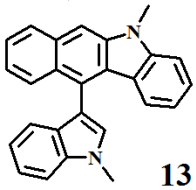

13

11-(1-Methyl-1*H*-indol-3-yl)-5-methyl-5*H*-benzo[b]carbazole (**13**). To a mechanically stirred solution of phthaldialdehyde (0.100 g, 0.746 mmol) and 1-methylindole (1.49 ml, 0.195 mmol) in chloroform (3ml), $POCl_3$ (0.069 ml, 0.746 mmol) was added drop-by-drop. The resulting solution was stirred at room temperature for 35 min and then quenched with saturated $NaHCO_3$ solution. The crude product was extracted with dichloromethane, filtered, and the solvent was evaporated. The product was purified by performing silica gel column chromatography using ethylacetate:hexane mixture (1:4) as an eluent. The obtained product was recrystallized from dichloromethane/methanol. The yield of yellowish crystals was 0.117 g (44%). MW=360.16 g/mol. $C_{26}H_{20}N_2$. M.p. 241 °C (DSC). ^{1}H NMR (400 MHz, $CDCl_3$) δ 8.05 (d, *J*=8.3 Hz, 1H), 7.97 (d, *J*=8.6 Hz, 1H), 7.75 (s, 1H), 7.56 (s, 1H), 7.54 (s, 1H), 7.49 (t, Ar., 1H), 7.40 (t, Ar., 1H), 7.34 (t, Ar., 3H), 7.18 (m, Ar., 1H), 7.08 (m, Ar., 1H), 7.02 (t, Ar., 1H), 6.84 (t, Ar., 1H), 4.01 (s, –C<u>H</u>$_3$, 3H), 3.91 (s, –C<u>H</u>$_3$, 3H). ^{13}C NMR (101 MHz, $CDCl_3$) δ 144, 141, 136, 132, 127, 126, 124, 123, 121, 119, 111, 109, 107, 102, 33, 28. ATR-IR (solid state on ATR, cm^{-1}): 3051 (Ar. C–H), 2925 (Alk. C–H), 1625, 1600, 1470, 1433 (Ar. C=C), 869, 829 (Alk. C–H). MS: *m*/*z* 361 [M^+].

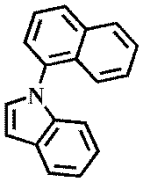

1-Naphthylindole was synthesized as described before [199].

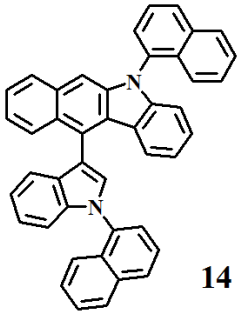

14

1-(1-(Naphthalen-1-yl)-1H-indol-3-yl)-5-(naphthalen-1-yl)-5H-benzo[b]carbazole (**14**). To a mechanically stirred solution of 1-naphthylindole

(0.520 g, 2.2 mmol) and *o*-phthaldialdehyde (0.143 g, 1.1 mmol) in chloroform (3ml), $POCl_3$ (0.097 ml, 1.06 mmol) was added drop-by-drop. The resulting solution was stirred at room temperature for 40 min and then quenched with saturated $NaHCO_3$ solution. The crude product was extracted with dichloromethane, filtered, and the solvent was evaporated. The obtained product was purified by performing silica gel column chromatography using ethylacetate:hexane mixture (1:4) as an eluent. The yield of a yellowish powder was 0.372 g (60%). MW=584.23 g/mol. $C_{44}H_{28}N_2$. ^{1}H NMR (400 MHz, $CDCl_3$) δ 8.24–8.03 (m, 5H), 8.02–7.94 (m, 1H), 7.89–7.79 (m, 3H), 7.79–7.66 (m, 3H), 7.64–7.51 (m, Ar., 4H), 7.50–7.39 (m, Ar., 4H), 7.37–7.26 (m, Ar., 4H), 7.22–7.13 (m, Ar., 2H), 7.04–6.94 (m, Ar., 2H). ^{13}C NMR (101 MHz, $CDCl_3$) δ 138, 134, 132, 131, 130, 128, 126, 125, 124, 123, 120, 119, 110, 109, 104. ATR-IR (solid state on ATR, cm^{-1}): 3051 (Ar. C–H), 1566, 1467, 1412 (Ar. C=C), 862, 834 (Alk. C–H). MS: *m*/*z* 585 [M^+].

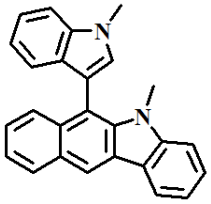

15

5-Methyl-6-(1-methyl-1H-indol-3-yl)-5H-benzo[b]carbazole (15). To a mechanically stirred solution of 1-methylindole (0.78 ml, 5.96 mmol) and *o*-phthaldialdehyde (0.4 g, 2.9 mmol) in methanol (10 ml), *p*-toluenesulfonic acid monohydrate (0.552 g, 2.9 mmol) was added. The product precipitated from the reaction mixture after stirring at room temperature for 15 min. The product was purified by performing silica gel column chromatography using ethylacetate:hexane mixture (1:4) as an eluent. The yield of yellowish-white crystals was 0.804 g (77%). MW=360.16 g/mol. $C_{26}H_{20}N_2$. M.p. 241 °C (DSC).^{1}H NMR (400 MHz, $CDCl_3$) δ 8.71 (s, Ar., 1H), 8.33 (d, *J*=7.6 Hz, Ar., 1H), 8.15 (d, *J*=7.8 Hz, 1H), 7.83 (d, *J*=8.6 Hz, Ar., 1H), 7.56 (d, *J*=8.6 Hz, Ar., 2H), 7.48–7.27 (m, Ar., 7H), 7.12 (dd, *J*=14.5, 6.8 Hz, Ar., 1H), 4.04 (s, –C<u>H</u>$_3$, 3H), 3.34 (s, –C<u>H</u>$_3$, 3H). ^{13}C NMR (101 MHz, $CDCl_3$) δ 144, 140, 136, 133, 130, 129, 128, 127, 125, 124, 123, 122, 120, 119, 118, 111, 110, 109, 108, 33, 31. ATR-IR (solid state on ATR , cm^{-1}): 3052 (Ar. C–H), 2923 (Alk. C–H), 1602, 1541, 1476, 1435 (Ar. C=C), 884, 860 (Alk. C-H). MS: *m*/*z* 361 [M^+].

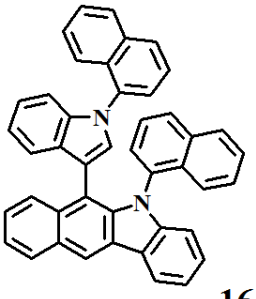

16

5-(Naphthalen-1-yl)-6-(1-(naphthalen-1-yl)-1H-indol-3-yl)-5H-benzo[b]carbazole (16). To a mechanically stirred solution of 1-naphthylindole (0.204 g, 0.838 mmol) and *o*-phthaldialdehyde (0.056 g, 0.419 mmol) in methanol (4 ml), *p*-toluenesulfonic acid monohydrate (0.0079 g, 0.042 mmol) was added. The product precipitated from the reaction mixture after stirring at room temperature for 24 h. The product was purified by performing silica gel column chromatography using ethylacetate:hexane mixture (1:4) as an eluent. The yield of a yellowish-white solid was 0.101 g (70%). MW=584.42 g/mol. $C_{25}H_{17}N_2$. ^{1}H NMR (400 MHz, $CDCl_3$) δ 8.21 (d, *J*=8.0 Hz, Ar., 1H), 8.05 (d, *J*=8.4 Hz, Ar., 1H), 7.87 (d, *J*=8.3 Hz, Ar., 1H), 7.84 (d, *J*=8.5 Hz, Ar., 1H), 7.59 (m, Ar., 2H), 7.50–7.27 (m, Ar., 6H), 7.10–7.03 (m, Ar., 1H), 6.99 (d, *J*=7.3 Hz, Ar., 1H), 6.77 (d, *J*=8.9 Hz, 1H), 6.70 (m, Ar., 1H), 6.67 (m, Ar., 1H). ^{13}C NMR (101 MHz, $CDCl_3$) δ 129, 128, 127, 127, 124, 123, 122, 120, 119, 118, 110, 110. ATR-IR (solid state on ATR, cm^{-1}): 3051 (Ar. C–H), 1596, 1467, 1439 (Ar. C=C), 881, 800 (Alk. C–H). MS: *m*/*z* 585 [M^+].

The general procedure was used for the synthesis of the following compounds **18**–**22**. 4,4'-Difluorobenzophenone (1.1 mmol) and an N-heterocyclic compound (1,2,3,4-tetrahydrocarbazole, 2-phenylindole, 3,6-di-(*tert*-butyl)-9H-carbazole, phenoxazine or 3-(4-vinylbenzyl)-2-phenyl-1H-indole (2.2 mmol) were dissolved in DMSO (8 mL). Potassium *tert*-butoxide (11 mmol) was added to the solution while vigorously stirring. The suspension mixture was stirred at room temperature for 24 h under nitrogen atmosphere. The mixture was poured into ice–water (60 mL) and filtered. The obtained crude product was purified by performing column chromatography on silica using ethylacetate:n–hexane mixture (1:3) as an eluent.

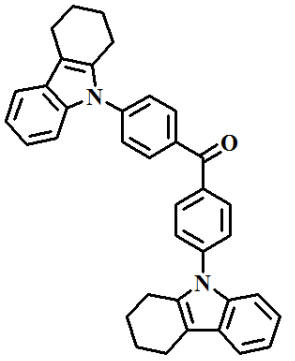

17

Bis[4-(1,2,3,4-tetrahydrocarbazol-9-yl)phenyl]methanone (17). The yield of yellowish crystals was 0.103 g (66%). MW=520 g/mol. $C_{37}H_{32}N_2O$. M.p. 168–169 ^{o}C. ^{1}H NMR (400 MHz, $CDCl_3$) δ 8.05 (s, 4H), 7.56 (s, 6H), 7.41 (s, 2H), 7.16 (s, 4H), 2.85 (s, 4H), 2.69 (s, 4H), 1.95 (s, 8H). ^{13}C NMR (101 MHz, CDCl3) δ 194, 144, 136, 135, 132, 130, 128, 126, 121, 119, 117, 109, 31, 23, 21. ATR-IR (solid

state on ATR, cm^{-1}): 3048 (Ar. C–H), 2927 (Alk. C–H), 1569 (Ar. C=O) 1230 (Alk. C–N), 827 (Alk. C–H). MS: m/z 521 [$(M+H)^+$].

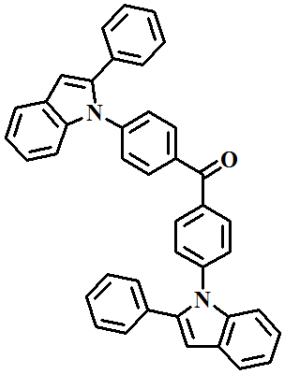

18

Bis[4-(2-phenyl-1H-indol-1-yl)phenyl]methanone (18). The yield of yellowish crystals was 0.173 g (68%). MW=564 g/mol. $C_{41}H_{28}N_2O$. M.p. 155–156 °C. ^{1}H NMR (400 MHz, CDCl3) δ 7.70–7.62 (m, 8H), 7.45 (s, 4H), 7.33 (t, J=7.4 Hz, 4H), 7.21 (d, J=7.1 Hz, 4H), 7.13 (t, J=7.4 Hz, 4H), 6.84 (s, 4H). ^{13}C NMR (101 MHz, CDCl3) δ 194, 137, 136, 132, 129, 127, 125, 122, 120, 110, 99, 77, 28. ATR-IR (solid state on ATR, cm^{-1}): 3048 (Ar. C–H), 2923 (Alk. C–H), 1598 (Ar. C=O) 1238 (Alk. C–N), 833 (Alk. C–H). MS: m/z 565 [$(M+H)^+$].

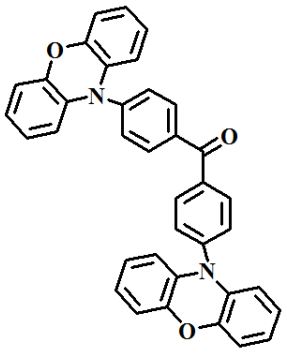

19

Bis[4-(10H-phenoxazin-10-yl)phenyl]methanone (19). [200] The yield of orange crystals was 0.074 g (37%). MW=544 g/mol. $C_{37}H_{24}N_2O_3$. M.p. 248–249 °C.^{1}H NMR (400 MHz, $CDCl_3$) δ 8.08 (d, *J*=8.4 Hz, 4H), 7.51 (t, *J*=8.6 Hz, 4H), 6.74–6.63 (m, 8H), 6.61 (td, *J*=7.6, 1.8 Hz, 4H), 5.99 (dt, *J*=10.9, 5.4 Hz, 4H). ^{13}C NMR (101 MHz, $CDCl_3$) δ 144, 143, 136, 133, 132, 130, 129, 128, 125, 123, 115, 113. ATR-IR (solid state on ATR, cm^{-1}): 3048 (Ar. C–H), 2970 (Alk. C–H), 1738 (Ar. C=O) 1290 (Alk. C–N),1268, 1044 (Alk. C–O), 833 (Alk. C–H). MS: m/z 544 [M^+].

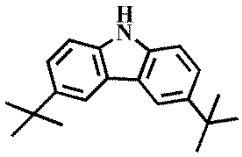

3,6-Di-(*tert*-butyl)-9H-carbazole was synthesized as described before [99].

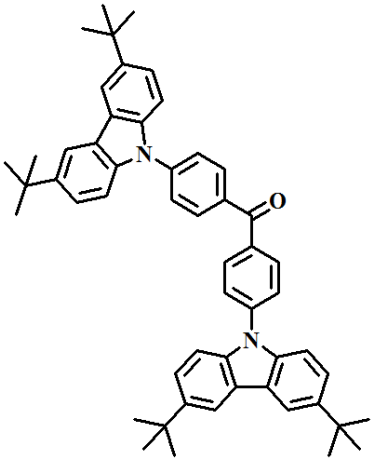

20

Bis[4-(3,6-di-*tert*-butyl-9H-carbazol-9-yl)phenyl]methanone (20). [201] The yield of yellowish crystals was 0.132 g (43%). MW=722 g/mol. $C_{53}H_{56}N_2O$. M.p.>270 °C. ^{1}H NMR (400 MHz, $CDCl_3$) δ 8.12 (d, *J*=7.7 Hz, 8H), 7.76 (d, *J*=8.4 Hz, 4H), 7.48 (d, *J*=0.8 Hz, 8H), 1.46 (s, 36H).^{13}C NMR (101 MHz, CDCl3) δ 193, 143, 142, 137, 131, 125, 123, 116, 109, 34, 31. ATR-IR (solid state on ATR, cm^{-1}): 3048 (Ar. C–H), 2955 (Alk. C–H), 1679 (Ar. C=O) 1291 (Alk. C–N), 843 (Alk. C–H). MS: m/z 723 [M+].

4. Results and Discussion

4.1. 2-Phenylindole Twin Compounds

4.1.1. Design and Synthesis

The aim of this research was the synthesis of a series of new 2-phenylindole twin compounds containing reactive functional groups with the direct and double C–C bond containing linkages between the aromatic moieties. The influence of the linking topology of the chromophores on the thermal, optical, photophysical and photoelectrical properties of the materials was explored.

The synthetic routes to the twin derivatives of 2-phenylindole are shown in Scheme 4.1. In the first step, 2-phenylindole-3-carbaldehyde was condensed via McMurry reaction so that to obtain the intermediate 1,2-bis(2-phenyl-*1H*-indol-3-yl)ethene. $TiCl_4$ and Zn were used as catalysts in this reaction. The resulting precursor compound was obtained after the crystallization in good yield (75%).

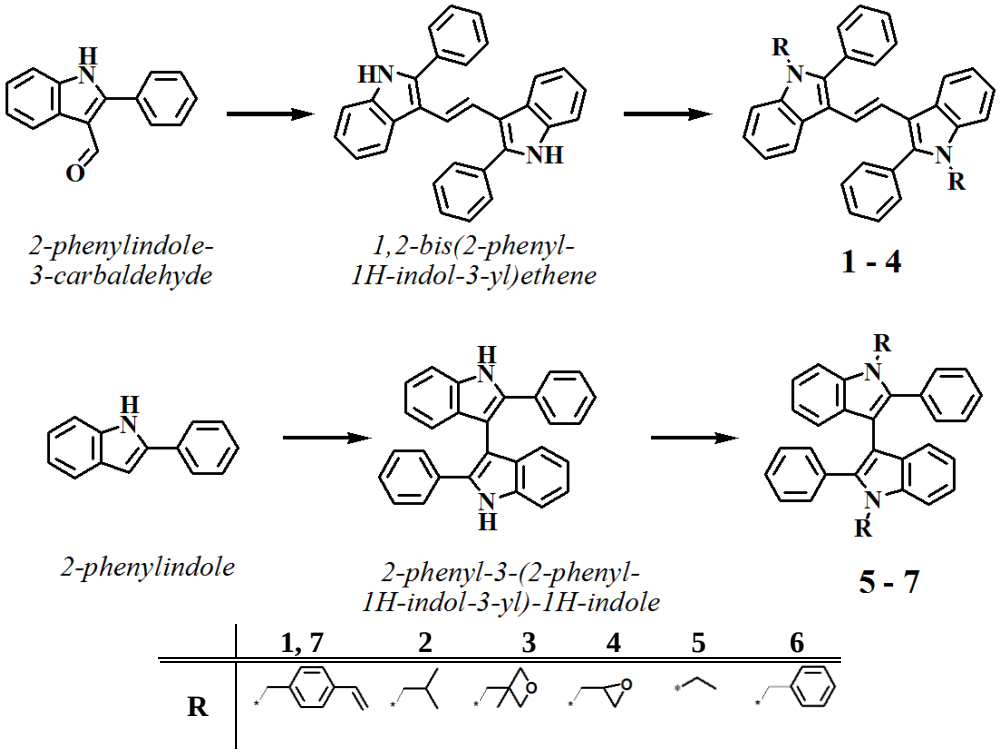

Scheme 4.1. Synthesis of 2-phenylindole derivatives

The other intermediate compound, 2-phenyl-3-(2-phenyl-1*H*-indol-3-yl)-1*H*-indole was prepared by the oxidative coupling of 2-phenylindole while using $FeCl_3$. This mild and selective method gave the yield of the precursor of 55%.

The last step in the synthesis of the target compounds was the introduction of the reactive functional groups, and, for the comparison of the properties, alkyl chains or benzyl groups by the interaction of the intermediate products with the

corresponding alkyl halides in the presence of potassium *tert*-butoxide. All the target compounds were isolated and purified by performing column chromatography and characterized by using NMR, IR and MS. The synthesized compounds are soluble in common organic solvents.

4.1.2. Thermal Properties and Polymerization

The thermal transitions and thermal stability of materials **1**–**7** were studied by performing DSC and TGA. The thermal characteristics are outlined in Table 4.1.

Table 4.1. Thermal characteristics of the twin derivatives of 2-phenylindole derivatives **1**–**7**

Compound	T_M, °C	T_G, °C	T_{CR}, °C	$T_{D\text{-}5\,\%}$, °C
1	181	-[a]	-	215[b]
2	-	95	-	245
3	191	68	-	214
4	187	44	-	228
5	75	-	-	252
6	156	-	133	207
7	-	120	-	220[b]

T_M – the melting point observed at the first heating scan of the DSC measurement; T_G – the glass transition temperature from the second DSC heating scan; T_{CR} – the crystallization temperature; $T_{D\text{-}5\%}$ – the 5% weight loss temperature obtained from TGA curves; [a] – not detected; [b] – the weight loss temperature of the products of thermal polymerization during the TGA measurement

Compounds **1, 3**–**6** were obtained as crystalline substances after crystallization from a solution whereas compounds **2** and **7** were obtained as amorphous materials. The crystalline nature of the materials was confirmed by DSC measurements. Such well-defined melting signals as sharp single endothermic peaks appeared in the curves of the first heating scans for the samples of **1, 3**–**6**. The difference between the T_M of the double-bonded (**1**, **3** and **4**) and single-bonded (**5**–**6**) compounds can be explained by the different molecular flexibility. The chromophores of the latter compounds can easily rotate as they are directly linked whereas the 2-phenylindole fragments in compounds **1**, **3** and **4** are linked via a double bond, and the molecules are almost fixed in planar conformations; thus they can hardly change their shapes.

During the cooling scans of DSC, the ability of glass-formation was confirmed for diindolylethenes **2**–**4** and for compound **7.** Their T_G ranged from 44 to 120 °C. The highest glass transition temperature was detected for the derivative with the vinylbenzyl group (**7**). It can be assumed that the incorporation of the relatively bulky vinylbenzyl group decreased the flexibility of the molecule. Compound **6** crystallized on cooling instead of forming molecular glass.

DSC thermograms of compound **1** are shown in Figure 4.1. Compound **1** containing two vinylbenzyl groups showed an exothermic signal after the melting signal in the first heating scan. This signal can be assigned to the self-polymerization [202] which starts at 180 °C. No glass-transition was observed for the product of polymerisation during the subsequent cooling and heating scans.

ATR-FTIR monitoring (Figure 4.1. b) of the polymerization process of monomer **1** revealed the decrease of the intensity of the signals of vinyl groups at 990–900 cm^{-1} in the IR spectra in the process of thermal curing. It can thus be stated that the cross-linked structure of compound **1** was formed [203].

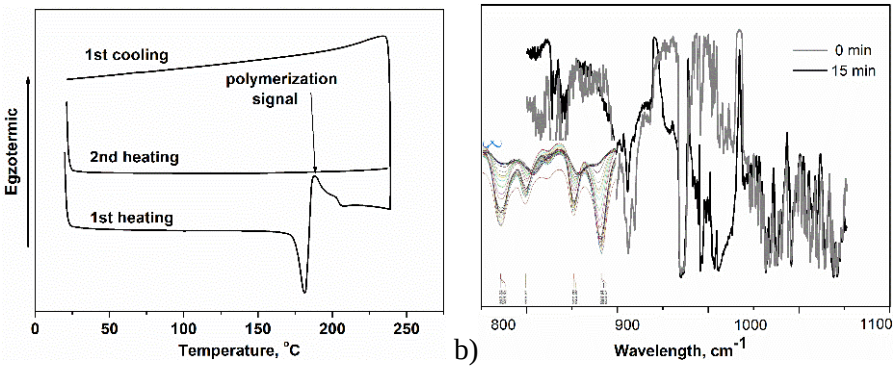

Figure 4.1. a) DSC thermograms of compound **1**; b) IR spectra of compound **1** recorded during thermal curing

Compounds **2**–**6** exhibited moderate thermal stability under nitrogen atmosphere with 5% weight loss temperatures reaching 252 °C. The highest thermal stability was observed for the alkyl-substituted derivatives **2** and **5.** Derivatives **1** and **7** may have undergone thermal polymerisation during TGA measurements. The values of 5% weight loss temperatures can be assigned to their products of polymerization. The temperatures of the onset of thermal degradation of all the compounds are rather similar; therefore, it can be assumed that the origin of the linkage between 2-phenylindole moieties and the nature of the substituents at N-1 position of the indole moiety do not have any significant impact on the thermal stability of the derivatives of 2-phenylindole.

4.1.3. *Computational Studies and Optical Properties*

Quantum chemical calculations were performed for compounds **1**–**7** by using DFT/B3LYP/ 6-31 (d, p) method. The theoretical ground state geometries of twin derivatives **1**–**7** showed that 2-phenylindole moieties of the central backbone are flip-sided and not planar (Fig. 4.2). The dihedral angle of the indole moiety is slightly twisted (~15°) in respect of the double bond linkage of compounds **1**–**4**. In the case of **5**–**7**, the main backbone is further rotated, and the dihedral angle between mirrored 2-phenylindole fragments is much higher (~60°). The attached phenyl rings are nearly perpendicular to the indole moieties, and the dihedral angles exceed 65°.

HOMO are localized on the indole moieties in all the compounds (**1**–**7**). LUMO are mostly localized on the phenyl rings with a small delocalization on the

indole moiety for compounds **2**–**6**. The orbitals of the LUMO of derivatives **1** and **7** are mainly localized on the vinylbenzyl fragments [204].

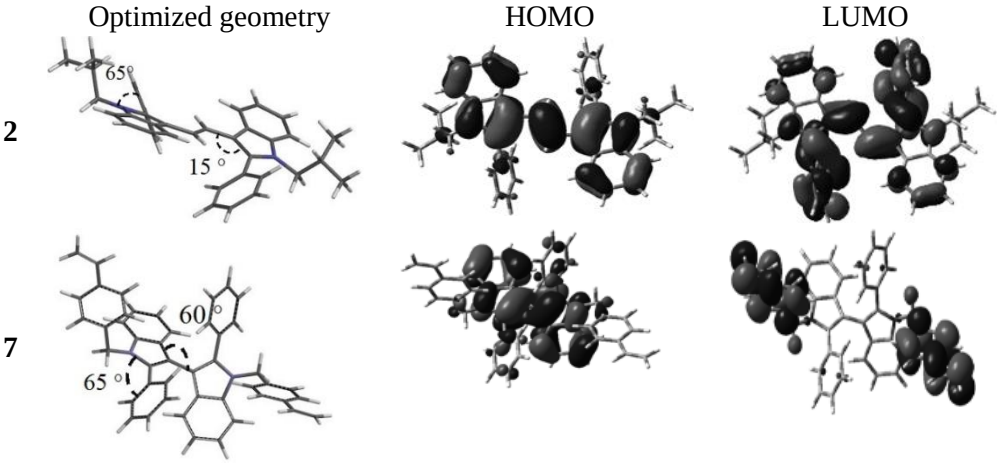

Figure 4.2. Optimized geometries and molecular orbital plots of compounds **2** and **7**

To get more insight into the nature of the absorption bands of **1**–**7**, TD-DFT calculations were performed. The lowest energy bands, the oscillator strengths and the molecular orbital contributions of the transitions from the ground state to the excited states of molecules **1**–**7** are presented in Table 4.2. Theoretical and experimental UV-VIS spectra are shown in Figure 4.3. The absorption spectra of the dilute THF solutions (10^{-4} M) were recorded at ambient conditions.

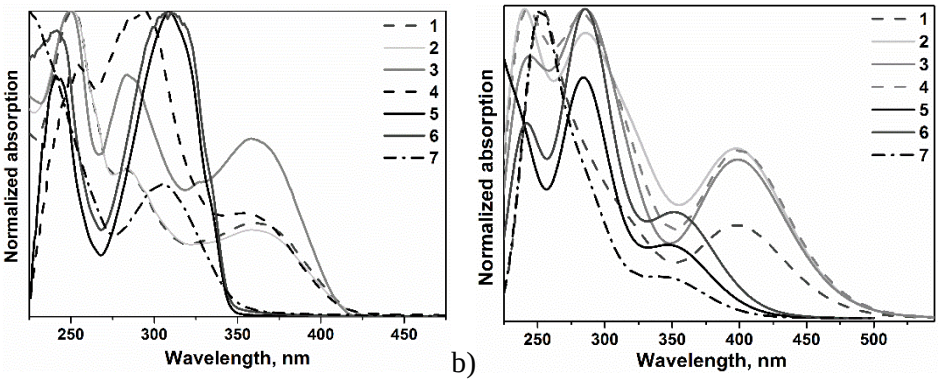

Figure 4.3. a) Experimental (10^{-4} M THF solutions) and b) theoretical UV-VIS spectra of compounds **1**–**7**

The nature of the theoretical and experimental absorption bands of compounds **1**–**4** is identical. However, two absorption bands overlap in the experimental spectra of compounds **5**–**7**. The lowest energy bands are characterized by small oscillator strengths, and they are hidden under more intensive absorption bands.

The lowest energy bands of the experimental UV spectra of compounds **1**–**4** are batochromically shifted in comparison with the ones of compounds **5**–**7**. This could be explained by the larger conjugation systems of molecules **1**–**4** resulting in

lower energy band gap values. The band gap values for compounds **1**–**4** are 2.84–2.86 eV whereas those for compounds **5**–**7** are 3.43–3.48 eV. The experimental lowest energy bands of the twin derivatives of 2-phenylindole **1**–**4** are influenced by transition S0→S1 with the maxima of absorption at ~360 nm. Transition S0→S1 corresponds to the transition from HOMO to LUMO for these compounds. In the case of compounds **5**–**7**, the experimental lowest energy bands at ca. 307 nm can be characterized as a combination of various transitions towards several excited states.

Table 4.2. Properties of the selected transitions and their contribution to UV-VIS spectra of compounds **1**–**7** calculated at the B3LYP/6-31G (d, p) level

Compound	Exp UV λ_{max}, nm	Calc UV λ_{max}, nm	Electronic Transition	Osc. strength, a.u	Contribution (%)
1	361	400	S0→S1	0.3656	H→L (60 %)
2	360	400	S0→S1	0.3128	H→L (95 %)
3	359	400	S0→S1	0.3218	H→L (97 %)
4	357	401	S0→S1	0.3130	H→L (96 %)
5	309	353 284	S0→S1 S0→S8	0.1311 0.3599	H→L (97 %) H-2→L (38 %) H-1→L+1 (48 %)
6	307	356 284	S0→S1 S0→S12	0.1800 0.3938	H→L (97 %) H-2→L (57 %) H-1→L+1 (29 %)
7	305	353 347 283	S0→S1 S0→S3 S0→S15	0.0635 0.0714 0.3149	H→L (79 %) H→L+2 (19 %) H→L (19 %) H→L+2 (78 %) H-2→L+2 (56 %) H-1→L+3 (20 %)

4.1.4. Luminescence Properties

Photoluminescence spectra of the dilute THF solutions (10^{-4} M) and of thin films were recorded at ambient conditions. The phosphorescence spectra of the dilute THF solutions were recorded at 77 °K. Luminescence was excited with the 325 nm wavelength. Figure 4.4 depicts the fluorescence spectra of the dilute THF solutions and of thin films of compounds **2** and **6** representing two different families of the twin derivatives of 2-phenylindole. The photophysical characteristics of compounds **1**–**7** are presented in Table 4.3.

The fluorescence spectra of the solutions of compounds are characterised by a single vibrational peak at ~ 460 nm. All the excited states involved in the absorption bands would relax and participate in the observed emission. The Stokes shift determines the difference between the lowest energy absorption maxima λ_{Abs} and the emission maxima λ_{PL}. Since λ_{PL} is in the same position, the Stokes shifts are determined by the positions of the lowest energy absorption maxima. The increase of the Stokes shift values of compounds **5**–**7** indicates that the latter compounds are

affected much more by the geometrical relaxation during electronic transitions as they are denoted by higher molecular flexibility.

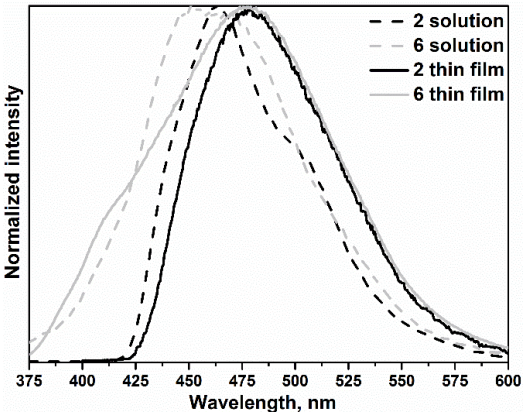

Figure 4.4. Fluorescence spectra of the dilute THF solutions and of the thin films of compounds **2** and **6**. λ_{ex}=325 nm

Table 4.3. Photophysical, electrochemical and photoelectrical characteristics of the twin derivatives of 2-phenylindole

	Compound	**1**	**2**	**3**	**4**	**5**	**6**	**7**
Solution	λ_{Abs}, nm	360	359	360	355	307	308	304
	λ_{PL}, nm	467	463	458	472	466	450	462
	Stokes shift, nm	107	104	98	117	159	142	158
	λ_{Abs}, nm	397	369	374	359	305	308	309
	E_T, eV	2.29	2.29	2.29	2.29	2.30	2.30	2.30
Neat film	λ_{PL}, nm	472	480	471	471	486	478	464
	λ_{PH}, nm	541	541	542	541	539	539	540
	Stokes shift, nm	101	111	98	112	181	170	155
	$E_{ox\ onset\ vs.Fc}$, V	0.20	0.06	0.13	0.12	0.51	0.42	0.57
	IP_{PE}, eV	5.22	5.16	5.52	5.51	5.54	5.79	5.61
	IP_{CV}, eV	5.22	5.16	5.23	5.22	5.61	5.52	5.67
	E_g^{opt}, eV	2.84	2.86	2.94	2.86	3.58	3.54	3.43
	EA_{CV}, eV	2.38	2.30	2.29	2.36	2.03	1.98	2.24
Theoretical calculations	HOMO, eV	-4.44	-4.35	-4.54	-4.56	-4.77	-4.80	-4.87
	LUMO, eV	-0.92	-0.79	-0.98	-1.02	-0.71	-0.78	-0.91
	E_G, eV	-3.52	-3.56	-3.56	-3.54	-4.06	-4.02	-3.96

λ_{Abs} – the wavelengths of the absorption maxima; λ_{PL}– the wavelengths of the emission maxima; Stokes shift=λ_{Fl}–λ_{Abs}; $E_{ox\ onset\ vs.Fc}$ – the onset oxidation potential of the sample vs. the onset oxidation potential of ferrocene; IP_{PE} – the ionization potential estimated by the electron photoemission in air method; IP_{CV} – the ionization potential estimated by CV as $IP_{CV}=E_{onset\ ox\ vs.Fc}$+5.1 eV; E_g^{opt} – the optical band gap

estimated as $1240/\lambda_{Abs\ onset}$ where $\lambda_{Abs\ onset}$ is the wavelength of the onset of absorption; EA_{CV} – electron affinity estimated as $EA_{CV}=IP_{CV}-E_g^{opt}$; HOMO – the theoretically calculated HOMO energy; LUMO – the theoretically calculated LUMO energy; E_G=HOMO–LUMO.

The solid samples of compounds **1**–**7** also exhibit well-resolved single peaks although a slight red shift is observed in the fluorescence of the films in respect to that of the solutions. This may indicate the influence of the neighbouring molecules.

The triplet energies E_T were calculated from the maxima of the phosphorescence spectra of the solid samples of compounds **1**–**7**. The values were found to be comparable (2.29–2.30 eV), and no influence of the linkage between 2-phenylindole moieties could be identified. Such E_T values make these compounds suitable as host materials for green OLEDs.

4.1.5.Electrochemical and Photoelectrical Characteristics

For the successful application in (opto)electronic devices, electroactive materials must be stable during electrochemical operation. During the application of current to the sample solution of a compound, various redox processes take place. Reversible oxidation may occur if, after the oxidation of the neutral molecule to the radical cation, the molecule reduces to its initial state. If changes, such as the appearance of a new wave, or the decrease of the current, occur in voltammograms of multiple scans, such an electrochemical process is irreversible.

In addition, the energy needed to withdraw one electron from a molecule can be determined from CV. The establishment of the energy level alignment is important when combining all the components of the devices. The electron affinity (EA_{CV}) and ionisation potential (IP_{CV}) values are obtained from CV measurements as these characteristics are of the condensed state. HOMO and LUMO levels can determine the isolated molecule at the vacuum level [205].

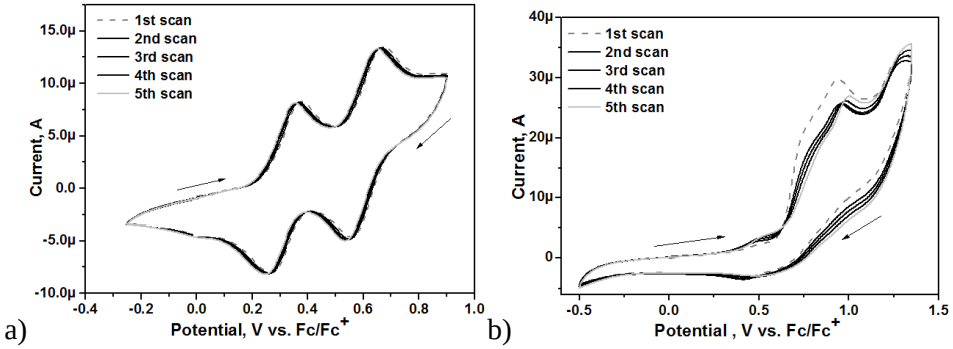

Figure 4.5. Cyclic voltammograms of compounds **2** (a) and **6** (b)

The electrochemical properties of derivatives **1**–**7** were studied by employing the cyclic voltammetry (CV) technique. The electrochemical characteristics are summarized in Table 4.3. The ionization potential values were determined from the onset oxidation potentials after calibration against ferrocene (Fc/Fc^+). The cyclic voltammograms of diindolylethene **2** are shown in Figure 4.5 a.

The 2nd and 3rd positions of the indole moiety can be easily oxidized. In the case of this series of compounds, both positions are blocked. Diindolylethene derivatives **1**–**4** were found to be electrochemically stable. They exhibited two reversible oxidation peaks in the repeated cycles of redox processes up to 1 V. During the multiple scans of compounds **1**–**4**, their CV curves retained their shape. The cyclic voltammograms of biindole **6** are shown in Figure 4.5 b. The similar CV curves were observed for compounds **5** and **7**. Twin compounds **5**–**7**, in which 2-phenylindole moieties are linked via the single bond, exhibited irreversible oxidation at 0.95 V, which can be attributed to the formation of radical cations, and to their coupling during further scans. The new peak of the reversible oxidation appeared at 0.48 V. The lower oxidation potential values and the formation of stable radical cations in the CV experiments of compounds **1**–**4** can apparently be explained by the extended conjugation system due to the presence of ethenyl-containing linking bridge of the diindolylethene derivatives. Whereas, in the case of compounds **5**–**7**, they are electrochemically stable only up to ~ 0.9 V.

Spectroelectrochemistry is a combination of two techniques: CV and spectroscopy. This method allows more complex analysis of single and multiple electron transfer processes through simultaneous determination of redox reactions and of the associated species at once. For the qualitative insight in such processes of compounds **1**–**4** observed on the electrodes during CV measurements, spectroelectrochemical measurements were performed. Figure 4.6 shows the results of UV-vis spectroelectrochemical measurements of compound **1**.

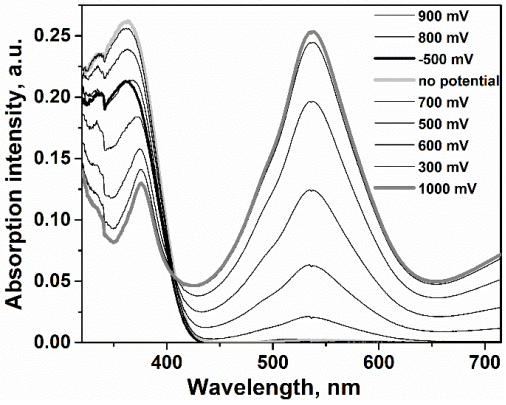

Figure 4.6. UV-vis spectra recorded during potentiostatic electrochemical oxidation of DCM solution of compound **1**

The process of electrochemical oxidation resulted in the decrease in the intensity of the absorption peak at 360 nm in the potential range of 0.3–1 V and the formation of one broad absorption band at 550 nm. This new absorption band can be associated with the newly formed radical cation (polaron). This polaron band disappears after applying the reduction potential of –0.5 V. The reversibility of the electrochemical process on the electrodes is confirmed as the absorption spectra after reduction of compound **1** are identical to the original one.

The ionization potentials of the solid samples of compounds **1**–**7** were also estimated by the electron photoemission in air method (Table 4.3). The trends were found to be in good agreement with those observed by CV and theoretically calculated HOMO levels. Derivatives **1**–**4** with the ethenyl-containing linkages between 2-phenylindole moieties showed lower ionization potentials than derivatives **5**–**7** in which the 2-phenylindole species are directly linked by the single bond indicating the larger π-conjugation system of the former compounds. The values of the ionization potentials of the researched diindolylethene derivatives **1**–**7** are also in the same trend with the experimentally and theoretically obtained energy band gap E_g^{opt} values. This is very important for the optimization of hole injection in the active layers, and thus for balancing the electron and hole transport in (opto)electronic devices.

4.1.6. Charge-Transporting Properties

Charge-transporting properties of the layers prepared by thermal vacuum deposition were studied by employing the TOF technique. Electric field dependencies of the hole-drift mobilities of the layers of compounds **1**–**4** are shown in Figure 4.7 a. The values of hole-mobility of the layer of compound **3** were found to be in the range from 2×10^{-5} to 7×10^{-4} cm^2/Vs at the electric fields ranging from 1×10^5 to 1×10^6 V/cm. This compound can be characterized as a low-dispersive charge-transporting material (Figure 4.7 b).

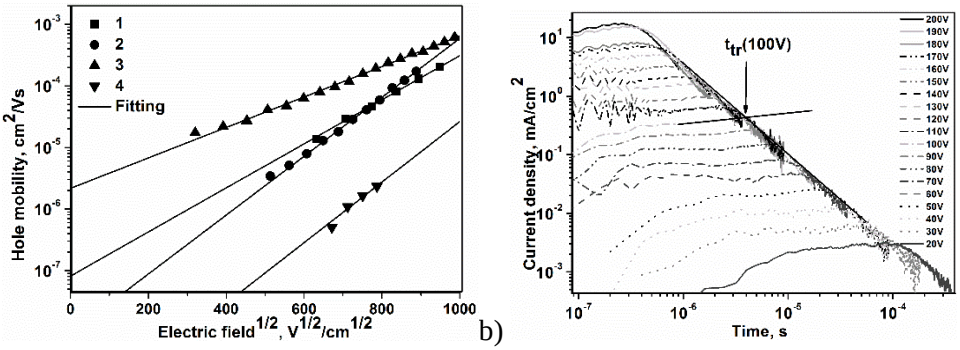

Figure 4.7. Electric field dependencies of the hole-drift mobilities of the layers of compounds **1**–**4** at room temperature (a) and current transient pulses at different electric fields for **3** (b)

The lower values of hole-mobility and the more dispersive charge transport were observed for compounds **1** and **2.** Such differences in the charge-transporting properties of the investigated compounds can apparently be explained by the different degree of ordering of the molecules in the solid layers [206]. The continuous increase of the hole drift mobility values of compounds **1**–**4** with the applied electric field implies the dominating role of energetic disorder. The values of the hole mobility of the synthesized indole twin compounds are close to those of the previously reported indole and N-phenyl-phenylenediamine-based enamines which were used as hole-transporting materials in bilayer green fluorescence OLEDs [207].

Hole mobilities of the layers of compounds **1**–**3** are higher than those of pyrido[2,3-b]indole derivatives which were used as the host materials for the fabrication of highly efficient blue phosphorescent OLEDs [52]. To sum up, it can be stated that these compounds could be used as hole-transporting layers of OLEDs.

4.2. Derivatives of 2-Phenylindole and Carbazole

4.2.1.Design and Synthesis

The strategy employed in this part of the work was to combine carbazole and indole moieties in the design and synthesis of host materials for phosphorescent OLEDs. The designed compounds were expected to exhibit high triplet energy values as well as charge-transporting and glass-forming abilities. The design of these materials was based on the idea that π-electron conjugation has to be interrupted in the compounds. This can be achieved by the incorporation of a hybridized sp^3 carbon atom.

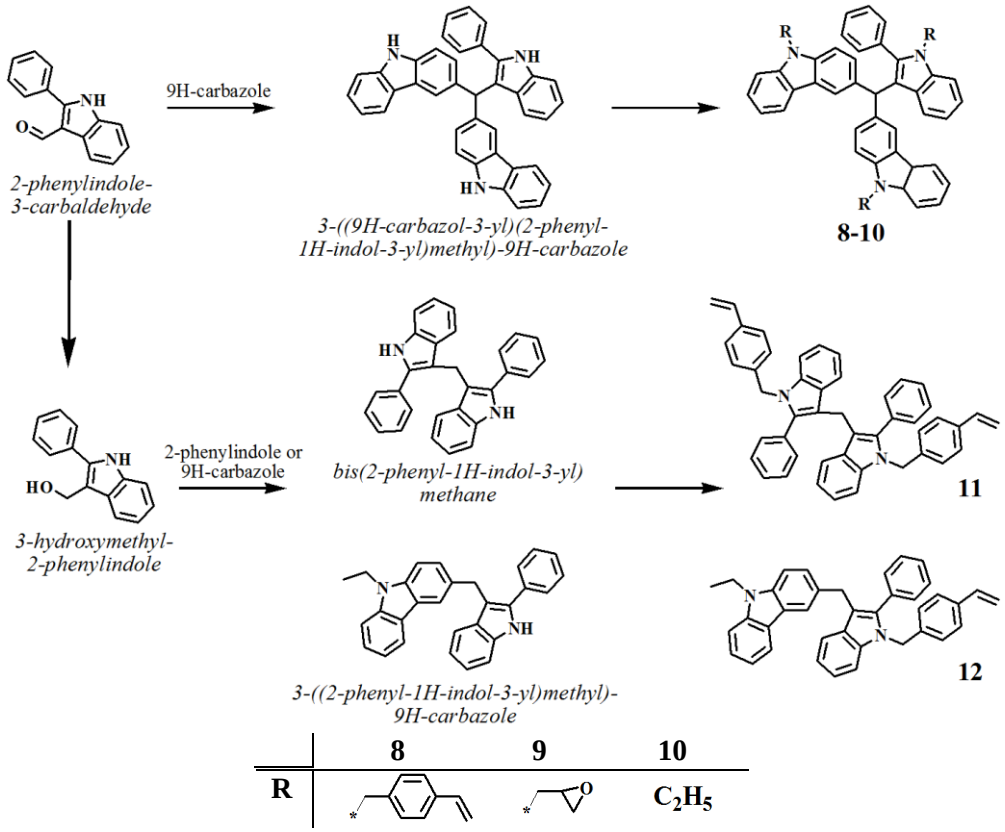

Scheme 4.2. Synthesis of 2-phenylindolylcarbazole derivatives

The routes to the synthesis of the derivatives of 2-phenylindole and carbazole are shown in Scheme 4.2. During the first step, the mixture of 2-phenylindole-3-carbaldehyde and 9*H*-carbazole was treated with HCl so that to obtain the intermediate compound 3-((9H-Carbazol-3-yl)(2-phenyl-1H-indol-3-yl)methyl)-9H-

carbazole. Friedel-Crafts alkylation is a convenient method for coupling different aromatic fragments. In this context, $FeCl_3$, $ZnCl_2$, $AlCl_3$ and HCl are most commonly used as catalysts [208]. The choice of hydrochloric acid resulted in a relatively fast reaction with a moderate yield (56%).

For the formation of compounds **11** and **12**, condensation of 3-hydroxymethyl-2-phenylindole with 2-phenylindole and 9-ethylcarbazole while using boron trifluoride diethyl etherate was performed. The rapid reaction resulted in moderate yields of intermediate compounds (58–62%). The final step in the synthesis of the target compounds was the introduction of the reactive functional groups by the interaction of the intermediate products with the corresponding alkyl halides in the presence of potassium *tert*-butoxide. All the target compounds were obtained and purified by performing column chromatography. The resulting yields of the alkylated compounds were 66–81%. The chemical structures were characterised by NMR, IR and MS. The compounds were found to be soluble in common organic solvents.

4.2.2. Thermal Properties

The thermal transitions and the thermal stability of materials **8**–**12** were studied by DSC and TGA. The thermal characteristics of compounds **8**–**12** are outlined in Table 4.4. TG curves and differential thermogravimetric (DTG) curves are presented in Figure 4.8 a, b.

Table 4.4. Thermal properties of compounds **8**–**12**

Compound	T_M, °C	T_G, °C	T_{CR}, °C	T_{ID}, °C
8	- [a]	-	-	228[b]
9	110	-	54	242
10	-	134	-	268
11	120	-	-	284[b]
12	-	85	-	404[b]

T_M – the melting point observed at the first heating scan of the DSC measurement; T_G – the glass transition temperature from the second DSC heating scan; T_{CR} – the crystallization temperature; T_{ID} – the initial weight loss temperature obtained from TGA curves; [a] – not detected; [b] – the weight loss temperature of the products of thermal polymerisation during the TGA measurement

Compounds **9** and **11** were isolated as crystalline substances. The T_M values were well defined from the sharp exothermic single peaks of the first heating scan during DSC. It was not possible to transform them to the glassy state by cooling from the melts. Compounds **8**, **10** and **12** were isolated as amorphous materials. The glass transition temperatures of compounds **10** and **12** were determined from the cooling scan of the melts. The higher glass transition temperature of compound **10** can be explained by its higher molecular weight which determines the stronger

intermolecular interaction in the solid state. We did not manage to detect the glass transition temperature of compound **8**. In the DSC heating scan, it only showed a sharp endothermic signal at 246 °C due to sublimation.

The temperatures of the onsets of the thermal degradation of most of the compounds were found to be rather moderate under nitrogen atmosphere. They were found to be up to 268 °C. Derivatives **8, 11** and **12** may have undergone thermal polymerisation during TGA measurements. The values of the onset weight loss temperatures can be assigned to their products of polymerization. The similar indole and carbazole hybrids reviewed in Chapter 4.2 also showed similar T_D values (281–321 °C).

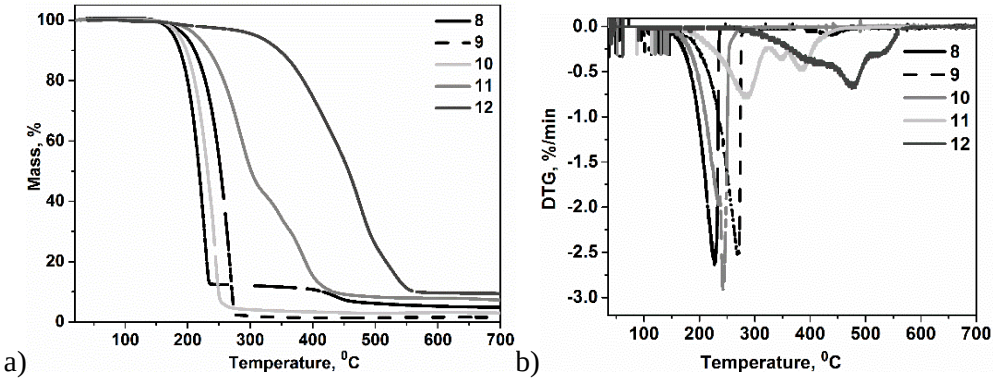

Figure 4.8. TG (a) and DTG (b) curves of 2-phenylindolo-carbazole derivatives **1**–**5**. (Heating rate: 10 °C/min, N_2 atm)

4.2.3. Polymerization

Photocross-linking of monomers **8** and **11** was studied by ATR-FTIR spectrometry. For the measurements, the solution of a monomer (0.5M) containing 3 mol % of photoinitiator cyclopentadienyl(fluorene)iron(II)hexafluorophosphate was drop-cast on the surface of the ATR-FTIR analysis crystal, the solvent was vapourised by heating at 40 °C for 15 min, and then the monitoring of the decrease of the intensity of the absorption band of the vinyl group under exposure to an UV radiation source was performed.

Figure 4.9 shows fragments of the FTIR spectra of the films of compounds **8** (a) and **11** (b) at different stages of photocuring. The fragments illustrate the decrease of the intensity of the absorption bands of vinyl groups at 997 cm^{-1} with the increase of the time of photocuring (they were being photocured for 15 min). The values of the insoluble fractions of the obtained materials were found to be 76% and 56%, respectively (estimated after the extraction of the samples with chloroform for 24h).

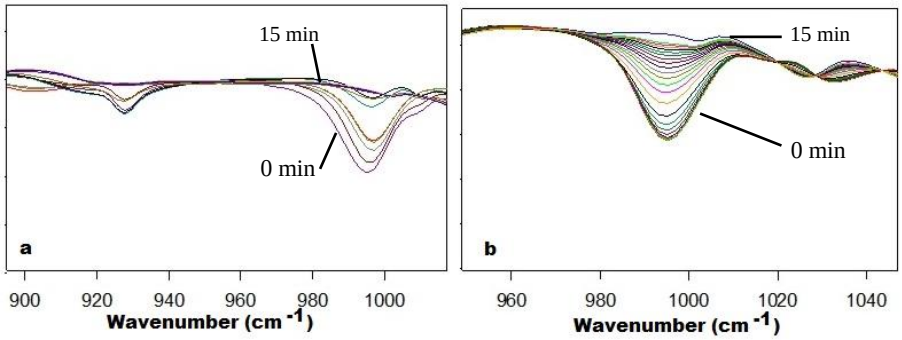

Figure 4.9. Fragments of FTIR spectra recorded during the photocuring of the films of compounds **8** (a) and **11** (b) containing 3 mol % of cyclopentadienyl(fluorene)iron(II)hexafluorophosphate

Polymerization of monomer **12** was performed in the solution, and the product was characterized by gel chromatography. The weight average relative molecular weight was determined to be 1870, and the number average molecular weight was found to equal 1110. The thermal degradation temperature (474 °C) of the resulting product was determined by the TG (see Figure 4.10), and it was 70 °C degrees higher than the thermally-induced polymerization product of the monomer **12** onset degradation temperature (404 °C). The glass transition temperature (120 °C) obtained from the DSC curves was detected to be 62 °C degrees higher than the monomer glass transition temperature (58 °C).

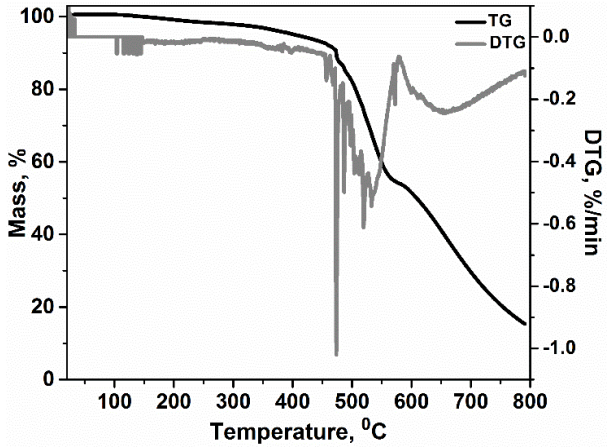

Figure 4.10. TG and DTG curves of the product of the polymerization of monomer **12**

4.2.4. Computational Studies

Quantum chemical calculations were performed for compounds **8**–**12** by using the DFT/B3LYP/ 6-31 (d, p) method. Theoretical ground state geometries revealed that the carbazole and 2-phenylindole moieties in all the compounds are not on the same plane. Figure 4.11 shows the molecular orbital plots of the optimised structures of **8**–**12**. The indole moiety is nearly perpendicular to the carbazole moieties (~85°)

of compounds **8**–**10** and **12**. The carbazole units in the molecules (**8**–**10**) are twisted by ca. 152° in respect to each other. In the case of compound **11**, the 2-phenylindole fragments are twisted by 58°.

π-Electrons in the HOMO of derivatives **8**–**10** and **12** are delocalized over all the carbazole-indole backbone, except for the phenyl- moiety, whereas the HOMO of indole twin derivative **11** is delocalized over both indole moieties with the same exception of the phenyl group. The LUMO of **8**, **11** and **12** are delocalized over vinylbenzyl fragments, while those of compounds **9** and **10** are delocalized on carbazole moieties (Figure 4.11).

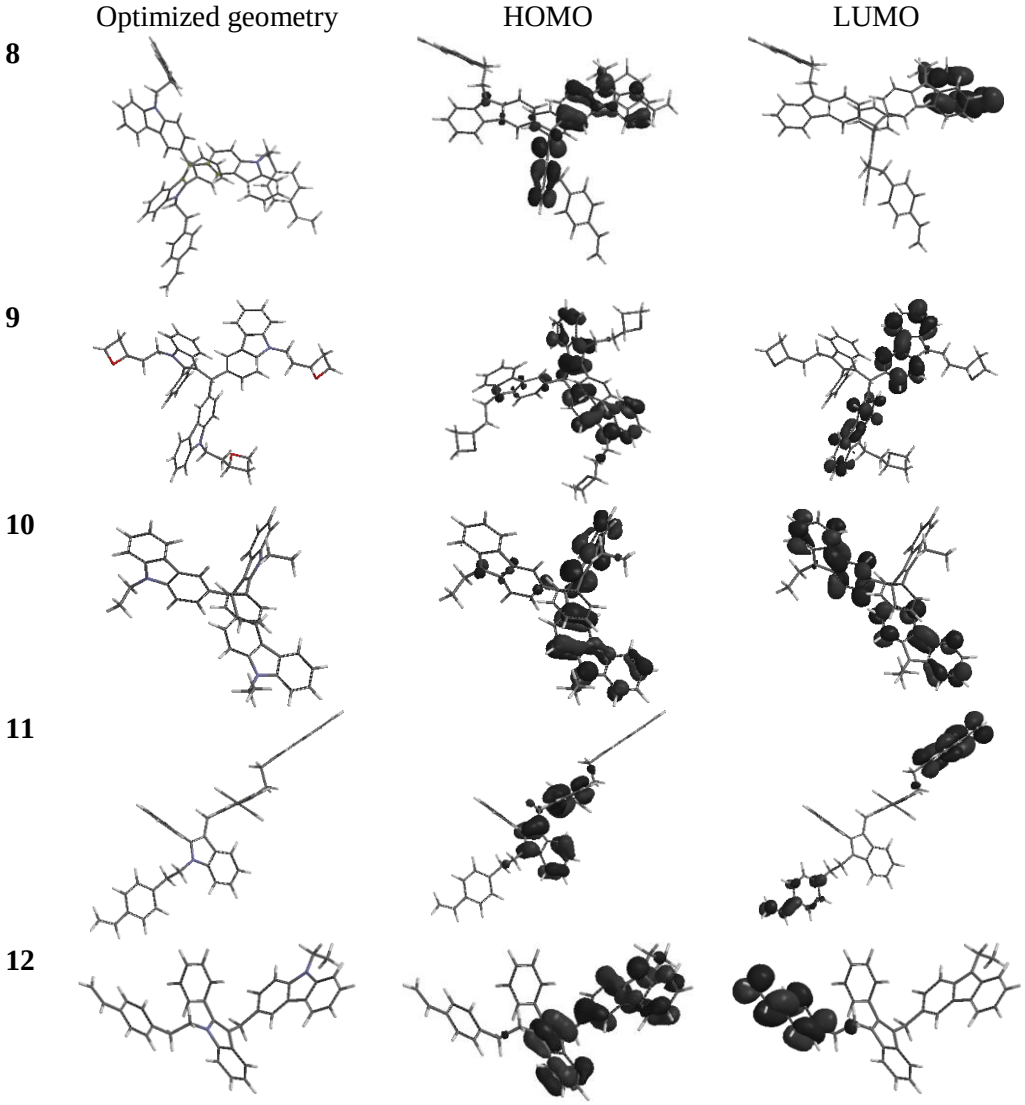

Figure 4.11. Optimized geometries and molecular orbital plots (B3LYP/ 6-31G**) of compounds **8**–**12**

4.2.5. Absorbance and Luminescence Properties

UV-vis and fluorescence spectra of the dilute THF solutions (10^{-4} M) of compounds **8**–**12** were recorded. The luminescence was excited with 320 nm wavelength. The UV-vis spectra of **8**, **11** and **12** representing two different families of the derivatives of 2-phenylindole and carbazole are shown in Figure 4.12 a. The wavelengths of the absorption maxima of compounds **8**–**12** are summarized in Table 4.5.

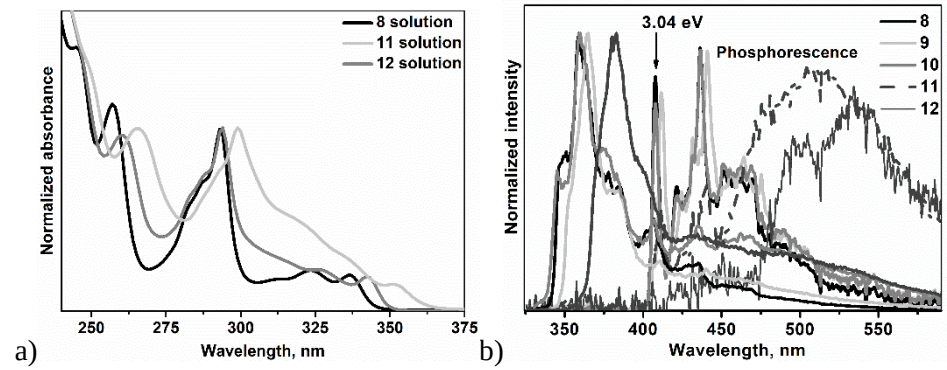

Figure 4.12. a) the absorption spectra of the dilute THF solutions of compounds **8**, **11** and **12**; b) the photoluminescence (the thick curves) and phosphorescence (the thin curves) spectra recoded at 77 °K (b) of the dilute THF solutions of compounds **8**–**12**. λ_{ex}=320 nm

The derivatives absorb UV-vis radiation up to 375 nm. A comparison with the absorption spectra of 9-ethylcarbazole (EtCz) and 2-phenylindole (PhI) can be made [104]. EtCz has absorption peaks at 348, 330 and 298 nm. The influence of this chromophore to the absorption behaviour of compounds **8** and **12** is significant as their spectra are of the same origin. The lowest energy absorption maxima of PhI is 300 nm [104]. The broad and bathochromically shifted absorption band of compound **11** with respect of the sole PhI moiety absorption band indicates the enhanced interaction of the chromophores in the molecule. As DFT calculations show that the delocalization of the HOMO of compound **11** differs mostly from the other series derivatives, the absence of the additional carbazole moiety in **11** is expected to have an impact on its photophysical and photoelectrical properties.

Photoluminescence spectra recorded at low (77 °K) temperatures of the dilute THF solutions of compounds **8**–**12** are shown in Figure 4.12 b. The wavelengths of the photoluminescence PL intensity maxima are summarized in Table 4.5. The PL spectra of compounds are characterized by the single peak. The fluorescence maxima of EtCz is at 351 nm [104]. The red-shifted fluorescence of the compounds can be attributed to the relaxation of the excited states in which the whole molecules are involved. The relatively low Stokes shift values show that the molecules are quite rigid and do not experience radical geometrical transformations upon photoexcitation.

The triplet energy values were established from the dilute THF solutions of the derivatives from their phosphorescence spectra at 77 °K. These values are higher

than those previously reported for other host materials such as indole-carbazole hybrids (2.62–2.99 eV) [104] and triindolylmethanes (2.97–2.99 eV) [209]. These luminescence properties make the 2-phenylindole and carbazole hybrids suitable as the hosts for blue PhOLEDS.

Table 4.5. Photophysical and electrochemical characteristics of compounds **8**–**12**

	Compound	**8**	**9**	**10**	**11**	**12**
Solution	λ_{Abs}, nm	259, 298, 325,337	259,298, 325,341	259,298, 325,336	262, 301, 352	360, 298, 327,342
	λ_{PL}, nm	359	363	359	363	381
	E_{S1}, eV	3.45	3.42	3.45	3.42	3.25
	Stokes shift, nm	40	22	25	11	39
	λ_{PH}, nm	407	410	407	425	430
	E_{T1}, eV	3.04	3.02	3.04	2.91	2.88
	ΔE_{ST}, eV	0.41	0.40	0.41	0.51	0.37
	$E_{ox\ onset\ vs.Fc}$, V	0.73	0.52	0.42	0.71	0.40
	IP_{PE}, eV	5.74	5.82	5.74	5.88	5.45
	IP_{CV}, eV	5.83	5.62	5.52	5.81	5.50
	E_g^{opt}, eV	3.42	3.46	3.40	3.29	3.36
	EA_{CV}, eV	2.41	2.16	2.12	2.45	2.21
Theoretical calculations	HOMO, eV	-4.99	-4.93	-4.95	-5.08	-5.01
	LUMO, eV	-0.91	-0.66	-0.66	-0.90	-0.92
	E_g, eV	4.08	4.27	4.29	4.18	4.09

λ_{Abs} – the wavelengths of the absorption maxima; λ_{PL}– the wavelengths of the emission maxima; Stokes shift=λ_{Fl}–λ_{Abs}; E_T – the triplet energy estimated as 1240/λ_{PH}; E_{ox} onset $_{vs.Fc}$ – the onset oxidation potential of the sample vs. the onset oxidation potential of ferrocene; IP_{PE} – the ionization potential estimated by the electron photoemission in air method; IP_{CV} – the ionization potential estimated by CV as $IP_{CV}=E_{onset\ ox\ vs.Fc}+5.1$ eV; E_g^{opt} – the optical band gap estimated as 1240/$\lambda_{Abs\ onset}$ where λ_{Abs} onset is the wavelength of the onset of absorption; EA_{CV} – electron affinity estimated as $EA_{CV}=IP_{CV}-E_g^{opt}$; HOMO – the theoretically calculated HOMO energy; LUMO – the theoretically calculated LUMO energy; E_G=HOMO–LUMO.

4.2.6. Electrochemical and Photoelectrical Properties

The electrochemical properties of the compounds were investigated by employing the CV technique. The obtained oxidation potential as well as the IP_{CV} and EA_{CV} values are summarized in Table 4.5. The oxidation potential was determined form the onset of the first cathodic wave, while the ionization potential

was determined from the oxidation potential after calibration against ferrocene. As an example, cyclic voltammograms of compound **8** are shown in Figure 4.13 a.

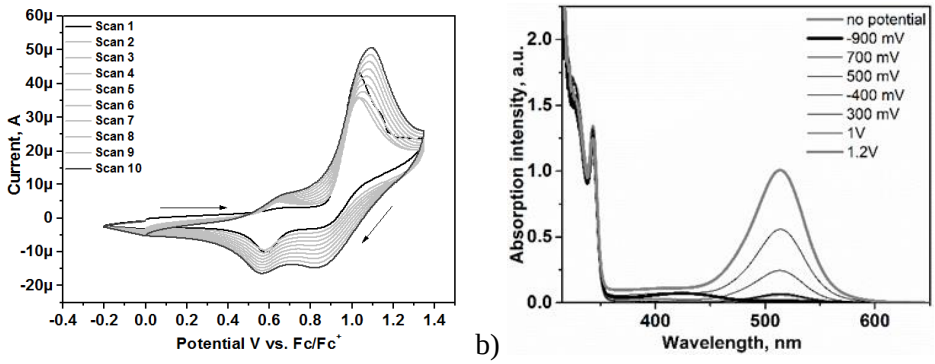

a) b)

Figure 4.13. a) Cyclic voltammograms of compound **8**; b) UV-vis spectra recorded during potentiostatic electrochemical oxidation of compound **8**

All the investigated compounds showed irreversible oxidation suggesting electrochemical coupling. During the multiple scans, new reversible oxidation peaks at around 0.65 V were observed for all the compounds. The ionisation potential (IP_{CV}) and the electron affinity (EA_{CV}) values were estimated from the oxidation onset potentials (E_{ox} onset vs. Fc) and the optical band gaps (E_g^{opt}). The theoretically calculated HOMO and LUMO energy values were found to be in the same trend as the experimental results. The resulting ionisation potential values as well as the optical band gap values are higher than for the previously presented series of 2-phenylindole derivatives **1**–**7** (see Chapter 4.1). This indicates a decreased π-conjugation system in derivatives **8**–**12**, which results in decreased delocalization of π-electrons and higher ionization potential values.

In order to get insight into the electrochemical processes of compounds **8**–**12** which occur on the electrodes during CV measurements, a spectroelectrochemical study was performed. Figure 4.13 b shows the results of UV-vis spectroelectrochemical measurements for compound **8**.

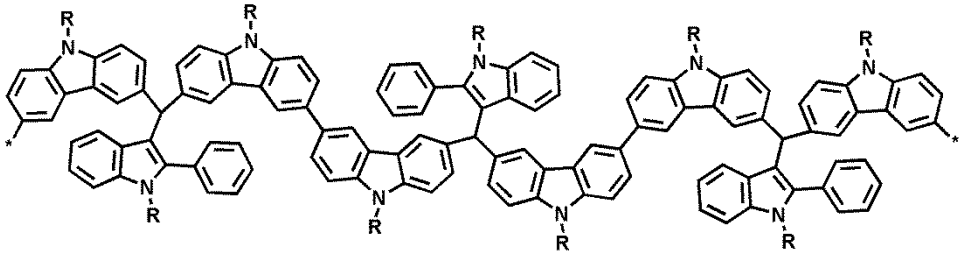

Figure 4.14. A possible structure of the product formed during the electrochemical coupling of 2-phenylindole and carbazole derivatives **8**–**10**. *R* refers to an alkyl group

During the process of electrochemical oxidation, the intensity of the absorption peak at 342 nm in the potential range of 0.3–1.2 V did not change. A new absorption band at ca. 520 nm was formed. This new absorption band can be associated with

the newly formed radical cation (polaron). This polaron band disappeared after applying the reduction potential of –0.9 V. The new broad absorption band also appeared at 420 nm thus indicating the formation of a new polymeric structure on the ITO working electrode. Although the newly detected polymeric structure was not further investigated, it is known, that the C-3 and C-6 positions of carbazole are the most active in anodic coupling reactions [210]. By taking these considerations into account, the possible structure of the derivative is depicted in Figure 4.14. The larger π-conjugation system of the formed polymeric structure is also confirmed by its lower oxidation potential value (Figure 4.13 a).

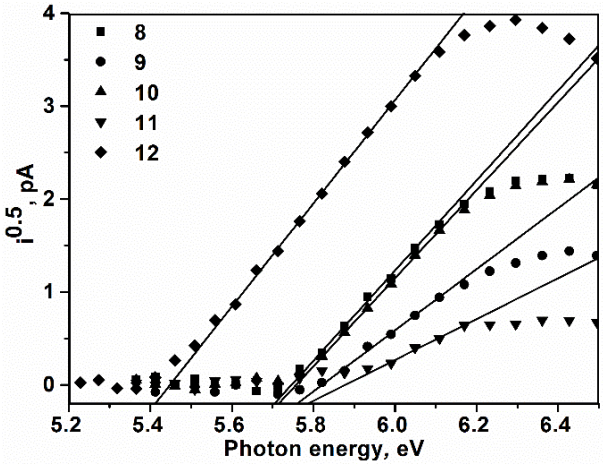

Figure 4.15. Electron photoemission spectra of compounds **8**–**12**

The ionization potentials of the solid samples of compounds **8**–**12** were estimated by the electron photoemission spectrometry in air. Electron photoemission spectra are shown in Figure 4.15, and the results are summarized in Table 4.5. The values of the ionization potentials recorded by electron photoemission spectrometry were found to be close to those estimated by CV and ranged from 5.74 eV to 5.88 eV. The IP values would be suitable for efficient hole injection to the layers of these materials.

4.2.7.Charge-Transporting and Layer Pattern Properties

Charge-transporting properties of the solid layers of compounds **9** and **12** were studied by employing the method of space-charge-limited current (SCLC). The hole-only devices with the following architectures were fabricated: ITO/m-MTDATA(20 nm)/ **9** or **12** (80 nm)/m-MTDATA(20 nm)/Al(60 nm). The layer of m-MTDATA (4,4′,4″-tris[3-methylphenyl(phenyl)amino]triphenylamine) was used as the hole-injecting and electron-blocking layer.

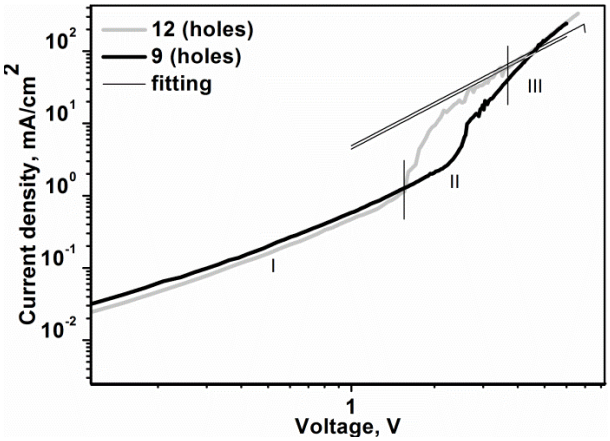

Figure 4.16. Current density vs voltage characteristics of the hole-only devices based on the compound **9** and **12** layer

The similar current density vs. voltage dependencies were observed for compounds **9** and **12** (Figure 4.16). The values of the zero-field hole mobility of 1.97×10^{-5} $cm^2V^{-1}s^{-1}$ and 1.78×10^{-5} $cm^2V^{-1}s^{-1}$ for compounds **9** and **12**, respectively, were obtained by fitting the region (III), in which the SCLC occurred, of the experimental current density vs. the voltage curve by employing Eq. 1 (see Figure 4.16). The disagreement between the experimental and fit curves can be explained by considering the existence of hole traps in **9** and **12** which can occur due to the volume or morphology effects in the solid state layers [211]. An additional explanation of this phenomenon can be the absent Ohmic contact which is required for the SCLC method in the hole-only devices [212]. Region I is the Ohmic region while Region II can be caused by injection-limited behaviour, trap filling, or built-in voltage [212].

The layer patterns were investigated by using two methods: atomic force microscopy and X-ray diffraction. AFM measurements were performed for vacuum deposited light-emitting layers **9**:$Ir(ppy)_3$ and **12**:$Ir(ppy)_3$ on glass substrates. The AFM topographical images are shown in Figure 4.17 a. The topography of **9**:$Ir(ppy)_3$ shows a relatively homogeneous surface with the morphological features having the mean height of 1.18 nm and the root mean square roughness (R_q) of 0.36 nm. The surface of **9**:$Ir(ppy)_3$ is dominated by peaks with the skewness (R_{sk}) value of 0.79 and has a leptokurtic distribution of the morphological features with the kurtosis (R_{ku}) value of 4.67 thus indicating relatively many high peaks and low valleys. In contrast to **9**:$Ir(ppy)_3$, the **12**:$Ir(ppy)_3$ surface is rougher with randomly oriented surface mounds having a mean height of 3.60 and the R_q value of 1.24 nm. The surface of **12**:$Ir(ppy)_3$ exhibited a relatively similar symmetry and the leptokurtic distribution of the morphological features with R_{sk} and R_{ku} values of 0.58 and 4.42, respectively. Both light-emitting layers, **9**:$Ir(ppy)_3$ and **12**:$Ir(ppy)_3$, exhibit quite low roughness values which are acceptable for structuring OLEDs as the low

roughness values of the host:guest emission layers contribute to the higher brightness and efficiency of PhOLEDs [213].

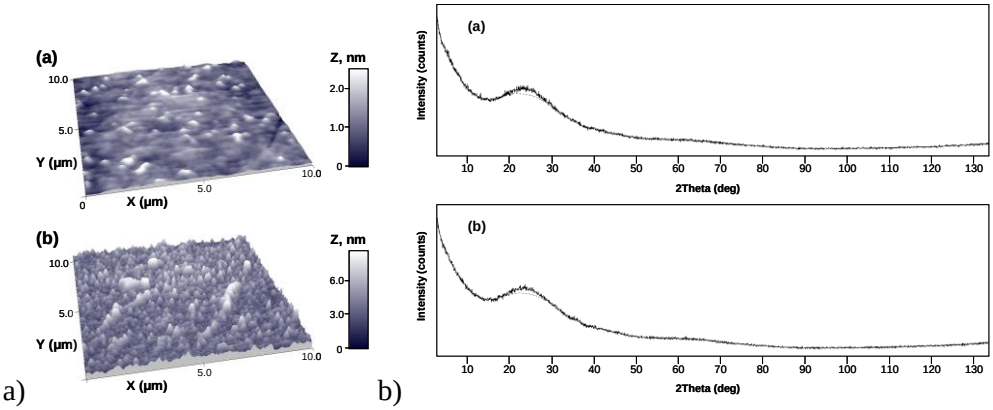

Figure 4.17. a) AFM topographical images with normalised Z axis in nm of light-emitting layers of **9**:Ir(ppy)$_3$ (a) and **12**:Ir(ppy)$_3$ (b). The images were acquired in air by using the contact mode; b) X-ray diffraction patterns of the light-emitting layers **9**:Ir(ppy)$_3$ (a) and **12**:Ir(ppy)$_3$ (b)

The X-ray diffraction patterns at the grazing incidence angle of 1.0º of **9**:Ir(ppy)$_3$ and **12**:Ir(ppy)$_3$ thin films are shown in Figure 4.17 b. The broad reflex at about 2θ=23.6º in both diffractograms indicates the amorphous character of thin films. Since crystallization and aggregation significantly affect the stability and lifetime of the device, such amorphous layers as those of **9**:Ir(ppy)$_3$ and **12**:Ir(ppy)$_3$ are favourable for OLEDs [214]. In addition, amorphous materials exhibit excellent processability, homogeneity and isotropic properties, which are also required for the highly efficient OLEDs [215].

4.2.8.Green and Blue Phosphorescent Organic Light Emitting Diodes

In order to study the performance of compounds **9** and **12** as hosts, simple green PhOLEDs were produced. In the devices with the structures of ITO/m-MTDATA (25 nm)/**9** or **12**:Ir(ppy)$_3$(15 nm)/Bphen (30 nm)/Ca:Al (devices A and B, respectively), 4,4′,4″-tris[phenyl(m-tolyl)amino]triphenylamine (m-MTDATA) was used as the hole-transporting material, and 4,7-diphenyl-1,10-phenanthroline (Bphen) was employed as the electron-transporting material. So that to prepare the emitting layers **9**:Ir(ppy)$_3$ and **12**:Ir(ppy)$_3$ for devices A and B, hosts **9** and **12** were doped with tris[2-phenylpyridinato-C2,N]iridium(III) (Ir(ppy)$_3$) as a green phosphorescent emitter. Efficient exciton confinement on the dopant Ir(ppy)$_3$ was expected due to the relatively high triplet levels of 3.02 eV and 2.88 for compounds **9** and **12** (Table 4.6) [193].

The electroluminescence (EL) spectra of devices A and B are shown in Figure 4.18. The fabricated PhOLEDs were characterized by green emissions with the intensity maxima at ca. 510 nm thus confirming the radiative recombination of excitons on Ir(ppy)$_3$. However, low intensity blue emission with the intensity maxima at ca. 430 nm was observed in the electroluminescence spectra of both

PhOLEDs. The wavelengths of these emissions were close to that of photoluminescence of m-MTDATA showing that the recombination of excitons occurred not only in the emitting layers but also in the hole-transporting layer of devices A and B. In order to avoid the recombination of excitons in the hole-transporting layer, either an additional electron-blocking layer or an exciton-blocking layer are required [216].

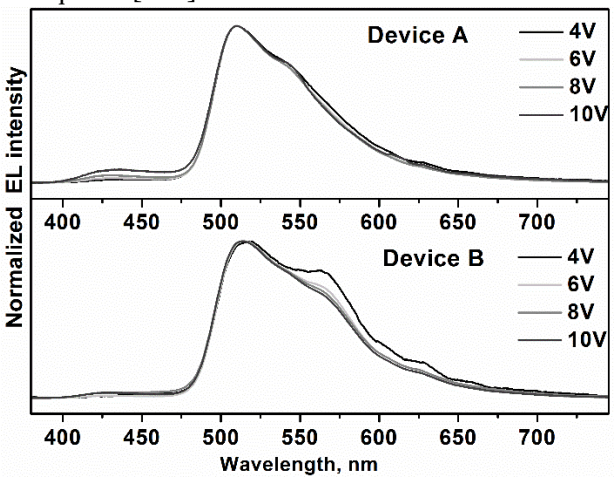

Figure 4.18. EL spectra of PhOLEDs recorded at different applied voltages

The similar shapes of electroluminescence spectra at the different applied voltages for both devices were observed. However, the intensity of the blue emissions increased in the EL spectra of the PhOLEDs with the increase of the applied voltage. The CIE coordinates were (0.29; 0.59) and (0.35; 0.64) which were calculated for the EL at 8 V for devices A and B, respectively. The superior colour purity was observed for device A.

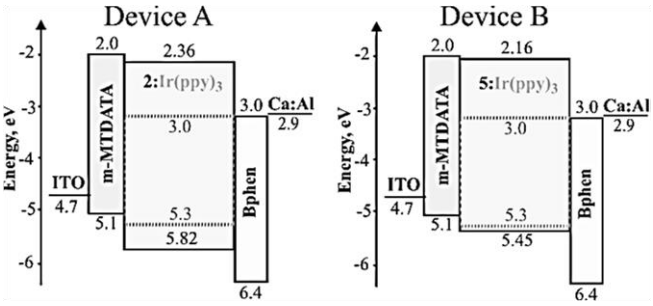

Figure 4.19. Energy-band diagrams of devices A and B

The efficiency curves of the PhOLEDs are shown in Figure 4.20 b–d. Devices A and B based on hosts **9** and **12** exhibited the maximum current efficiency, power efficiency, and external quantum efficiency of 4.2 and 10.3 cd/A, 2.5 and 7.2 lm/W, 1.2% and 2.9% respectively in the absence of light out-coupling enhancement. The external quantum efficiencies of 1.05% and 2.24% at 1000 cd/m^2 were recorded (Figure 20 b–d) thus showing efficiency roll-offs of 12.5% and 22.7% for devices A

and B, respectively. The external quantum efficiencies of PhOLEDs decreased at a high current density and high exciton concentrations apparently due to the unbalanced charges and quenching effects [217].

The luminance and efficiency characteristics of devices A and B are plotted in Figure 4.20.

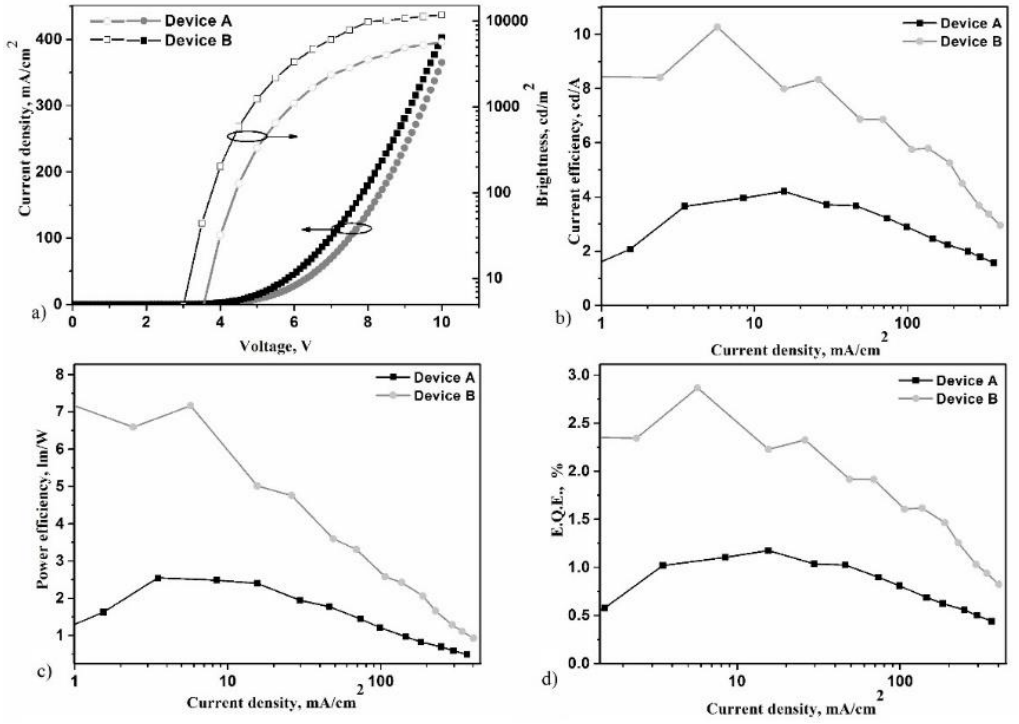

Figure 4.20. Electroluminescence characteristics of devices A and B: current density and luminance versus voltage (a), current efficiency versus current density (b), power efficiency versus current density (c), external quantum efficiency versus current density (d)

Both devices were characterised by the relatively low values of the turn-on voltage (V_{on}=3.7 for device A and V_{on}=3.1 V for device B), which confirms the highly efficient injection from the electrodes and the transport of holes and electrons to the emission layers (Figure 4.19). The driving voltage of 4.9 V at 1000 cd/m^2 was observed for device B, and it was 1 V lower than that observed for device A (Figure 4.20). This observation indicates a better charge balance in device B than that in device A owing to the better charge injection due to the more appropriate HOMO and LUMO levels of the active layers (Figure 4.19). The higher maximum brightness of ca. 11900 cd/m^2 was recorded for device B than that observed for device A (5700 cd/m^2) (Figure 4.20). The higher brightness and the lower driving voltages observed for device B compared to those recorded for device A shows the more effective exciton recombination and the radiative transition in the emitting layer with host **12** [218].

4.3.Benzo[b]carbazole Derivatives

4.3.1.Design and Synthesis

In this part of the work, for the synthesis of efficient luminescent and charge-transporting materials, regioselective acid-catalyzed reactions of 1-methyl and 1-naphthylindole with *o*-phthalbenzaldehyde in the presence of phosphorus (V) oxychloride or *p*-toluenesulfonic acid were employed. The influence of the substitution pattern of the benzo[b]carbazole moiety on the thermal, photophysical and photoelectrical properties was investigated.

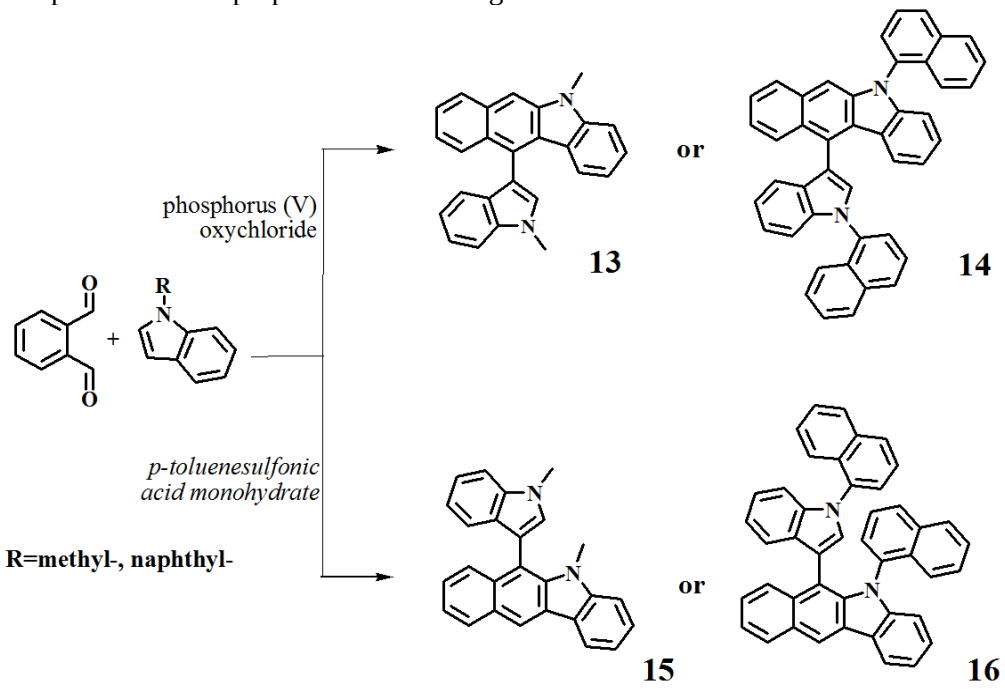

Scheme 4.3. Synthetic scheme of benzo[b]carbazole derivatives **13**–**16**

The synthesis of the derivatives of benzo[b]carbazoles is shown in Scheme 4.3. The combination of 2,3-unsubstituted indole and *o*-phthaldialdehyde in the presence of acid catalysts produces a promising aromatic fragment [219]. The use of phosphoryl chloride in chloroform produced methyl- and napthyl- substituted 6-(3-indolyl)benzo[b]carbazoles **13** and **14** in good yields (70–77%), whereas the use of *p*-toluenesulfonic acid in methanol allowed rapid reactions which yielded isomeric methyl- or naphtyl-substituted 11-(3-indolyl)benzo[b]carbazoles **15** and **16** in slightly lower yields (44–60%).

The efficient and easy synthesis of benzo[b]carbazoles employing different C-5 and N-substituted indoles significantly facilitated the synthesis of new efficient electroactive materials.

All the target compounds were obtained and purified by performing column chromatography and characterised by using NMR, IR and mass spectrometry methods. They were found to be soluble in common organic solvents.

4.3.2. Thermal Properties

The thermal transitions and stability of compounds **13**–**16** were investigated by DSC and TGA. The data is outlined in Table 4.6. DSC thermograms of compounds **13** and **15** are shown in Figure 4.21.

Table 4.6. Thermal characteristics of benzo[b]carbazole derivatives

Compound	**13**	**14**	**15**	**16**
T_G, ℃	90	107	89	116
T_M, ℃	241	-[a]	172, 186	-
T_{ID}[c], ℃	322	413	320	409

T_M – the melting point observed at the first heating scan of the DSC measurement; T_G – the glass transition temperature from the second DSC heating scan; T_{CR} – the crystallization temperature; T_{ID} – the initial weight loss temperature obtained from TGA curves; [a] – not detected.

Compounds **13** and **15** having lower molecular weights were isolated as crystalline substances. However, DSC studies (Figure 4.21) showed that these compounds can exist in both crystalline and amorphous states. The T_M of compound **13** was defined by a sharp single peak appearing during the first heating scan of DSC. In the case of compound **15**, two endothermal melting peaks appeared during the heating scan, which indicates polymorphism.

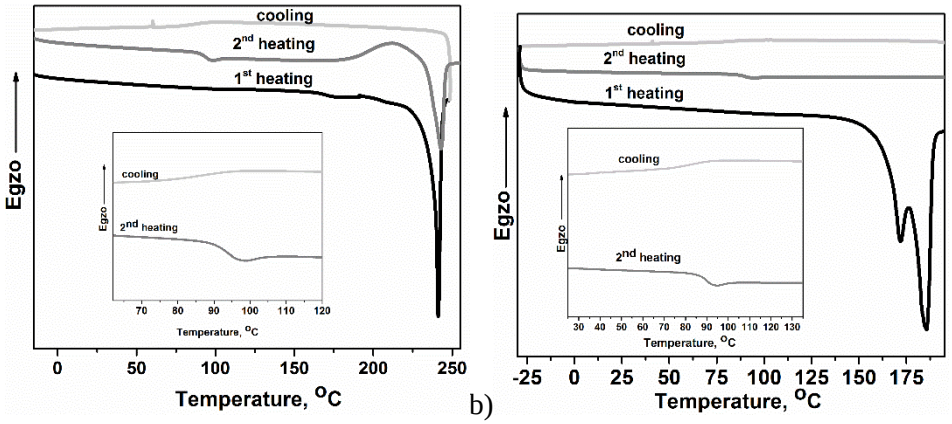

Figure 4.21. DSC thermograms of compounds **13** and **15**

During the cooling scans, both compounds showed transition to the glassy state. The isomers (**13** and **15**) showed comparable values of T_G (86 °C and 88 °C, respectively). Compounds **14** and **16** were isolated after the synthesis and purification as solid amorphous substances. No endothermic signals were observed during the heating scan of these compounds. These isomers also showed similar glass transition temperatures (107 °C and 116 °C, respectively). The slightly higher

T_G of compound **16** can apparently be explained by the steric hindrance preventing the rotation of naphthyl- and naphthylindolo substituents around the C–N and C–C bonds, respectively. In the case of compounds **13** and **15**, the plasticizing effect of methyl- substituents is apparently the reason for the lower T_G values.

The derivatives featuring naphthyl- substituents (**14** and **16**) exhibited considerably higher thermal stability than their methyl-substituted counterparts **13** and **15**. Thus the initial weight loss temperatures of compounds **13** and **15** were found to be 322 °C and 320 °C whereas those of **14** and **16** were 413 °C and 409 °C, respectively. The higher thermal stability of compounds **14** and **16** can apparently be explained by the stronger intermolecular interaction of the molecules of **14** and **16** due to their higher molecular weight and bulkier substituents.

4.3.3.Computational Studies

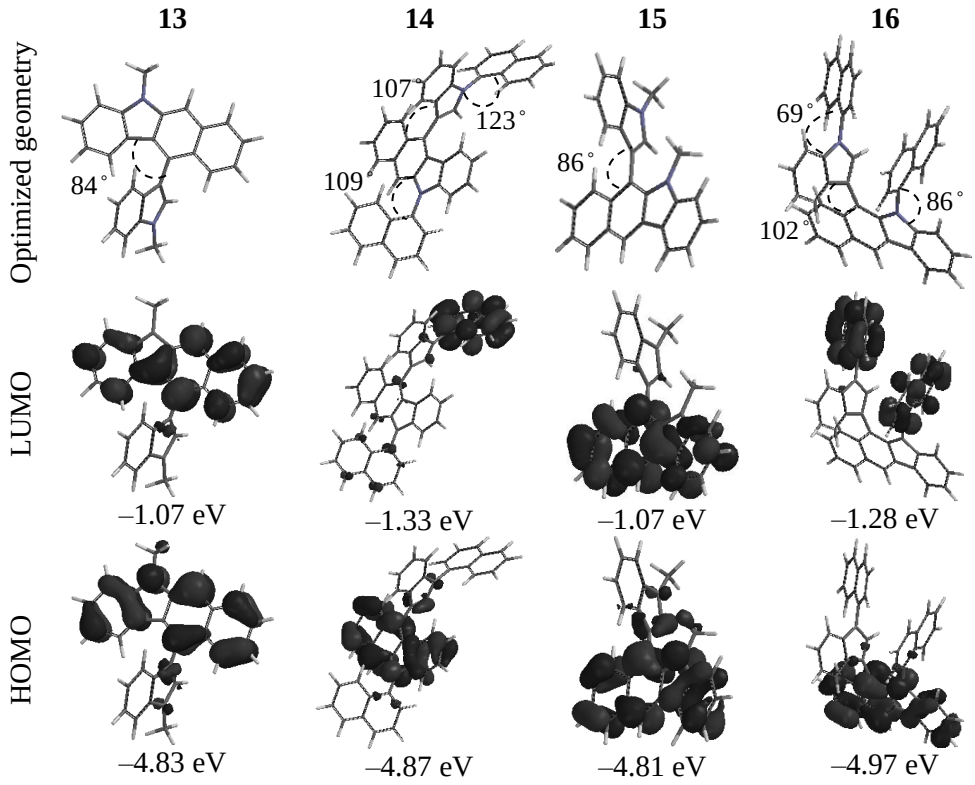

Figure 4.22. Optimized geometries and molecular orbital plots (B3LYP/ 6-31G**) of compounds **13**–**16**

In order to get an insight into the molecular and electronic structures of compounds **13**–**16**, density functional theory (DFT) calculations were performed. The ground-state geometries were optimised by using DFT with the B3LYP hybrid function at the basis-set level of 6-31 (d, p) method. The optimised geometries as

HOMO and LUMO for the optimized ground state geometries of the molecules are shown in Figure 4.22.

The theoretical ground state geometries of the benzo[b]carbazole derivatives **13**–**16** show that the substituents and the central benzo[b]carbazole moiety are not situated on one plane. The indole moieties are perpendicularly oriented (84–107°) to the benzo[b]carbazole backbone. In the case of compounds **14** and **16**, naphthyl-substituents form dihedral angles of 69–123° with respect to the benzo[b]carbazole or indole moieties.

The distribution of the electron density in HOMO is very similar for all the studied compounds. HOMO electrons are localized mainly on the benzo[b]carbazole moiety. The LUMO of **13** and **15** are localized over the benzo[b]carbazole fragment, whereas the LUMO of compounds **14** and **16** are localized on naphthyl moieties.

4.3.4. Photophysical Properties

The UV-vis and fluorescence spectra of the dilute THF (10^{-4} M) solutions and of thin films of compounds **13**–**16** were recorded at ambient conditions. The UV spectra are shown in Figure 4.23. The characteristic spectral data of the compounds are summarised in Table 4.7.

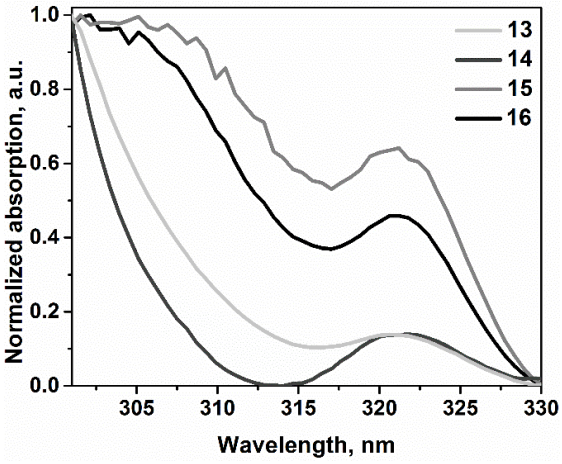

Figure 4.23. UV spectra of the THF solutions (10^{-4} M) of benzo[b]carbazole derivatives **13**–**16**

The derivatives absorb UV radiation in the range of up to 330 nm. The absorption bands of the solutions of the compounds are all in the similar range and are virtually not influenced by the nature of the substituent on the indole moiety. The optical band gap energy values estimated from the absorption band edges of the solutions of compounds **13**–**16** were found to be 3.76 eV. These values correlate well with the theoretically calculated optical band gap values ranging from 3.60 eV to 3.70 eV.

The emission spectra recorded at room and low (77 °K) temperatures of the dilute solutions and thin films of compounds **13**–**16** are shown in Figure 4.24 a, b.

The wavelengths of the photoluminescence (PL) intensity maxima are summarized in Table 4.7.

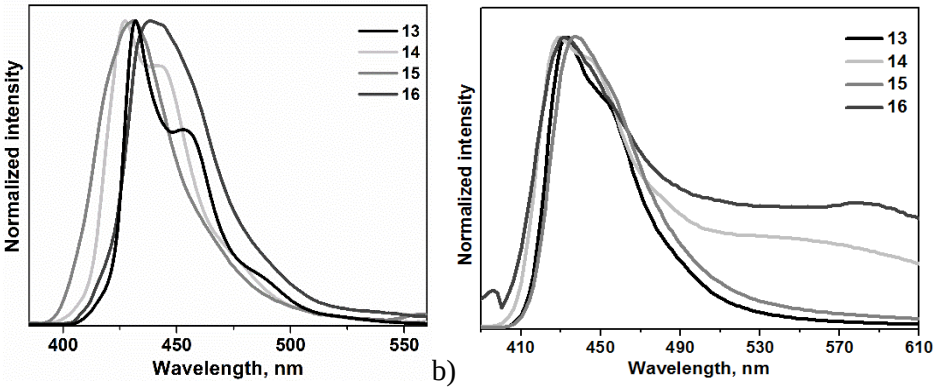

Figure 4.24. Photoluminescence (a – THF solutions; b – thin films) recorded at room temperature. λ_{ex}=320 nm

The emission spectra of the derivatives of indolylbenzo[b]carbazole THF solutions depend on the substitution pattern at the benzo[b]carbazole moiety. The PL spectra of derivatives **13** and **14**, showing a substitution at C-6 position, are characterized by two peaks. The PL spectra of derivatives **15** and **16** featuring substituents at C-11 position of the central backbone are characterized by a single peak at ca. 437 nm. The difference originates from the smaller conjugated π-electron system of compounds **13** and **14**. which results in the emission from two isolated fluorophores: naphthyl- and indole. The origin of the C–N substitution slightly impacts the blue shift of the spectra of methyl-substituted derivatives **13** and **15**. The PL spectra of the neat films are located at the similar wavelengths as those of dilute solutions but are less influenced by the origin of the substituents. They are characterized by the single peak at ca. 430 nm.

The triplet energy levels established from the phosphorescence spectra of the dilute solutions of the compounds at 77 K were found to be rather low (2.18–2.23 eV). These values correlate well with the theoretically calculated triplet energy values (2.21–2.26 eV).

The photoluminescence quantum yields (PLQY) of the dilute solutions of compounds **13**–**16** in THF solutions range from 39% to 69%. They were found to be dependent on the substitution pattern. The PLQY of the solutions of compounds **13** and **14** having substituents at C-6 position of the benzo[b]carbazole moiety were found to be considerably higher than those of compounds **15** and **16** featuring substituents at C-11 position. The PLQY values of the solid samples were found to be considerably lower than those of the dilute solutions and less dependent on the substitution pattern. The rather low PLQY of the solid samples can apparently be explained by the aggregation-induced quenching. For compound **14**, having bulky substituents on both sides of the benzo[b]carbazole moiety, aggregation-induced quenching is expressed to the less extent.

Table 4.7. Photophysical properties of benzo[b]carbazole derivatives

	Compound	**13**	**14**	**15**	**16**
THF solution	λ_{ABS}, nm	321, 336	321, 334	321, 336	321, 336
	λ_{PL}, nm	432, 454	427, 442	437	430
	λ_{PH}, nm	568	569	569	556
	Stokes shift, nm	96	93	101	94
	E_S, eV	2.73	2.81	2.84	2.88
	E_T, eV	2.18	2.18	2.18	2.23
	ΔE_{ST}, eV	0.55	0.63	0.66	0.65
	E_g^{opt}, nm	3.76	3.76	3.76	3.76
	QY, %	67	63	40	39
Thin film	λ_{ABS}, nm	252, 278, 286	277, 322, 336	221, 277, 286	287, 324, 339
	λ_{PL}, nm	430	428	437	430
	Stokes shift, nm	144	92	151	91
	QY, %	9	18	8	6

λ_{Abs} – the wavelengths of absorption maxima; λ_{PL}– the wavelengths of emission maxima; Stokes shift=λ_{Fl}–λ_{Abs}; E_T – the triplet energy estimated as 1240/λ_{PH}; E_{ox} onset vs.$_{Fc}$ – the onset oxidation potential of the sample vs. the onset oxidation potential of ferrocene.

The Stokes shift values of the indolo and benzo[b]carbazole derivatives are almost the same in solutions, whereas, in the solid state, the dependence of the C–N substituents on the Stokes shift is noticeable. The enhanced rigidity of the naphthyl-substituted indolylbenzo[b]carbazole does not influence the Stokes shift values as they remain the same in the solid state and the solution. The Stokes shift values of the unstacked methyl-substituted indolylbenzo[b]carbazole derivatives are highly influenced by the state of aggregation. The freely rotatable unstacked indole moiety is crucial to the large Stokes shifts of these folded chromophores in the solid state.

4.3.5. Electrochemical and Photoelectrical Properties

The electrochemical properties of the compounds were investigated by performing cyclic voltammetry (CV). The resulting data is summarised in Table 4.8. Cyclic voltammograms of compounds **13**–**16** are presented in Figure 4.25.

All the investigated compounds showed reversible oxidation thus suggesting electrochemical stability up to 1.2 V. During multiple scans, no new oxidation peaks were observed. The onset oxidation potential values of derivatives **13** and **15**

featuring methyl-substituted nitrogen atoms were found to be lower than those of the naphthyl-substituted compounds. The solid-state ionization potential (IP_{CV}) and the electron affinity (EA_{CV}) values were estimated from the oxidation onset potentials ($E_{ox\ onset\ vs.Fc}$) and the optical band gaps (E_g^{opt}).

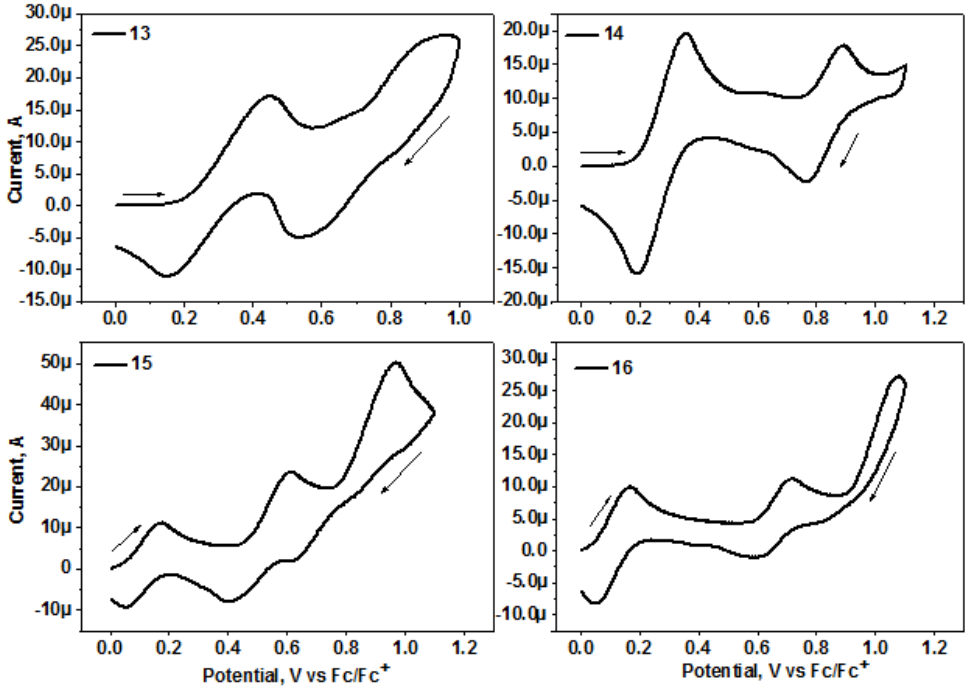

Figure 4.25. Cyclic voltammograms of 0.1M DCM solutions of compounds **13**–**15**. Ferrocene was used as the internal standard

The IP_{CV} values were found to be lower for the methyl-substituted compounds (**13** and **15**) than for the naphthyl-substituted derivatives (**14** and **16**). The theoretical energy values of HOMO and LUMO for compounds **13**–**16** were calculated by using the DFT/B3LYP/ 6-31 (d, p) method. Their values are summarized in Table 4.8. The theoretical HOMO energy values showed the same trend as the IP_{CV} values. Slightly shallower HOMO energy levels were estimated for compounds **13** and **15** relative to those of compounds **14** and **16**. The LUMO and EA_{CV} values showed the same trend thus indicating the influence of the naphthyl-substitution on the benzo[b]carbazole moiety.

In order to get insight into the electrochemical processes of compounds **13**–**16** observed on the electrodes during CV measurements, spectroelectrochemical measurements were performed. Figure 4.26 shows the results of UV-vis spectroelectrochemical measurements of compounds **13** and **15**.

The UV-vis absorption peak recorded during the electrochemical oxidation of compounds **13**–**15** without applying the potential was observed at 410 nm with a small shoulder in the shorter wavelength region.

Table 4.8. Electrochemical and photoelectrical characteristics of compounds **13**–**15**

Compound		**13**	**14**	**15**	**16**
	IP_{EP}, eV	5.16	5.26	5.29	5.29
	IP_{CV}, eV	5.53	5.60	5.45	5.58
	EA_{CV}, eV	1.77	1.84	1.69	1.82
Theorical calculations	E_{HOMO}, eV	-4.83	-4.87	-4.81	-4.97
	E_{LUMO}, eV	-1.07	-1.33	-1.07	-1.28
	E_g, eV	3.76	3.54	3.74	3.69
	E_S, eV	3.23	3.73	2.37	3.74
	E_T, eV	2.21	2.21	2.20	2.26
	ΔE_{S-T}	1.02	1.52	0.17	1.48

IP_{PE} – the ionization potential estimated by the electron photoemission in air method; IP_{CV} – the ionization potential estimated by CV as $IP_{CV}=E_{onset\ ox\ vs.Fc}+5.1$ eV; E_g^{opt} – the optical band gap estimated as $1240/\lambda_{Abs\ onset}$ where $\lambda_{Abs\ onset}$ is the wavelength of the onset of absorption; EA_{CV} – electron affinity estimated as $EA_{CV}=IP_{CV}-E_g^{opt}$; HOMO – the theoretically calculated HOMO energy; LUMO – the theoretically calculated LUMO energy; E_G=HOMO–LUMO.

During the process of electrochemical oxidation, compounds **13** and **15** behaved differently. Compound **13** showed one oxidation peak, and its UV-vis spectra changed only slightly. A small broad peak appeared at 550 nm in the potential range of 0.5–1.2 V. It can be attributed to the newly formed radical cation. Compound **15** showed two oxidation peaks during CV measurements. The intensity of the initial absorption peak of the latter compound in the potential range of 0.3–1.2 V decreased, and the shoulder disappeared. New very broad absorption bands at ~545 and 700 nm were formed. These new absorption bands can be associated with the newly formed radical cation (polaron) and dication (dipolaron).

The oxidation of both compounds was found to be reversible. In the case of compound **13**, the radical cation absorption band disappears, and the UV-vis spectra become identical to the initial spectrum. The polaron and dipolaron absorption bands of compound **15** disappear after applying reduction potential –0.3 V. Although the nature of the UV-vis spectra is not identical as it is broader, the characterisation peak at 410 nm with the small shoulder can be observed.

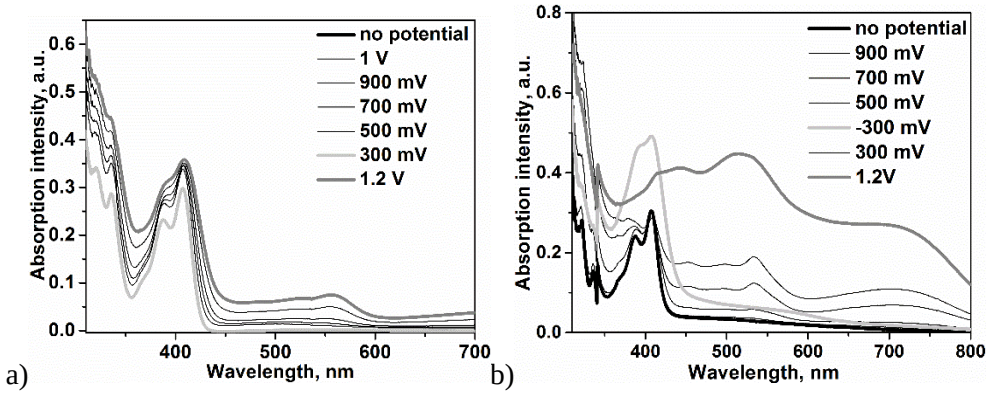

Figure 4.26. UV-vis spectra recorded during potentiostatic electrochemical oxidation of compounds **13** (a) and **15** (b)

Ionization potentials of the solid samples of compounds **13**–**16** were estimated by photoelectron emission spectrometry in air. The obtained photoelectron emission spectra are shown in Figure 4.27, and the results are summarized in Table 4.8.

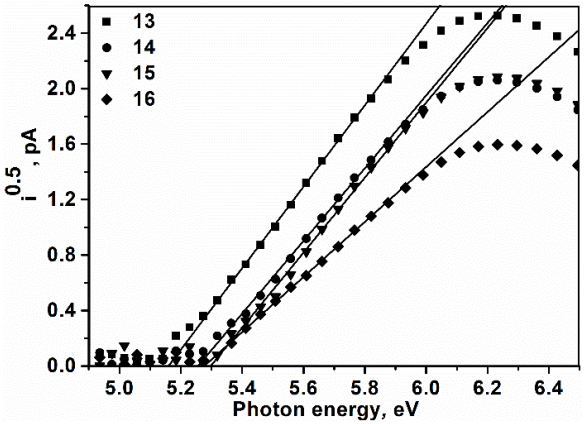

Figure 4.27. Photoelectron emission spectra of the amorphous films for vacuum-deposited compounds

The values of ionization potential recorded by photoelectron emission spectrometry were found to be comparable (5.16 eV–5.29 eV). This indicates that the energy levels are mainly determined by the main benzo[b]carbazole moiety. Compound **13** showed the lowest ionization potential (5.16 eV). The differences between the ionization potential values obtained by employing the different methods can apparently by explained by the different states of aggregation of the samples in use.

4.3.6.Charge-Transporting Properties

The charge-transporting properties of the layers of compounds **13**–**16** prepared by thermal vacuum deposition were studied by employing the TOF technique. The electric field dependencies on hole and electron-drift mobilities are shown in Figure 4.28.

The newly synthesized benzo[b]carbazole derivatives were found to be capable of transporting both holes and electrons. The values of hole-mobility of the layers of the derivatives were found to be up to 6×10^{-3} cm^2/Vs at the electric field of 5.7×10^5 V/cm. Electron mobilities reached 2.4×10^{-3} cm^2/Vs at the electric field of 5.4×10^5 V/cm. The layers of most of the investigated derivatives of benzo[b]carbazole showed close values of mobilities of holes and electrons. A balanced transport of both charges is essentially desirable for broad charge recombination zones in the active layers of the OLEDs [220].

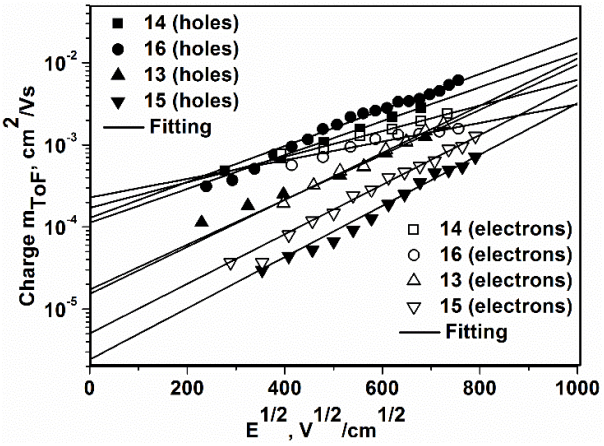

Figure 4.28. Electric field dependencies of hole-drift mobility for the amorphous films for vacuum-deposited compounds measured by the TOF method at room temperature

Derivatives **13** and **14** featuring substituents at C-11 position of the benzo[b]carbazole moiety exhibited higher charge drift mobilities than those substituted at C-6 position (**15** and **16**). Such differences in the charge-transporting properties of the researched compounds can apparently be explained by the different spatial orientation that is influenced by the substituents as well as the degree of ordering of the molecules in the solid layers [206]. The values of the hole mobility of the synthesized benzo[b]carbazole compounds are higher than those of the previously reported dibenzoindolocarbazole-based derivatives which were used in OFET devices [221].

4.3.7. Non-Doped Blue Emissive Electroluminescent Devices

In order to evaluate the EL performance of naphthyl-substituted indolylbenzo[b]carbazole derivatives **14** and **16** as blue emitters, non-doped unoptimized devices A and B were produced. Their structure and characteristics are described in Table 4.10. In these devices, CuI was used for the preparation of the hole injecting and transporting layer, 2-(4-biphenylyl)-5-(t-butylphenyl)1,3,4-oxidiazole (PDB) or BPhen were used for the fabrication of electron transporting layers (ETL) (devices A or B, respectively), Cs_2CO_3 was used as the electron injecting material, and the Al layer was used as the cathode.

Table 4.9. Characteristics of electroluminescent devices

Device	ITO/CuI(8nm)/ **A** or **B**/ Cs_2CO_3 (2nm)/Al(80nm)					
	V_{on}, V	η_c, Cd/A	η_p, lm/W	Brightness, Cd/m^2	CIE (x, y)	EQE, %
A(**14**(50nm)/ PDB(20nm))	3.4	9.8	3.2	17700	0.21, 0.16	3.4
B(**16**(50nm)/ BPhen(20nm))	3.6	5.7	3.6	14946	0.23, 0.20	2.0

The EL spectra of the single-layer devices (Figure 4.29 a and b) based on compounds **14** and **16** are slightly blue-shifted if compared to the PL spectra of the films of the corresponding compounds. This enhancement of singlet emission may be due to electric excitation. This enhancement of singlet emission may be due to electric excitation. The EL spectra of the devices based on compounds **14** and **16** are characterized by one well-defined narrow peak and a long-wavelength tail, which can be attributed to excimer formation. Excimers are formed due to resonance interactions of a molecular exciton with the neighbouring non-excited molecules [222].

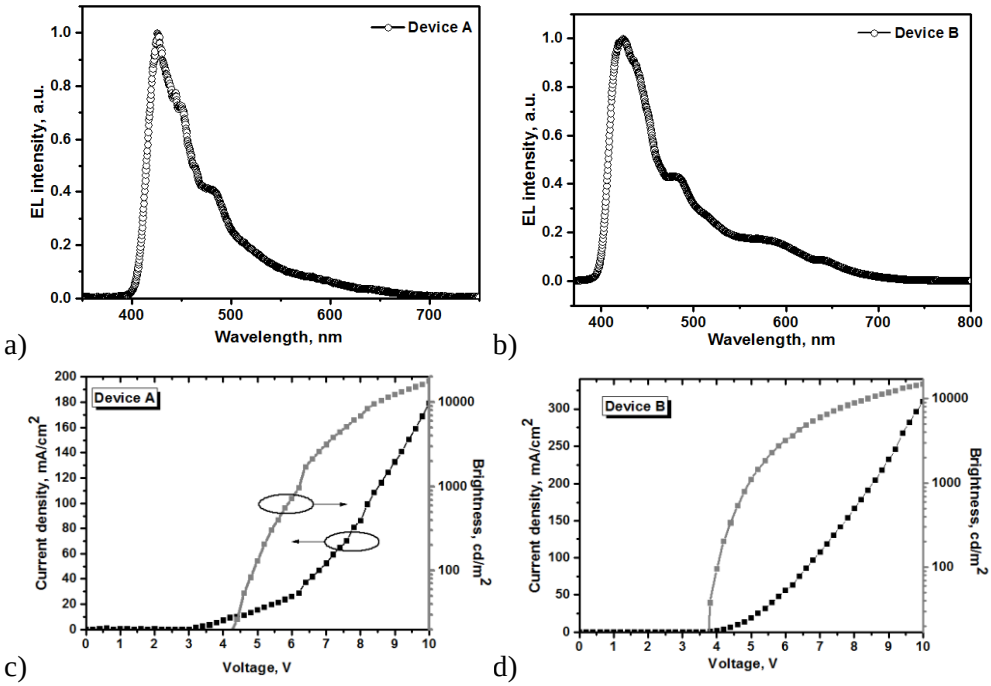

Figure 4.29. El spectra of devices A (a) and B (b) electroluminescence spectra; current density and luminance versus voltage plots for devices A (c) and B (d)

Different materials for the electron transport layer were chosen due to different electron mobility values of compounds **14** and **16**. The electron mobility of BPhen is

of the order of 10^{-4} cm^2 /Vs [223] whereas that of PBD is ranged between 2×10^{-5} and 4×10^{-5} cm^2/Vs [224].

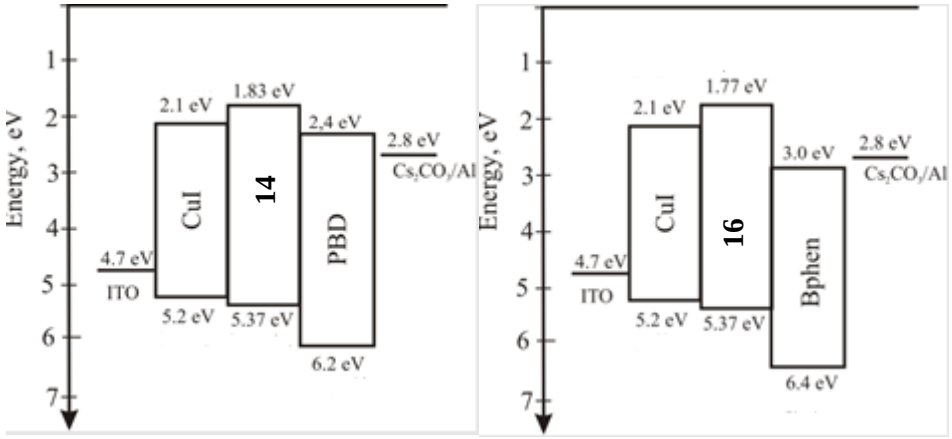

Figure 4.30. Energy level diagrams of devices A and B

Figure 4.29 c and d shows the characteristics of the single-layer OLEDs. The devices show relatively low turn-on voltage values and exhibit high brightness reaching 17700 Cd/m^2. The external quantum efficiency reaches 3.4%. The higher brightness and EQE of device A can be assigned to the improved HOMO/LUMO levels of the functional layers (Figure 4.30), higher charge drift mobility values and QY. The overall characteristics of the non-doped blue OLEDs are comparable to those of the similar blue OLEDs reported earlier [225, 226].

4.4. Benzophenone-Based Derivatives

4.4.1. Synthesis

A combination of donor and acceptor moieties in a single molecule enables to obtain materials exhibiting interesting photophysical properties such as triplet-triplet annihilation, delayed fluorescence or aggregation-induced emission [227, 228, 229]. The exploitation of these properties enables to obtain efficient OLEDs without using expensive heavy metal-based emitters [230, 231, 232]. In this part of the work, new compounds were designed by using benzophenone as an acceptor and various donors such as phenylindole and tetrahydrocarbazole. As it was mentioned in Chapter 2, these donors are not widely investigated in donor-acceptor compounds. Phenoxazine and 3,6-di-*tert*-butylcarbazole moieties were used for the comparison. Bis[4-(10H-phenoxazin-10-yl)phenyl]methanone (**19**) [200] and bis[4-(3,6-di-*tert*-butyl-9H-carbazol-9-yl)phenyl]methanone (**20**) [201] were reported when this work was in process. Researchers used conventional coupling methods, such as Buchwald-Hartwig and Ullmann methods. These synthesis methods require air-senstitive Pd and Cu metal catalysts which are relatively expensive compared to ordinary chemicals.

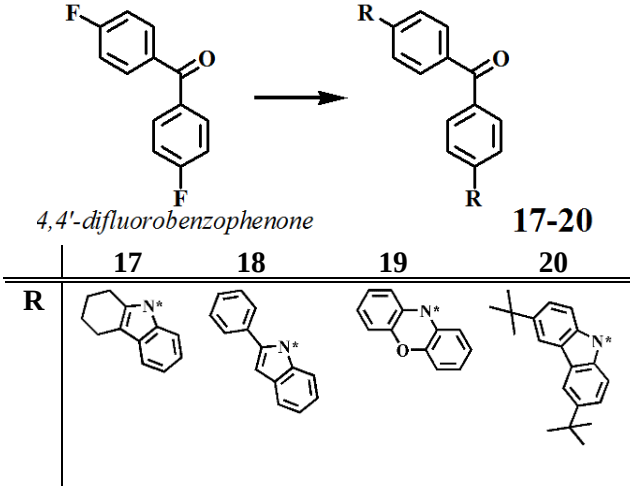

Scheme 4.4. Synthesis of benzophenone derivatives **17**–**20**

The target compounds discussed in this chapter were obtained by using one step synthesis as illustrated in Scheme 4.4. The C–N bond formation was conducted via the nucleophilic aromatic substitution reaction. 4,4'-difluorobenzophenone and various N-heterocyclic compounds reacted by using potassium *tert*-butoxide as a base in DMSO. Although the yields of compounds **19** and **20** were lower (37% and 43%) than those obtained by employing different synthetic routes (84% and 68% [200, 201]), this synthesis method is comparatively mild and cheaper as no metal catalysts are used.

All the target compounds were found to be soluble in common organic solvents.

4.4.2. Thermal Properties

The thermal transitions and thermal stability of compounds **17**–**20** were researched by DSC and TGA. The thermal characteristics of the compounds are outlined in Table 4.11. The TG curves are presented in Figure 4.31.

Table 4.10. Thermal characteristics of benzophenone derivatives

Compound	**17**	**18**	**19**	**20**
T_G, ℃	82	-[a]	145	160
T_M, ℃	200	179	258	343
T_{CR}, ℃	-	160	157	222
T_D, ℃	447	251	476	485

T_M – the melting point observed at the first heating scan of the DSC measurement; T_G – the glass transition temperature from the second DSC heating scan; T_{CR} – the crystallization temperature; T_{ID} – the initial weight loss temperature obtained from TGA curves; [a] – not detected.

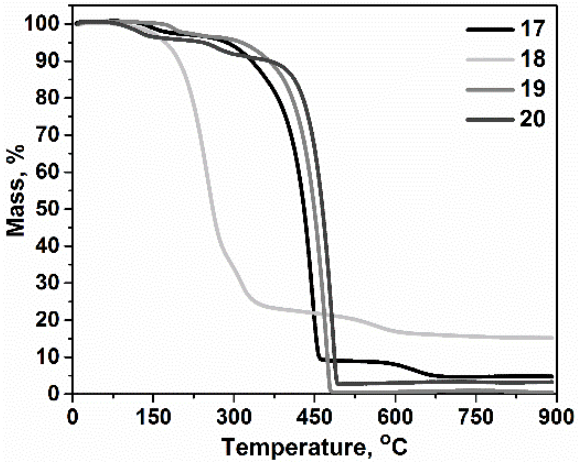

Figure 4.31. TG curves of benzophenone derivatives **17**–**20**. Heating rate 10 °C/min, N_2 atmosphere

Benzophenone derivatives (**17**–**20**) were isolated after purification as crystalline compounds. The T_M was defined as sharp single endothermic peaks during the first DSC heating scans. The high T_M values of the compounds can be attributed to the molecular symmetry of the compounds. The highest T_M was observed for the di-*tert*-butylcarbazole containing derivative **20** (343 °C). Exothermic crystallization peaks were observed during the cooling scans of compounds **18**–**20**. Tetrahydrocarbazole, phenoxazine and di-*tert*-butylcarbazole-substituted benzophenone derivatives **17, 19** and **20** were found to be capable of

forming molecular glasses with the glass transition temperatures ranging from 82 to 160 °C.

Benzophenone derivatives **17**, **19**, **20** exhibited high thermal stability. The temperatures of the onsets of their thermal degradation ranged from 447 to 485 °C. The temperature of the onset of thermal degradation of 2-phenylindole moiety containing compound **18** was found to be comparatively low (251 °C). The relatively modest thermal stability of the 2-phenylindole substituted compound **18** can apparently be explained by the lower thermal stability of the phenylindole moiety as similar values were observed for the previously discussed indole derivatives (Chapter 4.1 and 4.2). Compounds **8**–**11** discussed in Chapter 4.2 showed close values of the temperatures of the onsets of thermal degradation. The TG of compound **18** revealed a rather high amount of carbonized residue indicating thermochemical decomposition. The weight loss of compounds **19** and **20** resulted in evaporation rather than in decomposition as their weight loss reached ca.100%.

4.4.3. Computational Studies

All the compounds (**17**–**20**) exhibit clear separation of HOMO and LUMO distributions. As shown in Figure 4.32, for compounds **17**–**20**, LUMO are located on the central electron-accepting benzophenone core, whereas HOMO are mainly localized on the electron-donating peripheral substituents because of the highly twisted donors with respect of the acceptor.

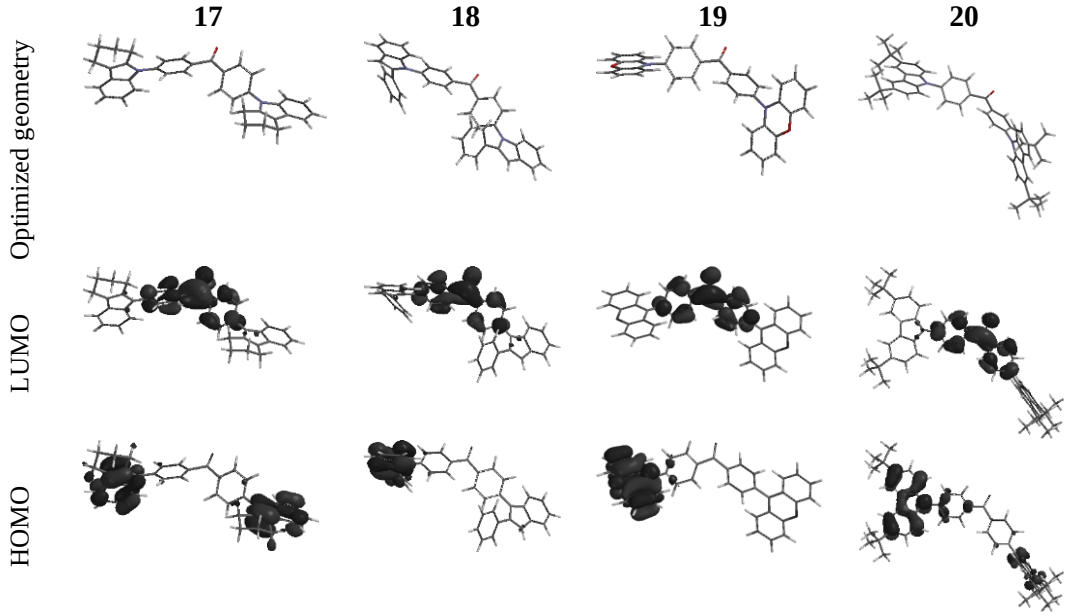

Figure 4.32. Optimized geometries and HOMO–LUMO distributions of compounds **17**–**20**

In their optimized ground-state geometries, dihedral angles between the phenyl rings of the benzophenone unit and the respective donors were calculated to be 177° for compound **17**, 22° for **18**, 94° for **19**, and 47° for **20**. In order to predict the energy difference (ΔE_{ST}) between the lowest S_1 and the lowest T_1 levels, time

dependent density functional theory (TD-DFT) calculations were performed based on the ground state geometries when optimized by the DFT (B3LYP/6-31G(d,p)). The spatial separation of the frontier orbitals of all these molecules resulted in rather small calculated ΔE_{ST} of 0.52 eV, 0.39 eV, 0.13 eV and 0.14 eV, respectively, indicating the potential of the compounds as TADF emitters.

4.4.4. Photophysical Properties

UV-vis absorption, photoluminescence and phosphorescence spectra of the dilute toluene solutions (10^{-5} M) and of thin films of compounds **17**–**20** were recorded. The luminescence of compounds **17**, **19**–**20** was excited with λ=365 nm wavelength, whereas the emission of compound **18** was excited with 325 nm. The spectra are shown in Figure 4.33. The photophysical characteristics of compounds **17**–**20** are summarized in Table 4.12.

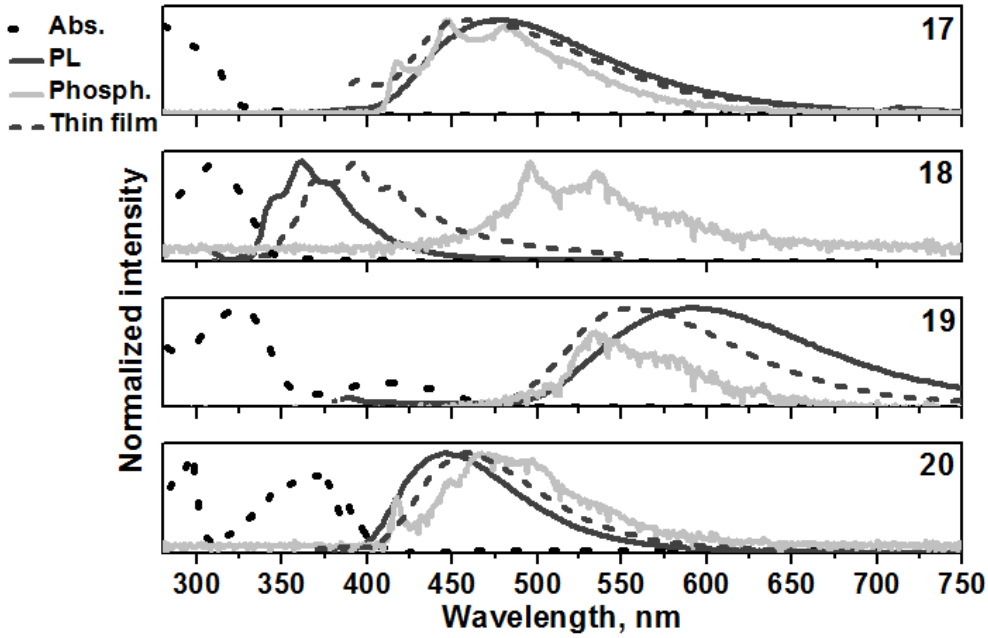

Figure 4.33. Absorption (at RT), photoluminescence and phosphorescence (77 °K) spectra of toluene solutions (10^{-5} M) of compounds **17–20**

UV-vis spectra of the derivatives were found to be very different and dependent on the nature of the substituents. 2-Phenylindole substituted benzophenone derivative **18** absorbs UV radiation up to 350 nm and has one absorption band with the maximum at 309 nm. This lowest energy absorption peak is bathochromically shifted with respect to that of unsubstituted 2-phenylindole. This observation can be attributed to the interaction between benzophenone and the donor fragments in the molecule. Tetrahydrocarbazole and ditertbutyl-carbazole substituted derivatives **17** and **20** have two absorption bands at 290 and 375 nm which can be attributed to n–π* and π–π* transitions of carbazole and the intramolecular charge transfer, respectively [201]. Phenoxazine-substituted

derivative **19** absorbs up to 450 nm, and its UV spectrum band is bathochromically shifted with respect to the spectra bands of the other researched benzophenone derivatives. Its lowest energy absorption peak can be attributed to the intramolecular charge transfer. The band gap values estimated from the absorption edges also depend on the nature of the substituents.

Table 4.11. Photophysical characteristics of compounds **17**–**20**

Compound		**17**	**18**	**19**	**20**
Toluene solution	λ_{ABS}, nm	310, 375	309	325, 425	295, 375
	λ_{PL}, nm	480	344, 362, 377	590	450
	Stokes shift, nm	105	35	165	75
	E_{Sonset}, eV	3.05	3.73	2.49	3.12
	E_{Tonset}, eV	3.03	2.84	2.49	3.02
	ΔE_{ST}, eV	0.02	0.89	~0	0.10
	E_g^{opt}, nm	3.03	3.42	2.52	3.04
	QY, %	7	18	9	5
	τ_1, ns	4.2	3.7	4.3	1.7
	τ_2, ns	-	-	61.2	-
	χ^2	1.29	1.17	1.10	0.92
Thin film	λ_{PL}, nm	458	370, 392, 414	556	460
	QY, %	5	3	3	3
	τ_1, ns	14.6	0.5	76.6	15.5
	τ_2, ns	152.6	3.3	855.3	987.8
	χ^2	1.29	1.13	1.31	1.03

λ_{Abs} – the wavelengths of the absorption maxima; λ_{PL}– the wavelengths of the emission maxima; Stokes shift=λ_{Fl}–λ_{Abs}; E_T – the triplet energy estimated as 1240/λ_{PH}; $\Delta E_{ST}=E_T-E_S$; $E_{ox\ onset\ vs.Fc}$ – the onset oxidation potential of the sample vs. the onset oxidation potential of ferrocene; IP_{PE} – the ionization potential estimated by employing the electron photoemission in air method; IP_{CV} – the ionization potential estimated by CV as $IP_{CV}=E_{onset\ ox\ vs.Fc}+5.1$ eV; E_g^{opt} – the optical band gap estimated as 1240/$\lambda_{Abs\ onset}$ where $\lambda_{Abs\ onset}$ is the wavelength of the onset of absorption; EA_{CV} – electron affinity estimated as $EA_{CV}=IP_{CV}-E_g^{opt}$; HOMO – the theoretically calculated HOMO energy; LUMO – the theoretically calculated LUMO energy; E_G=HOMO–LUMO.

The photoluminescence spectra of derivatives **17**–**20** are also highly influenced by the substitution pattern. The spectra of the solutions of compounds **17** and **20** are similarly broad and are characterized by a single peak in the blue region. The spectrum of the solution of compound **18** is blue-shifted with respect to those of

solutions of **17** and **20**. It is characterized by the vibrational structure. The photoluminescence spectrum of the solution of compound **19** is red-shifted with respect to those of the solutions of the other investigated derivatives of benzophenone.

The fluorescence spectra of thin films of compounds **17**–**20** are similar to the spectra of solutions. They are slightly red-shifted with respect to those of the solutions. The red shifts can be attributed to the intramolecular interaction in the solid state.

The solutions of compounds **17**–**20** showed rather low PLQY values ranging from 5% to 18%. The solid samples showed even lower PLQY values which can be explained by aggregation-induced fluorescence quenching.

The Stokes shift values of the dilute solutions of compounds **17**–**20** were estimated to range from 35 to 165 nm. It is known that the Stokes shift is highly dependent on the rigidity of the molecule [233]. High Stokes shift values of tetrahydrocarbazole- and phenoxazine-substituted benzophenones **17** and **19** implies that they are denoted by large rotational degrees of freedom.

Triplet energy values were obtained from the phosphorescence spectra of the toluene solutions of compounds **17**–**20**. These values are required for the estimation of the materials as the hosts of the emitting layers of OLEDs and for the evaluation of the differences between singlet and triplet energies (ΔE_{ST}). Compound **18** possesses a high triplet energy value but its ΔE_{ST} is the highest among this series. Low ΔE_{ST} values of compounds **17**, **19**–**20** allow to expect efficient singlet-triplet up-conversion. Similarly, low ΔE_{ST} values for compounds **19** and **20** were earlier reported [200, 201].

In order to determine the origin of the emission, the fluorescence decay curves of compounds **17**–**20** were recorded and analysed. Dilute solutions of benzophenone derivatives **17**, **18** and **20** exhibited single-exponential decays. The accuracy of the fits was characterized by $\chi 2$ values of 0.92–1.29. The dilute solution of compound **20** exhibited the shortest fluorescence lifetime of 1.7 ns. The solutions of **17** and **18** exhibited longer emission lifetimes of 4.2 and 3.7 ns, respectively. The solution of compound **19** exhibited bi-exponential fluorescence decay with the lifetimes of 4.28 and 61.24 ns. For the mathematical representation of the decay curve, the following equation was used:

$$F(t)= A + B1\exp(-t/\tau_1) + B2\exp(-t/\tau_2);$$

where where $\tau 1$ and $\tau 2$ represent the time constants, and B1 and B2 represent the amplitudes of the fast and slow components, respectively [234].

Fluorescence decays of the vacuum-deposited thin films of **17**–**20** exhibited double-exponential behaviour. The accuracy of the fits (χ^2) was characterised by values of 1.03–1.31. Compound **18** showed the shortest relaxation pathway with the τ_1 value of 0.51 and the τ_2 value of 3.3 ns indicating its origin as prompt fluorescence. The films of compounds **17**, **19**–**20** demonstrated significantly longer-lived excited species with the τ_2 values of 152.3–855.3 ns of delayed fluorescence.

The longest fluorescence lifetime values of the film of compound **19** correlates with its smallest singlet-triplet energy splitting (ΔE_{ST}).

The newly synthesized and characterized compound **17** can be considered as a potential TADF emitter based on its photophysical characteristics described above. Compound **18**, due to its high triplet energy value and the large optical band gap, can be regarded as a potential host material.

4.4.5. Electrochemical and Photoelectrical Properties

The electrochemical properties of the compounds were investigated by performing CV. The resulting data is summarized in Table 4.13. The ionization potential values were determined from oxidation potential after calibration against ferrocene. Cyclic voltammograms of compounds **17**–**20** are shown in Figure 4.34.

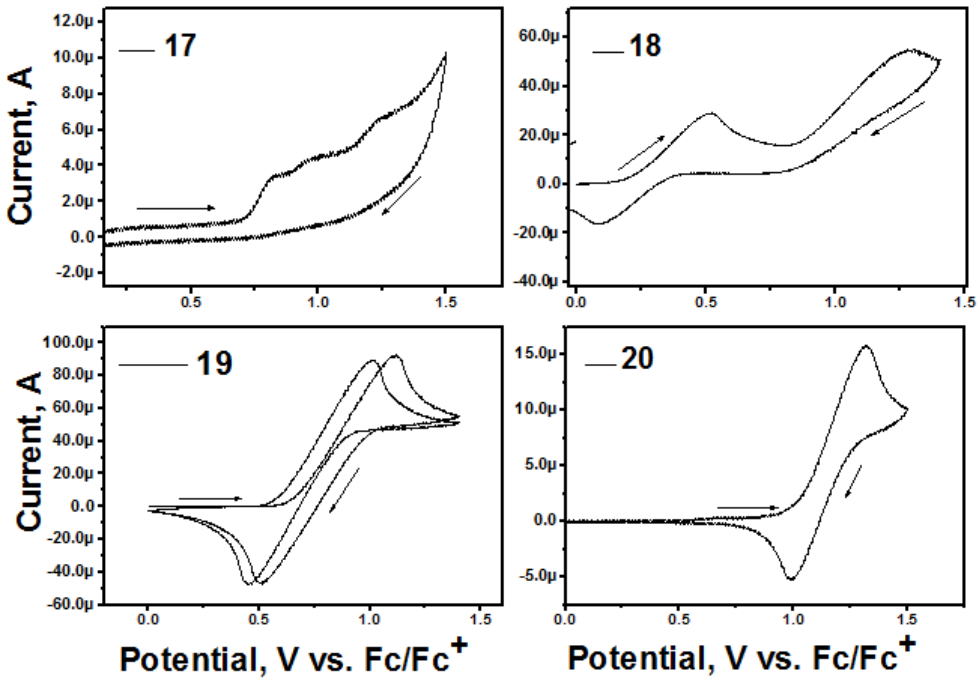

Figure 4.34. Cyclic voltammograms of 0.1M DCM solutions of compounds **17**–**20**

All the researched compounds except for **17** showed reversible oxidation suggesting electrochemical stability up to 1.5 V. During the multiple scans, no new oxidation peaks were observed. The solid-state ionization potential (IP_{CV}) and electron affinity (EA_{CV}) values were estimated from the oxidation onset potentials (E_{ox} onset vs. Fc) and optical band gaps (E_g^{opt}).

The theoretical energy values of HOMO and LUMO of compounds **17**–**20** were calculated by using the DFT/B3LYP/ 6-31 (d, p) method. The obtained values are summarized in Table 4.10. The theoretical HOMO energy values showed a similar trend to those of IP_{CV} values. The lowest HOMO level was estimated for compound **19**. The LUMO and EA_{CV} values are also in good agreement. These

values also correlate well with the optical band gap values estimated from the absorption band edges.

In order to get insight into the electrochemical processes of compounds **17**–**20** taking place on the electrodes during CV measurements, spectroelectrochemical analysis was performed. Figure 4.35 shows the results of UV-vis spectroelectrochemical measurements for compounds **18** and **19**.

Compound **19,** as well as compound **20**, showed fully reversible electrochemical oxidation during CV scans. Their UV-vis absorption bands have two peaks at 325 and 420 nm. In contrast to the previously described compounds **1**–**18**, the intensity of those peaks in the potential range of 0.4–1.2 V increased. A new absorption band appeared at 550 nm indicating the formation of the radical cations. This polaron band disappeared, and the increased peaks decreased to the initial state after applying the reduction potential of –0.4 V. The reversibility of the electrochemical process on the electrodes is confirmed as the absorption spectra after the reduction of compound **19** is identical to the original one, only with the difference of the increased intensity.

Table 4.12. Electrochemical and photoelectrical characteristics of compounds **17**–**20**

	Compound	**17**	**18**	**19**	**20**
	IP_{EP} , eV	5.54	5.53	5.46	5.74
	IP_{CV}, eV	5.70	5.72	5.45	5.84
	EA_{CV}, eV	2.67	2.30	2.93	2.80
Theoretical calculations	HOMO, eV	-5.27	-5.45	-4.81	-5.32
	LUMO, eV	-2.00	-1.99	-2.21	-1.91
	E_g^{opt}, eV	3.27	3.46	2.60	3.41
	E_S, eV	2.81	3.0	3.23	2.97
	E_T, eV	3.33	3.39	3.36	3.11
	ΔE_{S-T}	0.52	0.39	0.13	0.14

IP_{PE} – the ionization potential estimated by the photoelectron emission spectrometry in air; IP_{CV} – the ionization potential estimated by CV as $IP_{CV}=E_{onset\ ox\ vs.Fc}$ + 5.1 eV; E_g^{opt} – the optical band gap estimated as $1240/\lambda_{Abs\ onset}$ where $\lambda_{Abs\ onset}$ is the wavelength of the onset of absorption; EA_{CV} – electron affinity estimated as $EA_{CV}=IP_{CV}-E_g^{opt}$; HOMO – the theoretically calculated HOMO energy; LUMO – the theoretically calculated LUMO energy; E_G=HOMO–LUMO.

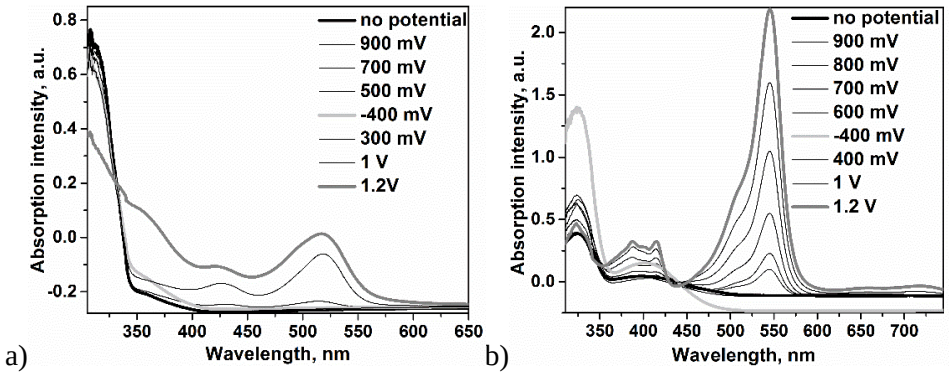

Figure 4.35. UV-vis spectra recorded during potentiostatic electrochemical oxidation of compounds **18** (a) and **19** (b)

The ionization potentials of the solid samples of compounds **17**–**20** were estimated by the electron photoemission in air method. The obtained electron photoemission spectra are shown in Figure 4.36 a, and the results are summarized in Table 4.13.

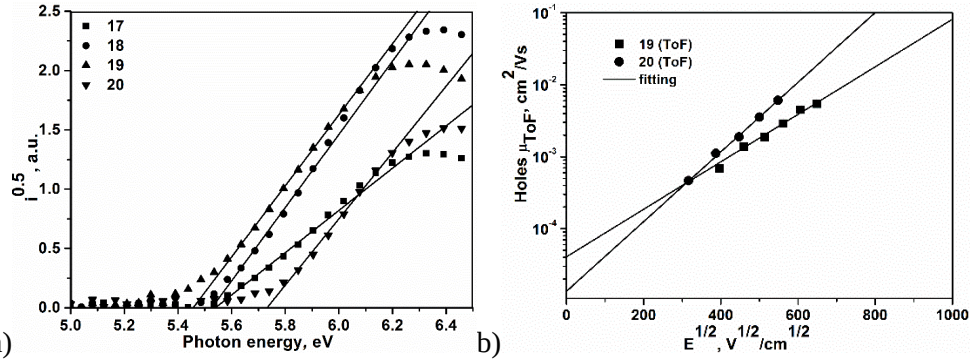

Figure 4.36. a) Photoelectron emission spectra of the films for vacuum deposited compounds **17**–**20**; b) electric field dependencies of hole-drift mobility for the vacuum deposited layers of compounds **19** and **20** measured by employing the TOF method at room temperature

The values of ionization potentials recorded by photoelectron emission spectrometry ranged from 5.46 eV to 5.79 eV. Compound **19** showed the lowest ionization potential (5.46 eV). The IP values obtained by employing both methods are in good agreement, and the decrease in the sequence is obtained: **20**>**17**≈**18**>**19**. These values also correlate well with optical band gap values. Small differences in the values of ionization potentials obtained by employing different methods can be explained by different environments in the solution and the solid state.

4.4.6.Charge-Transporting Properties

The charge-transporting properties of the layers prepared by thermal vacuum deposition were studied by using the TOF technique. Electric field dependencies of hole-drift mobilities on the layers of compounds **19** and **20** are shown in Figure 4.36 b. Charge mobilities of the other compounds (**17** and **18**) could not be measured by the employing the TOF method due to the fast recombination of the charges.

The values of hole-mobility of the layers of derivatives **19** and **20** were found to reach 2.9 $\times 10^{-3}$ cm^2/Vs and 6.1×10^{-3} cm^2/Vs, respectively, in the 3×10^5 V/cm electric field. Both compounds have been reported before [200, 201], but their charge-drift mobilities were not discussed. The hole-drift mobility values of derivatives **19** and **20** are characterised similarly to the previously discussed materials (see Chapters 4.1 and 4.3) by the continuous increase of the applied electric field which implies the dominating role of the energetic disorder.

In summary, it can be stated that the newly synthesized tetrahydrocarbazole- and 2-phenylindole-substituted benzophenone derivatives **17** and **18** can be used for the preparation of active layers of OLEDs as their properties adhere to the requirements.

The Main Results and Conclusions

1. Twin derivatives 2-phenylindole with different linkages between chromophores were synthesized, and their properties were investigated. It was established that:

1.1. 1,2-Bis(1-(4-vinylbenzyl)-2-phenylindol-3-yl)ethane can be subjected to thermally initiated self-polymerisation.

1.2. The synthesised compounds form molecular glasses with the glass transition temperatures ranging from 44 °C to 120 °C. The addition of the vinylbenzylgroup to the molecule increases its rigidity and consequently increases the glass transition temperature.

1.3. The calculated triplet energies E_T (2.29–2.30 eV) make these compounds suitable to serve as host materials for green OLEDs.

1.4. The ionization potential values estimated by photoelectron emission spectrometry are in the range of 5.16–5.79 eV.

1.5. The hole-drift mobilities in the layers of the compounds exceed 10^{-4} cm^2/Vs at high electric fields.

2. Derivatives of phenylindole and carbazole were synthesised and studied. It was established that:

2.1. Self-photopolymerization of the compounds featuring vinylbenzyl- reactive functional groups can occur both in the solid films and in solutions.

2.2. Electrochemical polymerization of the obtained derivatives can be performed at 0.4–0.7 V.

2.3. The synthesized compounds form glasses with the glass transition temperatures ranging from 85 °C to 134 °C.

2.4. The narrowly localized π-conjugation systems in the molecules determine their high triplet energies (2.88–3.01 eV) and low ionisation potential values (5.45–5.88 eV).

2.5. 9-[(Oxiran-2-yl)methyl]-3-[[1-{(oxiran-2-yl)methyl}-2-phenyl-indol-3-yl][9-{(oxiran-2-yl)methyl}-carbazol-3-yl]methyl]-carbazole and 3-{[1-(4-vinylbenzyl)-2-phenyl-1H-indol-3-yl]methyl}-9-ethyl-9H-carbazole were tested as the host materials for iridium-based light emitting guests. The devices exhibited the turn-on voltage of 3.1 V, the brightness up to 11900 cd/m^2, and the external quantum efficiency up to 2.9%.

3. Indole and benzo[b]carbazole derivatives were easily synthesised and fully characterized. It was established that:

3.1. These derivatives form molecular glasses with the glass transition temperatures in the range of 86–116 °C.

3.2. The solutions of derivatives featuring substituents at C-11 position of the benzo[b]carbazole moiety exhibit higher fluorescence quantum yield values (63–67%) than the solutions of the compounds having substituents at C-6 position (~40%).

3.3. The ionisation potential values estimated by cyclic voltammetry are in the range of 5.45–5.60 eV, while the values obtained by photoelectron emission spectrometry are in the range of 5.16–5.29 eV.

3.4. Hole and electron drift mobilities of the layers of the benzo[b]carbazole derivatives clearly exceed 10^{-3} $cm^2/(Vs)$ at high electric fields at room temperature.

3.5. 1-(1-(Naphthalen-1-yl)-1H-indol-3-yl)-5-(naphthalen-1-yl)-5H-benzo[b]carbazole and 5-(naphthalen-1-yl)-6-(1-(naphthalen-1-yl)-1H-indol-3-yl)-5H-benzo[b]carbazole were used as the blue emitters in non-doped light emitting diodes. The devices exhibited the turn-on voltage of 3.6 V, the brightness up to 17700 cd/m^2, and the external quantum efficiency up to 3.4%.

4. Benzophenone derivatives with various donor moieties were easily synthesised and investigated. It was established that:

4.1. These derivatives form glasses with glass transition temperatures of 82 °C and 160 °C respectively.

4.2. Tetrahydrocarbazole- and 2-phenylindole-substituted derivatives have high triplet energy values exceeding 2.84 eV, which makes them suitable as the host materials in blue PhOLEDs.

4.3. The ionization potential values depend on the nature of the donor substituents and range from 5.46 eV to 5.74 eV. The lowest ionization potential was shown by phenoxazine-substituted benzophenone.

4.4. Hole drift mobilities of the layers of donor-substituted benzophenone derivatives clearly exceeded 10^{-3} $cm^2/(Vs)$ at high electric fields at room temperature.

REFERENCES

1. TREMBLAY, J.F. The Rise of OLED Displays. *Chemical & Engineering News.* 2016, 94(28), 30–34. ISSN 0009–2347.

2. HIRATA, S., and SHIZU, K. Organic Light-Emitting Diodes: High-Throughput Virtual Screening. *Nature Materials*. 2016, 15, 1056–1057. ISSN 1476–4660.

3. SOKOLOV, A.N., *et al*. Chemical and Engineering Approaches to Enable Organic Field-Effect Transistors for Electronic Skin Applications. *Accounts of Chemical Research*. 2012, 45(3), 361–71. ISSN 0001–4842.

4. GÓMEZ-BOMBARELLI, R., *et al*. Design of Efficient Molecular Organic Light-Emitting Diodes by a High-Throughput Virtual Screening and Experimental Approach. *Nature Materials.* 2016, 15, 1120–1127. ISSN 1476–4660.

5. DUGGAL, A.R., *et al*. Solution-Processed Organic Light-Emitting Diodes for Lighting. *Journal of Display Technology.* 2007, 3(2), 184–192. ISSN 1558–9323.

6. NAGAI, Y. *et al*. Effect of Substituents in a Series of Carbazole-Based Host-Materials toward High-Efficiency Carbene-Based Blue OLEDs. *Journal of Materials Chemistry C*. 2016, 4, 9476–9481. ISSN 2050–7526.

7. IWAN, A., and SEK, D. Polymers with Triphenylamine Units: Photonic and Electroactive Materials. *Progress in Polymer Science.* 2011, 36(10), 1277–1325. ISSN 0079–6700.

8. SLODEK, A., et al. Highly Luminescence Anthracene Derivatives as Promising Materials for OLED Applications. *European Journal of Organic Chemistry.* 2016, 23, 4020–4031. ISSN: 1099–0690.

9. HATAKEYAMA, T., *et al*. Ultrapure Blue Thermally Activated Delayed Fluorescence Molecules: Efficient HOMO–LUMO Separation by the Multiple Resonance Effect. *Advanced Materials*. 2016, 28(14), 2777–2781. ISSN 1521–4095.

10. ZOSTAUTIENE, R., *et al*. Electro-Active Oligomers Containing Pendent Carbazolyl or Indolyl Groups as Host Materials for OLEDs. *Journal of Applied Polymer Science*. 2011, 122(2), 908–913. ISSN 1097–4628.

11. TANG, C.W. and VAN SLYKE, S.A. Organic Electroluminescent Diodes. *Applied Physics Letters*. 1987, 51(12), 913–915, ISSN 1077–3118.

12. SEKINE, C. *et al*. Recent Progress of High Performance Polymer OLED and OPV Materials for Organic Printed Electronics. *Science and Technology of Advanced Materials.* 2014, 15(3), 034203–034218, ISSN 1878–5514.

13. ZHOU, G., *et al*. Functionalization of Phosphorescent Emitters and Their Host Materials by Main-Group Elements for Phosphorescent Organic Light-Emitting Devices. *Chemical Society Reviews*. 2015, 44, 8484–8575, ISSN 0306–0012.

14. SASABE, H. *et al*. Extremely Low Operating Voltage Green Phosphorescent Organic Light-Emitting Devices. *Advanced Functional Materials*. 2013, 23, 5550–5555. ISSN 1616–3028.

15. HAN, T.H., *et al*. Extremely Efficient Flexible Organic Light-Emitting Diodes with Modified Graphene Anode. *Nature Photonics*. 2012, 6(2), 105–110. ISSN 1749–4885.

16. XU, R., *et al*. Resent Advances in Flexible Organic Light-Emitting Diodes. *Journal of Materials Chemistry C.* 2016, 4, 9166 – 9142. ISSN 2050–7526.

17. HÖFLE, S. *et al*. Solution Processed, White Emitting Tandem Organic Light-Emitting Diodes with Inverted Device Architecture. *Advanced Materials.* 2014, 26(30), 5155–5159. ISSN 1521–4095.

18. LEE, S.J. *et al*. Effect of a Broad Recombination Zone with a Triple-Emitting Layer on the Efficiency of Blue Phosphorescent Organic Light-Emitting Diodes. *Electronic Materials Letters.* 2014, 10(6), 1127–1131. ISSN 2093–6788.

19. HA, T., *et al*. Organic Light-Emitting Devices Based on Solution-Processable Small Molecular Emissive Layers Doped with Interface-Engineering Additives. *RSC Advances*. 2016, 6, 33063–33071. ISSN 2046–2069.

20. IRMIA-VLADU, M. "Green" Electronics: Biodegradable and Biocompatible Materials and Devices for Sustainable Future. *Chemical Society Reviews*. 2014, 43, 588. ISSN 1460–4744.

21. KROTKUS, S., *et al*. Photo-Patterning of Highly Efficient State-of-The-Art Phosphorescentoleds Using Orthogonal Hydrofluoroethers. *Advanced Optical Materials*. 2014, 2(11), 1043–1048. ISSN 2195–1071.

22. KIM, H.S., *et al*. Fabrication of a Microball Lens Array for OLEDs Fabricated Using a Monolayer Microsphere Template. *Electronic Materials Letters*. 2013, 9(1), 39–42. ISSN 2093–6788.

23. CHOU, H.H., *et al*., A Chameleon-Inspired Stretchable Electronic Skin with Interactive Colour Changing Controlled by Tactile Sensing. *Nature Communications.* 2015, 6, 8011–8021. ISSN 2041–1723.

24. CHANG, Y.L. and LU, Z.H. White Organic Light-Emitting Diodes For Solid-State Lighting. *Journal of Display Technology*. 2013, 9(6), 459–468. ISSN 1551–319X.

25. LIU, X.K., *et al*. Novel Blue Fluorophor with High Triplet Energy Level for High Performance Single-Emitting-Layer Fluorescence and Phosphorescence Hybrid White Organic Light-Emitting Diodes. *Chemistry of Materials*. 2013, 25(21), 4454–4459. ISSN 1520–5002.

26. XIAO, L., *et al*. Recent Progresses on Materials for Electrophosphorescent Organic Light-Emitting Devices. *Advanced Materials*. 2011, 23(8), 926–952. ISSN 1521–4095.

27. CHEN, Y.X., *et al*. Internal Quantum Efficiency Drop Induced by the Heat Generation Inside of Light Emitting Diodes (LEDs). *Chinese Physics B*. 2011, 20, 017204. ISSN1674–1056

28. SCHAER, M., *et al*. Water Vapor and Oxygen Degradation Mechanisms in Organic Light Emitting Diodes. *Advanced Functional Materials*. 2001, 11, 116–121. ISSN 1616–3028.

29. KANG, J.W., *et al*. A Host Material Containing Tetraphenylsilane for Phosphorescent OLEDs with High Efficiency and Operational Stability. *Organic Electronics*. 2008, 9(4), 452–460. ISSN 1566–1199.

30. SASABE, H., *et al*. 2-Phenylpyrimidine Skeleton-Based Electron-Transport Materials for Extremely Efficient Green Organic Light-Emitting Devices. *Chemical Communications*. 2008, (44), 5821–5823. ISSN 1364–548X.

31. HOU, L., *et al*. Efficient Solution-Processed Small-Molecule Single Emitting Layer Electrophosphorescent White Light-Emitting Diodes. *Organic Electronics*. 2010, 11(8), 1344–1350. ISSN 1566–1199.

32. ALLWOOD, J.M., *et al*. Material Efficiency: A White Paper. *Resources, Conservation and Recycling*. 2011, 55, 362–381. ISSN 0921–3449.

33. YANG, X.H., and NEHER, D. Polymer Electrophosphorescence Devices with High Power Conversion Efficiencies. *Applied Physics Letters*. 2004, 84(14), 2476–2478. ISSN 1077–3118

34. LAMANSKY, S., *et al*. Molecularly Doped Polymer Light Emitting Diodes Utilizing Phosphorescent Pt(II) and Ir(III) Dopants. *Organic Electronics*. 2001, 2(1), 53–62. ISSN 1566–1199.

35. DUAN, L., *et al*. Solution Processable Small Molecules for Organic Light-Emitting Diodes. *Journal of Materials Chemistry*. 2010, 20, 6392–6407. ISSN 1364–5501.

36. YOOK, K.S., and LEE, J.Y. Small Molecule Host Materials for Solution Processed Phosphorescent Organic Light-Emitting Diodes. *Advanced Materials*. 2014, 26(25), 4218–4233. ISSN 1521–4095.

37. XIANG, C., *et al*. Phosphorescent Organic Light Emitting Diodes with a Cross-Linkable Hole Transporting Material. *Organic Electronics*. 2014, 15(7), 1702–1706. ISSN 1566–1199.

38. BURROUGHES, J.H. *et al*. Light-Emitting Diodes Based on Conjugated Polymers. *Nature*. 1990, 347, 539–541. ISSN 0028−0836.

39. YANG, X. *et al*. Highly Efficient Polymeric Electrophosphorescent Diodes. *Advanced Materials*. 2006, 18(7), 948–954. ISSN 1521–4095.

40. GONG, X., *et al*. High-Efficiency Polymer-Based Electrophosphorescent Devices. *Advanced Materials*. 2002, 14(8), 581–585. ISSN 1521–4095.

41. MÜLLEN, K., SCHERF, U. *Organic Light-Emitting Devices: Synthesis, Properties and Applications.* Wiley-VCH Verlag GMbH & Co. KGaA: Weinheim, 2006.

42. HUANG, J., *et al*. The Development of Anthracene Derivatives for Organic Light-Emitting Diodes. *Journal of Materials Chemistry*. 2012, 22, 10977−10989. ISSN 1364–5501.

43. BALDO, M.A., *et al*. Highly Efficient Phosphorescent Emission from Organic Electroluminescent Devices. *Nature*. 1998, 395, 151−154. ISSN 0028–0836.

44. XIAO, L., *et al*. Nearly 100% Internal Quantum Efficiency in an Organic Blue-Light Electrophosphorescent Device Using a Weak Electron Transporting Material with a Wide Energy Gap. *Advanced Materials*. 2009, 21, 1271−1274. ISSN 1521–4095.

45. ADACHI, C., *et al*. Nearly 100% Internal Phosphorescence Efficiency in an Organic Light-Emitting Device. *Journal of Applied Physics*. 2001, 90(10), 5048−5051. ISSN 1089–7550.

46. MATSUI, N., *et al*. Charge-Carrier Transport and Triplet Exciton Diffusion in a Blue Electrophosphorescent Emitting Layer. *Journal of Applied Physics.* 2005, 97(12), 123512–123517. ISSN 1089–7550.

47. CHOUKRI, H., *et al*. White Organic Light-Emitting Diodes with Fine Chromaticity Tuning via Ultrathin Layer Position Shifting. *Applied Physics Letters.* 2006, 89, 183513–183517. ISSN 1077–3118.

48. YOU, Y., and PARK, S.Y. Phosphorescent Iridium(III) Complexes: toward High Phosphorescence Quantum Efficiency through Ligand Control. *Dalton Transactions.* 2009, 1267–1282. ISSN 1477–9234.

49. YANG, X.L., *et al*. Highly Efficient Phosphorescent Materials Based on Platinum Complexes and Their Application in Organic Light-Emitting Devices (OLEDs). *Platinum Metals Review*. 2013, 57(1), 2–16. ISSN 2056–5135.

50. LIAO, J.L., *et al*. Os(II) Metal Phosphors Bearing Tridentate 2,6-di(pyrazol-3-yl)pyridine Chelate: Synthetic Design, Characterization and Application in OLED Fabrication. *Journal of Materials Chemistry C*. 2014, 2, 6269–6282. ISSN 2050–7526.

51. KIM, S.Y., *et al*. Organic Light-Emitting Diodes with 30% External Quantum Efficiency Based on a Horizontally Oriented Emitter. *Advanced Functional Materials*. 2013, 23, 3896–3900. ISSN 1616–3028.

52. LEE, C.W., and LEE, J.Y. Above 30% External Quantum Efficiency in Blue Phosphorescent Organic Light-Emitting Diodes Using Pyrido[2,3-b]indole Derivatives as Host Materials. *Advanced Materials*. 2013, 25, 5450–5454. ISSN 1521–4095.

53. KAPPAUN, S., *et al*. Phosphorescent Organic Light-Emitting Devices: Working Principle and Iridium Based Emitter Materials. *International Journal of Molecular Sciences.* 2008, 9(8), 1527–1547. ISSN 1661–6596.

54. REINEKE, S. Organic Light-Emitting Diodes: Phosphorescence Meets Its Match. *Nature Photonics*. 2014, 8, 269–270. ISSN 1749–4885.

55. HOLMES, R.J. *et al*. Blue Organic Electrophosphorescence Using Exothermic Host–Guest Energy Transfer. *Applied Physics Letters.* 2003, 82, 2422–2424. ISSN 1077–3118.

56. YANG, X., *et al*. Functionalization of Phosphorescent Emitters and Their Host Materials by Main-Group Elements for Phosphorescent Organic Light-Emitting Devices. *Chemical Society Reviews*. 2015, 44(23), 8484–8575. ISSN 1460–4744.

57. LEE, B.M. *et al*., Highly Efficient Blue Organic Light-Emitting Diodes Using Dual Emissive Layers with Host-Dopant System. *Journal of Photonics for Energy*. 2013, 3, 33598. ISSN 1947–7988.

58. ADAMOVICH, V.I. High-Performance Phosphorescent White-Stacked Organic Light-Emitting Devices For Solid-State Lighting. *Journal of Photonics for Energy.* 2012, 2(1), 21202. ISSN 1947–7988.

59. ZHAO, Y. *et al*. New Benzimidazole-Based Bipolar Hosts: Highly Efficient Phosphorescent and Thermally Activated Delayed Fluorescent Organic Light-Emitting Diodes Employing the Same Device Structure. *ACS Applied Materials and Interfaces*, 2016, 8(4), 2635–2643. ISSN 1944–8244.

60. GUDEIKA, D. *et al*., Derivative of Oxygafluorene and di-tert-butyl Carbazole as the Host with very High Hole Mobility for High-Efficiency Blue Phosphorescent Organic Light-Emitting Diodes. *Dyes and Pigments.* 2016, 130, 298–305. ISSN 0143–7208.

61. PARKER, C.A., and HATCHARD, C.G. Triplet–Singlet Emission in Fluid Solutions. Phosphorescence of Eosin. *Transactions of the Faraday Society*. 1961, 57, 1894. ISSN 0014–7672.

62. UOYAMA, H., *et al*. Highly Efficient Organic Light-Emitting Diodes from Delayed Fluorescence. *Nature*. 2012, 492(7428), 234–238. ISSN 0028–0836.

63. GOUSHI, K., *et al*. Organic Light-Emitting Diodes Employing Efficient Reverse Intersystem Crossing for Triplet-to-Singlet State Conversion. *Nature Photonics.* 2012, 6(4), 253–258. ISSN 1749–4885.

64. MÉHES, G., *et al*. Influence of Host Matrix on Thermally-Activated Delayed Fluorescence: Effects on Emission Lifetime, Photoluminescence Quantum Yield, and Device Performance. *Organic Electronics.* 2014, 15(9), 2027–2037. ISSN 1566–1199.

65. SUZUKI, K., *et al*. Triarylboron-Based Fluorescent Organic Light-Emitting Diodes with External Quantum Efficiencies Exceeding 20%. *Angewandte Chemie – International Edition*. 2015, 54(50), 15231–15235. ISSN 1521–3773.

66. DEATON, J.C., *et al*. E-Type Delayed Fluorescence of a Phosphine-Supported $Cu_2(mu\text{-}NAr_2)_2$ Diamond Core: Harvesting Singlet and Triplet Excitons in OLEDs. *Journal of American Chemical Society*. 2010, 132(27), 9499–9508. ISSN 0002–7863.

67. DATA, P. *et al*. Exciplex Enhancement as a Tool to Increase OLED Device Efficiency. *Journal of Physical Chemistry C*. 2016, 120(4), 2070–2078. ISSN 1932–7447.

68. GIBSON, J., *et al*. The Importance of Vibronic Coupling for Efficient Reverse Intersystem Crossing in Thermally Activated Delayed Fluorescence Molecules. *Chemical Physics and Physical Chemistry*. 2016, 11, 1–7. ISSN 1439–7641.

69. DOS SANTOS, P.L., *et al*. Engineering the Singlet-Triplet Energy Splitting in a TADF Molecule. *Journal of Materials Chemistry C*. 2016, 4, 3815–3824. ISSN 2050–7526.

70. HASHIMOTO, M., *et al*. Highly Efficient Green Organic Light-Emitting Diodes Containing Luminescent Three-Coordinate Copper(I) Complexes. *Journal of American Chemical Society*. 2011, 133(27), 10348–10351. ISSN 0002–7863.

71. ZINK, D.M. *et al*. Synthesis, Structure, and Characterization of Dinuclear Copper(I) Halide Complexes with P^N Ligands Featuring Exciting Photoluminescence Properties. *Inorganic Chemistry*. 2013, 52(5), 2292–2305. ISSN 0020–1669.

72. DOS SANTOS, P.L., *et al*. Investigation of the Mechanisms Giving Rise to TADF in Exciplex States. *Journal of Physical Chemistry C.* 2016, 120 (32), 18259–18267. ISSN 1932–7447.

73. ISHIMATSU, R., *et al*. Electrogenerated Chemiluminescence of Donor–Acceptor Molecules with Thermally Activated Delayed Fluorescence. *Angewandte Chemie – International Edition*. 2014, 53, 6993–6996. ISSN 1521–3773.

74. DOS SANTOS, P.L., *et al*. Using Guest–Host Interactions to Optimize the Efficiency of TADF OLEDs. *The Journal of Physical Chemistry Letters*. 2016, 7(17), 3341–3346. ISSN 1948–7185.

75. BALEIZÃO, C., and BERBERAN-SANTOS, M.N. Thermally Activated Delayed Fluorescence as a Cycling Process between Excited Singlet and Triplet States: Application to the Fullerenes. *The Journal of Chemical Physics.* 2007, 126, 204510. ISSN 1089–7690.

76. REINEKE, S. Novel Emission Types in Organic Molecules: TADF and Biluminescence, *Proccedings of SPIE*. 2015, 9566. ISSN 1996–756X.

77. YERSIN, H., *et al*. The Triplet State of Organo-Transition Metal Compounds. Triplet Harvesting and Singlet Harvesting for Efficient OLEDs. *Coordination Chemistry Reviews*. 2011, 255, 2622−2652. ISSN 0010−8545.

78. KÖHLER, A. and BÄSSLER, H. Triplet States in Organic Semiconductors. *Material Science and Engineering Reports*. 2009, 66, 71−109. ISSN 0927−796X.

79. VOLTZ, D. Review of Organic Light-Emitting Diodes with Thermally Activated Delayed Fluorescence Emitters for Energy-Efficient Sustainable Light Sources and Displays. *Journal of Photonics for Energy*. 2016, 6(2), 020901. ISSN 1947−7988.

80. KONDAKOV, D., *et al*. Triplet Annihilation Exceeding Spin Statistical Limit in Highly Efficient Fluorescent Organic Light-Emitting Diodes. *Journal of Applied Physics*. 2009, 106(12), 124510. ISSN 0021−8979.

81. SHIZU, K. *et al*. Strategy for Designing Electron Donors for Thermally Activated Delayed Fluorescence Emitters. *Journal of Physical Chemistry C*. 2015, 119(3), 1291–1297. ISSN 1932–7447.

82. OH, C.S. *et al*. Molecular Design of Host Materials for High Power Efficiency in Blue Phosphorescent Organic Light-Emitting Diodes Doped with an Imidazole Ligand Based Triplet Emitter. *Journal of Materials Chemistry C*. 2016, 4, 3792–3797. ISSN 2050–7526.

83. UDAGAWA, K., *et al*. Low-Driving-Voltage Blue Phosphorescent Organic Light-Emitting Devices with External Quantum Efficiency of 30%. *Advanced Materials.* 2014, 26(29), 5062–5066. ISSN 1521–4095.

84. WEBER, E., and OTHMER, K. *Encylopedia of Chemical Technology*. Wiley, Chichester, 1995.

85. ENACHE, T.A., and OLIVEIRA-BRETT, A.M. Pathways of Electrochemical Oxidation of Indolic Compounds. *Electroanalysis*. 2011, 23(6), 1337–1344. ISSN 1521–4109.

86. GEIGER, T., *et al*. Low-Band Gap Polymeric Cyanine Dyes Absorbing in the NIR Region. *Macromolecular Rapid Communications*. 2008, 29(8), 651–658. ISSN 1521–3927

87. CHANG, G. *et al*. Synthesis of Indole-Based Functional Polymers with Well-Defined Structures via a Catalyst-Free C–N Coupling Reaction. *RSC Advances*. 2014, 4(58), 30630. ISSN 2046–2069.

88. SURAMWAR, N.V., *et al*. Green Synthesis of Predominant (1 1 1) Facet CuO Nanoparticles: Heterogeneous and Recyclable Catalyst for N-Arylation of Indoles. *Journal of Molecular Catalysis A: Chemical.* 2012, 359, 28–34. ISSN 1381–1169.

89. POTAVATHRI, S., *et al*. Regioselective Oxidative Arylation of Indoles Bearing N-Alkyl Protecting Groups: Dual C−H Functionalization via a Concerted Metalation−Deprotonation Mechanism. *Journal of the American Chemical Society*. 2010, 132, 14676. ISSN 0002−7863.

90. GŁOWACKI, E.D., *et al*. 25th Anniversary Article: Progress in Chemistry and Applications of Functional Indigos for Organic Electronics. *Advanced Materials*. 2013, 25, 6783. ISSN 1521–4095.

91. SHARMA, G.D., *et al*. Indole and Triisopropyl Phenyl as Capping Units for a Diketopyrrolopyrrole (DPP) Acceptor Central Unit: an Efficient Dead Type Small Molecule for Organic Solar Cells. *RSC Advances*. 2014, 4, 732–742. ISSN 2046–2069.

92. KRASOVITSKII, B.M., and BOLOTIN, B.M. *Organic Luminescent Materials.* VCH, New York, 1988.

93. HWU, J.R. *et al*. Fine Tuning of Blue Photoluminescence from Indoles for Device Fabrication. *Journal of Materials Chemistry*. 2009, 19(19), 3084. ISSN 1364–5501.

94. LI, Q. *et al*. New Indole-Based Metal-Free Organic Dyes for Dye-Sensitized Solar Cells. *The journal of physical chemistry B.* 2009, 113(44), 14588–95. ISSN 1520–6106.

95. NEWMAN, S.G., and LAUTENS, M. The Role of Reversible Oxidative Addition in Selective Palladium (0)-Catalyzed Intramolecular Cross-Couplings of Polyhalogenated Substrates: Synthesis of Brominated Indoles. *Journal of the American Chemical Society*. 2010, 132, 11416−11417. ISSN 0002−7863.

96. JEON, S., *et al*. N-Phenylindole-Diketopyrrolopyrrole-Containing Narrow Band-Gap Materials for Dopant-Free Hole Transporting Layer of Perovskite Solar Cell. *Organic electronics*. 2016, 37, 134–140. ISSN 1566–1199.

97. SHI, H., *et al*. The Synthesis of Novel AIE Emitters with the Triphenylethene-Carbazole Skeleton and Para-/Meta-Substituted Arylboron Groups and Their Application in Efficient Non-Doped OLEDs. *Journal of Materials Chemistry C*. 2016, 4(6), 1228–1237. ISSN 2050–7526.

98. SUZUKI, K., *et al*. Triarylboron-Based Fluorescent Organic Light-Emitting Diodes with External Quantum Efficiencies Exceeding 20%. *Angewandte Chemie - International Edition*. 2015, 54(50), 15231–15235. ISSN 1521–3773.

99. MOONSIN, P., *et al*. Carbazole Dendronised Triphenylamines as Solution Processed High Tg Amorphous Hole-Transporting Materials for Organic Electroluminescent Devices. *Chemical Communications*. 2012, 48(28), 3382. ISSN 1364–548X.

100. SHIH, P.I., *et al*., Novel Carbazole/Fluorene Hybrids: Host Materials for Blue Phosphorescent OLEDs. *Organic Letters*. 2006, 8(13), 2799–2802. ISSN 1523–7060.

101. RADENKOVIĆ, S., *et al*. Effect of Benzo-Annelation on Local Aromaticity in Heterocyclic Conjugated Compounds. *Journal of Physical Chemistry A*. 2014, 118(49),11591–11601. ISSN 1089–5639.

102. KIRKUS, M. *et al*. Triindolylmethane-Based High Triplet Energy Glass-Forming Electroactive Molecular Materials. *Synthetic Metals*. 2008, 158(6), 226–232. ISSN 0379–6779.

103. CHEN, Y.C., *et al*. High Triplet Energy Polymer as Host for Electrophosphorescence with High Efficiency. *Journal of the American Chemical Society*. 2006, 128(26), 8549. ISSN 0002−7863.

104. KIRKUS, M. *et al*., New Indole-Carbazole Hybrids as Glass-Forming High-Triplet-Energy Materials. *Synthetic Metals*. 2009, 159(7–8), 729–734. ISSN 0379–6779.

105. TSAI, M.H., *et al*. 3-(9-carbazolyl)carbazoles and 3,6-Di(9-carbazolyl)carbazoles as Effective Host Materials for Efficient Blue Organic Electrophosphorescence. *Advanced Materials*. 2007, 19(6), 862–866. ISSN 1521–4095.

106. BORISEVICH, N.A. *et al*. Nature of Delayed Luminescence of N-methylindole and Indole in the Gas Phase. *Journal of Applied Spectroscopy*. 2007, 74(3), 379–384. ISSN 1573–8647.

107. BARONAS, P., *et al*. High-Triplet-Energy Carbazole and Fluorene Tetrads. *Journal of Luminescence*. 2016, 169, 256–265. ISSN 0022–2313.

108. DUMUR, F. Carbazole-Based Polymers as Hosts For Solution-Processed Organic Light-Emitting Diodes: Simplicity, Efficacy. *Organic Electronics*. 2015, 25, 345–361. ISSN 1566–1199.

109. KERUCKAS, J., *et al*. 3,6-Bis(indol-1-yl)-9-phenylcarbazoles as Electroactive Materials for Electrophosphorescent Diodes. *Dyes and Pigments*. 2014, 100, 66–72. ISSN 0143–7208.

110. GRAZULEVICIUS, J.V., et al. Photophysics of Carbazole-Containing Systems. 3. Fluorescence of Carbazole-Containing Oligoethers in Dilute Solution. *Macromolecules* 1998, 31, 4820–7. ISSN 0024–9297.

111. ENDO, A., and ADACHI, C. Photoluminescence Characteristics of tris(2-phenylquinoline)iridium (III) Dispersed in an Iridium Complex Host Layer. *Chemical Physics Letters*. 2009, 483, 224–6. ISSN 0009–2614.

112. SHEN, H., *et al*. Highly Efficient Blue Green Quantum Dot Light-Emitting Diodes Using Stable Low-Cadmium Quaternary-Alloy ZnCdSSe/ZnS Core/Shell Nanocrystals. *ACS Applied Materials and Interfaces.* 2013, 5, 4260–5. ISSN 1944–8252.

113. KÖHLER, A., and BÄSSLER, H. Triplet States in Organic Semiconductors. *Materials Science and Engineering R.* 2009, 66, 71–109. ISSN 0927–796X.

114. KALINOWSKI, J., *et al*. Mixing of Excimer and Exciplex Emission: a New Way to Improve White Light Emitting Organic Electrophosphorescent Diodes. *Advanced Materials*, 2007, 19(22), 4000–4005. ISSN 1521–4095.

115. TSAI, T.C., *et al*. A New Ambipolar Blue Emitter for NTSC Standard Blue Organic Light-Emitting Device. *Organic Electronics.* 2009, 10, 158−162. ISSN 1566–1199.

116. UOYAMA, H., *et al*. Highly Efficient Organic Light-Emitting Diodes from Delayed Fluorescence. *Nature.* 2012, 492, 234−238. ISSN 0028–0836.

117. TOMKEVICIENE, A., *et al*. Dimethyldiphenylamino-Substituted Carbazoles as Electronically Active Molecular Materials. *Dyes and Pigments.* 2013, 96, 574−580. ISSN 0143–7208.

118. VOLYNIUK, D., *et al*. Highly Efficient Blue Organic Light-Emitting Diodes Based on Intermolecular Triplet-Singlet Energy Transfer. *The Journal of Physical Chemistry C*. 2013, 117(44), 22538–22544. ISSN 1932–7455.

119. DONG, Q., *et al*., Novel Spirofluorene/Indole/Carbazole-Based Hole Transport Materials with High Triplet Energy for Efficient Green Phosphorescent Organic Light-Emitting Diodes. *Dyes and Pigments*. 2017, 137, 84–90. ISSN 0143–7208.

120. TAO, Y., *et al*. Highly Efficient Phosphorescent Organic Light-Emitting Diodes Hosted by 1,2,4-Triazole-Cored Triphenylamine Derivatives: Relationship between Structure and Optoelectronic Properties. *The Journal of Physical Chemistry C.* 2010, 114, 601–9. ISSN 1932–7455.

121. JEON, S.O., and LEE, Y.J. Fluorenobenzofuran as the Core Structure of High Triplet Energy Host Materials for Green Phosphorescent Organic Light-Emitting Diodes. *Journal of Materials Chemistry.* 2012, 22, 10537–41. ISSN 1364–5501.

122. CARDONA, C.M., *et al*. Electrochemical Considerations for Determining Absolute Frontier Orbital Energy Levels of Conjugated Polymers for Solar Cell Applications. *Advanced Materials*. 2011, 23, 2367–2371. ISSN 1521–4095.

123. RYBAKIEWICZ, R., *et al*. Electronic Properties of Semiconducting Naphthalene Bisimide Derivatives–Ultraviolet Photoelectron Spectroscopy versus Electrochemistry. *Electrochimica Acta*. 2013, 96, 13–17. ISSN 0013–4686.

124. SAKUDA, E., *et al*. Extremely Large Dipole Moment in the Excited Singlet State of tris{[p-(N,N-dimethylamino)phenylethynyl]duryl}borane. *The Journal of Physical Chemistry A*. 2010, 114, 9144–50. ISSN 1520–5215.

125. CHEN, Y., *et al*. Highly Efficient Bipolar Host Material Based on Indole and Triazine Moiety for Red Phosphorescent Light-Emitting Diodes. *Dyes and Pigments*. 2016, 124, 188–195. ISSN 0143–7208.

126. HUANG, H., *et al*. Controllably Tunable Phenanthroimidazole-Carbazole Hybrid Bipolar Host Materials for Efficient Green Electrophosphorescent Devices. *Journal of Materials Chemistry C*. 2013, 1, 5899–5908. ISSN 2050–7526.

127. TONZOLA, C. J., *et al*. New n-Type Organic Semiconductors: Synthesis, Single Crystal Structures, Cyclic Voltammetry, Photophysics, Electron Transport, and Electroluminescence of a Series of Diphenylanthrazolines. *Journal of the American Chemical Society*. 2003, 125, 13548–13558. ISSN 0002−7863.

128. KIM, D., *et al*. Highly Efficient Red Phosphorescent Dopants in Organic Light-Emitting Devices. *Advanced Materials*. 2011, 23, 2721−2726. ISSN 1521–4095.

129. Hwu, J.R. *et al*., Fine Tuning of Blue Photoluminescence from Indoles for Device Fabrication. *Journal of Materials Chemistry*. 2009, 19(19), 3084. ISSN 1364–5501.

130. WANG, S., *et al*. Synthesis, Morphology, and Optical Properties of Tetrahedral Oligo(phenylenevinylene) Materials. *Journal of the American Chemical Society*. 2000, 122, 5695. ISSN 0002−7863.

131. WEN, S.W., *et al*. Recent Development of Blue Fluorescent OLED Materials and Devices. *IEEE/OSA Journal of Display Technology*. 2005, 1(1), 90–99. ISSN 1551–319X.

132. YAN, H., *et al*. Enhanced Polymer Light-Emitting Diode Performance Using a Crosslinked-Network Electron-Blocking Interlayer. *Advanced Materials*. 2004, 16, 1948–1953. ISSN 1521–4095.

133. NIU, Y.H., *et al*. Highly Efficient Red Electrophosphorescent Devices Based on an Iridium Complex with Trifluoromethyl-Substituted Pyrimidine Ligand. *Applied Physics Letters*. 2004, 85(9), 1619. ISSN 1077–3118.

134. PARK, M.S. *et al*. Fused Indole Derivatives as High Triplet Energy Hole Transport Materials for Deep Blue Phosphorescent Organic Light-Emitting Diodes. *Journal of Materials Chemistry*. 2012, 22(7), 3099–3104. ISSN 1364–5501.

135. JEON, S.O., *et al*. External Quantum Efficiency Above 20% in Deep Blue Phosphorescent Organic Light-Emitting Diodes. *Advanced Materials*. 2011, 23(12), 1436. ISSN 1521–4095.

136. JEON, S.O., *et al*. High-Efficiency Deep-Blue-Phosphorescent Organic Light-Emitting Diodes Using a Phosphine Oxide and a Phosphine Sulfide High-Triplet-Energy Host Material with Bipolar Charge-Transport Properties. *Advanced Materials*. 2010, 22(16), 1872–1876. ISSN 1521–4095.

137. SUN, D., *et al*. A Versatile Hybrid Polyphenylsilane Host for Highly Efficient Solution-Processed Blue and Deep Blue Electrophosphorescence. *Journal of Materials Chemistry C*. 2014, 2, 8277–8284. ISSN 2050–7526.

138. PARK, M.S., and LEE, J.Y. An Indole Derivative as a High Triplet Energy Hole Transport Material for Blue Phosphorescent Organic Light-Emitting Diodes. *Thin Solid Films.* 2013, 548, 603–607. ISSN 0040–6090.

139. YANG, X., *et al*. Functionalization of Phosphorescent Emitters and Their Host Materials by Main-Group Elements for Phosphorescent Organic Light-Emitting Devices. *Chemical Society Reviews.* 2015, 44(23), 8484–8575. ISSN 1460–4744.

140. LEE, S.H., *et al*. Enhanced Lifetime of Organic Light-Emitting Diodes Using an Anthracene Derivative with High Glass Transition Temperature. *Journal of Nanoscience and Nanotechnology*. 2013, 13(6), 4216–22. ISSN 1533–4899.

141. SHI, H., *et al*. Two Novel indolo[3,2-b]carbazole Derivatives Containing Dimesitylboron Moieties: Synthesis, Photoluminescent and Electroluminescent Properties. *New Journal of Chemistry*, 38(6), 2368–2378. ISSN 1369–9261.

142. JANOSIK, T., *et al*. Recent Progress in the Chemistry and Applications of Indolocarbazoles. *Tetrahedron*. 2008, 64(39), 9159–9180. ISSN 0040–4020.

143. WU, Y., *et al*. Indolo[3,2-b]carbazole-Based Thin-Film Transistors with High Mobility and Stability. *Journal of the American Chemical Society*. 2005, 127(2), 614–618. ISSN 0002−7863.

144. SIMOKAITIENE, J., *et al*. Synthesis and Properties of Methoxyphenyl-Substituted Derivatives of Indolo[3,2-b]carbazole. *The Journal of Organic Chemistry*. 2012, 77(11), 4924–4931. ISSN 1520–6904.

145. ZHAO, H. P., *et al*., Indolo[3,2-b]carbazole: Promising Building Block for Highly Efficient Electroluminescent Materials. *Organic Electronics: Physics, Materials, Applications*, 2009, 10(5), 925–931. ISSN 1566–1199.

146. KIM, Y. H., *et al*. High-Purity-Blue and High-Efficiency Electroluminescent Devices Based on Anthracene. *Advanced Functional Materials*. 2005, 15(11), 1799–1805. ISSN 1616–3028.

147. SHIH, P. I., *et al*. Stable and Efficient White Electroluminescent Devices Based on a Single Emitting Layer of Polymer Blends. *Advanced Functional Materials*. 2006, 16(12), 1582–1589. ISSN 1616–3028.

148. ZHAO, Z., *et al*. Fluorescent, Carrier-Trapping Dopants for Highly Efficient Single-Layer Polyfluorene LEDs. *Advanced Functional Materials*. 2007, 17(13), 2203–2210. ISSN 1616–3028.

149. ZHAO, H.P. *et al*., Structure and Electronic Properties of Triphenylamine-Substituted indolo[3,2-b]carbazole Derivatives as Hole-Transporting Materials for Organic Light-Emitting Diodes. *Chemical Physics Letters*. 2007, 439(1–3), 132–137. ISSN 0009-2614.

150. ADAMOVICH, V.I., *et al*. New Charge-Carrier Blocking Materials for High Efficiency OLEDs. *Organic Electronics*. 2003, 4(2–3), 77–87. ISSN 1566–1199.

151. ZACHARIAS, P., *et al*. New Crosslinkable Hole Conductors for Blue-Phosphorescent Organic Light-Emitting Diodes. *Angewandte Chemie – International Edition*. 2007, 46(23), 4388–4392. ISSN 1521–3773.

152. YANG, X., *et al*. Highly Efficient Polymeric Electrophosphorescent Diodes. *Advanced Materials*. 2006, 18(7), 948–954. ISSN 1521–4095.

153. ZUNIGA, C.A., *et al*. Crosslinking Using Rapid Thermal Processing for the Fabrication of Efficient Solution-Processed Phosphorescent Organic Light-Emitting Diodes. *Advanced Materials*. 2013, 25, 1739–1744. ISSN 1521–4095.

154. KANG, B.G., *et al*. Thermally Cross-Linkable Hole Transporting Polymer Synthesized by Living Anionic Polymerization for Effective Electron Blocking and Reduction of Exciton Quenching in Multilayerpolymer Light Emitting Diodes. *Polymer Chemistry*. 2013, 4, 969–977. ISSN 1099–0518.

155. HONG, H., *et al*. Synthesis and Characterization of Thermally Cross-Linkable Trimer Based on Triphenylamine. *Macromolecular Research*. 2013, 21, 321–326. ISSN 2092–7673.

156. HUNG, W.Y., *et al*. A New Thermally Crosslinkable Hole Injection Material for OLEDs, *Organic Electronics.* 2012, 13, 2508–2515. ISSN 1566–1199.

157. ZUNIGA, C.A., *et al*. Approaches to Solution-Processed Multilayer Organic Light-Emitting Diodes Based on Cross-Linking. *Chemistry of Materials.* 2011, 23(3), 658–681. ISSN 0897–4756.

158. KHUONG, K.S., *et al*. The Mechanism of the Self-Initiated Thermal Polymerization of Styrene. Theoretical Solution of a Classic Problem. *Journal of the American Chemical Society*. 2005, 127(4), 1265–1277. ISSN 0002−7863.

159. HUANG, J., *et al*. Achieving High-Efficiency Polymer White-Light-Emitting Devices. *Advanced Materials*. 2006, 18(1), 114–117. ISSN 1521–4095.

160. CHUANG, C.Y., *et al*. Bright-White Light-Emitting Devices Based on a Single Polymer Exhibiting Simultaneous Blue, Green, and Red Emissions. *Macromolecules.* 2007, 40(2), 247–252. ISSN 0024-9297.

161. HUANG, F., *et al*. Crosslinkable Hole-Transporting Materials for Solution Processed Polymer Light-Emitting Diodes. *Journal of Materials Chemistry.* 2008, 18, 4495–4509. ISSN 1364–5501.

162. LIU, M.S., *et al*. Thermally Cross-Linkable Hole-Transporting Materials for Improving Hole Injection in Multilayer Blue-Emitting Phosphorescent Polymer Light-Emitting Diodes. *Macromolecules.* 2008, 41(24), 9570–9580. ISSN 0024–9297.

163. YEOH, K.H., *et al*. The Efficiency Enhancement of Single-Layer Solution-Processed Blue Phosphorescent Organic Light Emitting Diodes by Hole Injection Layer Modification. *Journal of Physics D: Applied Physics.* 2014, 47(20), 205103. ISSN 1361–6463.

164. CHARAS A., and MORGADO, J. Oxetane-functionalized Conjugated Polymers in Organic (Opto)Electronic Devices. *Current Physical Chemistry*. 2012 , 2(3), 241–264. ISSN 1877–9468.

165. LIAPTSIS, G., and MEERHOLTZ, K. Crosslinkable TAPC-Based Hole-Transport Materials for Solution-Processed Organic Light-Emitting Diodes with Reduced Efficiency Roll-Off. *Advanced Functional Materials*. 2013, 23(3), 359–365. ISSN 1616–3028.

166. LEE, J., *et al*. Utilization of “thiol-ene” Photo Cross-Linkable Hole-Transporting Polymers for Solution-Processed Multilayer Organic Light-Emitting Diodes. *Journal of Materials Chemistry C*. 2014 , 2, 1474–1481. ISSN 2050–7526.

167. AIZAWA, N., *et al*. Thermally Cross-Linkable Host Materials For Enabling Solution-Processed Multilayer Stacks in Organic Light-Emitting Devices. *Organic Electronics*. 2013, 14, 1614–1620. ISSN 1566–1199.

168. KIM, Y.H., *et al*. Highly Efficient, Simplified, Solution-Processed Thermally Activated Delayed-Fluorescence Organic Light-Emitting Diodes. *Advanced Materials.* 2016, 28(4), 734–741. ISSN 1521–4095.

169. CHEN, S., *et al*. Hole Injection Polymer Effect on Degradation of Organic Light-Emitting Diodes. *Organic Electronics*. 2013, 14(10), 2518–2522. ISSN 1566–1199.

170. CHENG, Y.J., *et al*. Exciplex Electroluminescence Induced by Cross-Linked Hole-Transporting Materials for White Light Polymer Light-Emitting Diodes. *Macromolecules*. 2011, 44(15), 5968–5976. ISSN 0024-9297.

171. SUN, K., *et al*. Thermally Cross-Linkable Thermally Activated Delayed Fluorescent Materials for Efficient Blue Solution-Processed Organic Light-Emitting Diodes. *Journal of Materials Chemistry C*. 2016, 4(38), 8973–8979. ISSN 2050–7526.

172. PARK, J., *et al*. Facile Photo-Crosslinking of Azide-Containing Hole-Transporting Polymers for Highly Efficient, Solution-Processed, Multilayer Organic Light Emitting Devices. *Advanced Functional Materials*. 2014, 24(48), 7588–7596. ISSN 1616–3028.

173. CHENG, Y.-J., *et al*. Thermally Cross-Linkable Hole-Transporting Materials on Conducting Polymer: Synthesis, Characterization, and Applications for Polymer Light-Emitting Devices. *Chemistry of Materials*. 2007, 20(2), 413–422. ISSN 1520–5002.

174. LENGVINAITE, S., *et al*. Indolo[3,2-b]carbazole-Based Functional Derivatives as Materials for Light Emitting Diodes. *Dyes and Pigments*. 2010, 85(3), 183–188. ISSN 0143–7208.

175. SANGERMANO, M., *et al*. Synthesis of an Oxetane-Functionalized Hemispiroorthocarbonate Used as a Low-Shrinkage Additive in the Cationic Ultraviolet Curing of Oxetane Monomers. *Journal of Applied Polymer Science*. 2009, 112(3), 1780–1787. ISSN 1097–4628.

176. LENGVINAITE, S., *et al*. Polyethers Containing 2-phenylindol-1-yl Moieties as Host Materials for Light Emitting Diodes. *Synthetic Metals*. 2010, 160(15–16), 1793–1796. ISSN 0379–6779.

177. NOBUMITSU, N., *et al*., Synthesis and Property of Noria (Water-Wheel Like Macrocycle) Derivatives with Pendant Alkoxyl And Adamantyl Ester Groups, and Their Application for Extreme Ultraviolet Resist. *Thin Solid Films*. 2013, 544, 459–464, ISSN 0040–6090.

178. GRIGALEVICIUS, S., *et al*. Polymers Containing Diphenylvinyl-Substituted Indole Rings as Charge-Transporting Materials for OLEDs. *Journal of Electronic Materials*. 2016, 45(2), 1210–1215. ISSN 1543–186X.

179. KIRKUS, M., *et al*. Hole-Transporting Glass-Forming indolo[3,2-b]carbazole-based Diepoxy Monomer and Polymers. *European Polymer Journal.* 2009, 45(2), 410–417. ISSN 0014–3057.

180. WEN, G.A., *et al*. Synthesis and Characterization of a Main-Chain-Type Conjugated Copolymer Containing Rare Earth With Photocrosslinkable Group. *Journal of Polymer Science Part A: Polymer Chemistry*. 2007, 45(3), 388–394. ISSN 1099–0518.

181. ZHANG, Y.D., *et al*. Photo-Crosslinkable Polymers as Hole-Transport Materials for Organic Light-Emitting Diodes. *Journal of Materials Chemistry.* 2002, 12, 1703–1708. ISSN 1364–5501.

182. ZILINSKAITE, V., *et al*. Synthesis and Cationic Polymerization of Oxyranyl-Functionalized Indandiones. *Polymer Bulletin*. 2016, 73(1), 229–239. ISSN 1436–2449.

183. LI, Y., *et al*. 3,6-Di(furan-2-yl)pyrrolo[3,4-c]pyrrole-1,4(2H,5H)-dione and Bithiophene Copolymer with Rather Disordered Chain Orientation Showing High Mobility in Organic Thin Film Transistors. *Journal of Materials Chemistry*. 2011, 21, 10829–10835. ISSN 1364–5501.

184. LENGVINAITE, S., *et al*. Carbazol-3-yl Substituted Aromatic Amines Containing Crosslinkable Groups as Materials for Multilayer Light Emitting Diodes. *Molecular Crystals and Liquid Crystals*. 2008 497(1), 164–172. ISSN 1563–5287.

185. US Patent PCT/US99/07876 (WO 00/46321).

186. MIYAMOTO, E., *et al*. Ionization Potential of Organic Pigment Film by Atmospheric Photoelectron Emission Analysis. *Denshi Shashin Gakkaishi (Electrophotography)*. 1989, 28, 364–70. ISSN 1880-5108

187. GRITZNER, G., and KUTA, J. Recommendations on Reporting Electrode Potentials in Nonaqueous Solvents. *Pure and Applied Chemistry.* 1984, 6(4), 461–66. ISSN 2541–0733.

188. BECKE, A.D. Density-Functional Exchange-Energy Approximation with Correct Asymptotic Behavior. *Physical Review A.* 1988, 38, 3098. ISSN 2469–9934.

189. *SPARTAN'14 for Windows Version 1.1.2*. 1840 Von Karman Avenue, Suite 370, Irvine, CA 92612: Wavefunction, Inc., 2013.

190. FRISCH, M.J, *et al*. *Gaussian 09, Revision A. 02*. Gaussian, Inc., Wallingford CT, 2009.

191. TSE, S.C., *et al*. Materials, Processing, Devices and Applications (edited by Franky So). Chapter 3. Charge Transport and Injection in Amorphous Organic Semiconductors. Taylor & Francis Group. New York. Organic Electronics. 71–74.

192. BLAKESLEY, J.C., *et al*. Towards Reliable Charge-Mobility Benchmark Measurements for Organic Semiconductors. *Organic Electronics*. 2014, 15, 1263–72. ISSN 1566–1199.

193. TOMKUTE-LUKSIENE, D., *et al*. 2-Phenyl-1,2,3-benzotriazole Ir(III) Complexes with Additional Donor Fragment for Single-Layer PhOLED Devices. *Dyes and Pigments*. 2013, 96, 278–86. ISSN 0143–7208.

194. OKAMOTO, S., *et al*. Simple Measurement of Quantum Efficiency in Organic Electroluminescent Devices. *Japanese Journal of Applied Physics.* 2001, 40, 783–84. ISSN 0021–4922.

195. KRUZINAUSKIENE, A., *et al*. Carbazolyl- and Diphenylamino Substituted Fluorenes as Hole Transport Materials. *Synthetic Metals.* 2007, 157, 401–06. ISSN 0379–6779.

196. RAJAKUMAR, P., and SWAROOP, M. The Use of McMurry Coupling for the Synthesis of Indolophanes and Cis-Stilbenophanes. *Tetrahedron Letters*. 2004, 45(32), 6165–6167. ISSN 0040–4039.

197. NIU, T., and ZHANG, Y. Iron-Catalyzed Oxidative Homo-Coupling of Indoles via C–H Cleavage. *Tetrahedron Letters.* 2010, 51(29), 6847–6851. ISSN 0040–4039.

198. LEETE, E. 3-Hydroxymethylindoles. *Journal of the American Chemical Society.* 1959, 81, 6023–26. ISSN 0002–7863.

199. CHANDRASEKHAR, S., *et al*. Copper-Catalyzed N-Arylation of Amines/Amides in Poly(ethylene glycol) as Recyclable Solvent Medium. *Synthesis*. 2006, 5, 839–842. ISSN 0039–7881.

200. LEE, S.Y., *et al*. Luminous Butterflies: Efficient Exciton Harvesting by Benzophenone Derivatives for Full-Color Delayed Fluorescence OLEDs. *Angewandte Chemie – International Edition*. 2014, 53(25), 6402–6406. ISSN 1521–3773.

201. HUANG, B., *et al*. Thermally Activated Delayed Fluorescence Materials Based on Benzophenone Derivative as Emitter for Efficient Solution-Processed non-Doped Green OLED. *Dyes and Pigments*. 2016, 133, 380–386. ISSN 0143–7208.

202. CHIN-CHUAN, Ch. Thermal Polymerization of Uninhibited Styrene Investigated by Using Microcalorimetry. *Journal of Hazardous Materials* 2009. 163(2–3), 1385–1390. ISSN 0304–3894.

203. CHUAN, Ch. *et al*. Thermal Polymerization of Uninhibited Styrene Investigated by Using Microcalorimetry. *Journal of Hazardous Materials.* 2009, 163, 11385–1390. ISSN 0304–3894.

204. KONDO, Sh., *et al*. Mechanochemical Solid-State Polymerization. VI. Quantum Chemical Considerations for Structural Criteria of Mechanically Polymerizable Vinyl Monomers. *Chemical and Pharmaceutical Bulletin.* 2008, 42(4), 768–773. ISSN 1347–5223.

205. PRON, A., *et al*. Electroactive Materials for Organic Electronics: Preparation Strategies, Structural Aspects And Characterization Techniques. *Chemical Society Reviews*. 2010, 39(7), 2577–2632. ISSN 0306–0012.

206. YOKOYAMA, D., *et al*. Orientation Control of Linear-Shaped Molecules in Vacuum-Deposited Organic Amorphous Films and Its Effect on Carrier Mobilities. *Advanced Functional Materials*. 2010, 20, 386–391. ISSN 1616–3028.

207. PASPIRGELYTE, R., *et al.* Indole and Phenylenediamine Based Enamines as Amorphous Hole-Transporting Materials. *Synthetic Metals*. 2010, 160, 162–168. ISSN 0379–6779.

208. SUBRAMANIAPILLAI, S.G., and GANESAN, A. $ZnCl_2$ Promoted Efficient, One-Pot Synthesis of 3-Arylmethyl and Diarylmethyl Indoles. *Tetrahedron Letters.* 2014, 55(3), 694–698. ISSN 0040–4039.

209. STANISLOVAITYTE, E., *et al*. Carbazole Based Polymers as Hosts for Blue Iridium Emitters: Synthesis, Photophysics and High Efficiency PLEDs. *Journal of Materials Chemistry C.* 2013, 1, 8209–21. ISSN 2050–7526.

210. BLACK, D.S., *et al*. Mechanism-Controlled Regioselective Synthesis Of Indolyl benzo[b]carbazoles. *Tetrahedron Letters.* 1999, 40, 6653–6656. ISSN 0040–4039.

211. ANGIONI, E., *et al*. A Single Emitting Layer White OLED Based on Exciplex Interface Emission. *Journal of Materials Chemistry C.* 2016, 4, 3851–56. ISSN 2050–7526.

212. MINAEV, B., *et al*. Principles of Phosphorescent Organic Light Emitting Devices. *Physical Chemistry Chemical Physics*. 2014, 16, 1719–58. ISSN 1463–908.

213. BAGDZIUNAS, G., *et al*. Green and Red Phosphorescent Organic Light Emitting Diodes with Ambipolar Hosts Based on Phenothiazine and Carbazole Moieties: Photoelectrical Properties, Morphology And Efficiency. *RSC Advances.* 2016, 6, 61544–61554. ISSN 2046–2069.

214. SUN, Y.H., *et al*. Potential Solution Processible Phosphorescent Iridium Complexes toward Applications in Doped Light-Emitting Diodes: Rapid Syntheses and Optical and Morphological Characterizations. *Journal of Organic Chemistry*. 2006, 71, 6281–6284. ISSN 0022–3263.

215. SHIROTA, Y., and KAGEYAMA, H. Charge Carrier Transporting Molecular Materials and Their Applications in Devices. *Chemical Reviews*. 2007, 107(4), 953–1010. ISSN 1520–6890.

216. HE, G., *et al*. High-Efficiency and Low-Voltage p-i-n Electrophosphorescent Organic Light-Emitting Diodes with Double-Emission Layers. *Applied Physics Letters*. 2004, 85, 3911–13. ISSN 0003–6951.

217. BLAKESLEY, J.C., *et al*. Towards Reliable Charge-Mobility Benchmark Measurements for Organic Semiconductors. *Organic Electronics*. 2014, 15, 1263–72. ISSN 1566–1199.

218. ZHANG, Z., *et al*. Selectively Investigating Molecular Configuration Effect on Blue Electrophosphorescent Host Performance through a Series of Hydrocarbon Oligomers. *The Journal of Physical Chemistry C.* 2014, 118, 20559−70. ISSN 1932−7455.

219. YANG, X.L., *et al*. Recent Advances of the Emitters for High Performance Deep-Blue Organic Light-Emitting Diodes. *Journal of Materials Chemistry C.* 2015, 3, 913−944. ISSN 2050–7526.

220. TSAI, Y.W., *et al*. Bipolar Transport Materials for Electroluminescence Applications. O*rganic Electronics.* 2016, 30, 265–274. ISSN 1566–1199.

221. LEVICK, M.T.A Sm(II)-Mediated Cascade Approach to Dibenzoindolo[3,2-b]carbazoles: Synthesis and Evaluation. *Organic Letters*. 2014, 16 (8), 2292−2295. ISSN 1523−7060.

222. KALINOWSKI, J. Excimers and Exciplexes in Organic Electroluminescence. *Material Science – Poland*. 2009, 27, 735–56. ISSN 2083–134X.

223. NAKA, S. High Electron Mobility in Bathophenanthroline. *Applied Physics Letters*. 2000, 76 (2), 197–199. ISSN 1077–3118.

224. SASAKI, F. Electron Mobility Measurement Using Exciplex-Type Organic Light-Emitting Diodes. *Applied Physics Letters*. 2002, 81 (3), 391–393. ISSN 1077–3118.

225. COOK, J.H. Efficient Deep Blue Fluorescent Polymer Light Emitting Diodes (PLEDs). *Journal of Material Chemistry C.* 2014, 2, 5587–5592. ISSN 2050–7534.

226. CEKAVICIUTE, M. Arylfluorenyl-Substituted Metoxytriphenylamines as Deep Blue Exciplex Forming Bipolar Semiconductors for White and Blue Organic Light Emitting Diodes. *Dyes and Pigments*. 2017, 140, 187–202. ISSN 0143–7208.

227. WANG, W., *et al*. Efficient Triplet–Triplet Annihilation-Based Upconversion for Nanoparticle Phototargeting. *Nano Letters*. 2015, 15 (10), 6332−6338. ISSN 1530−6992.

228. MEI, J., et al. Aggregation-Induced Emission: Together We Shine, United We Soar! *Chemical Reviews*. 2015, 115 (21), 11718−11940. ISSN 1520−6890.

229. SHIZU, K., *et al*. Highly Efficient Blue Electroluminescence Using Delayed-Fluorescence Emitters with Large Overlap Density between Luminescent and Ground States. *The Journal of Physical Chemistry C*. 2015, 119 (47), 26283−26289. ISSN 1932−7455.

230. SHAHROOSVAND, H., *et al*. Going from Green to Red Electroluminescence Through Ancillary Ligand Substitution in Ruthenium(II) Tetrazole Benzoic Acid Emitters. *Journal of Materials Chemistry C.* 2013, 1, 6970–6980. ISSN 2050–7526.

231. YANG, X.L., *et al*. Highly Efficient Phosphorescent Materials Based on Platinum Complexes and Their Application in Organic Light-Emitting Devices (OLEDs). *Platinum Metals Review*. 2013, 57(1), 2–16. ISSN 0032–1400.

232. LIAO, J., *et al*. Near Infrared-Emitting Tris-Bidentate Os(II) Phosphors: Control of Excited State Characters and Fabrication of OLEDs. *Journal of Materials Chemistry C.* 2015, 3, 4910–4920. ISSN 2050–7526.

233. HE, B., *et al*. High Fluorescence Efficiencies and Large Stokes Shifts of Folded Fluorophores Consisting of a Pair of Alkenyl-Tethered, π-Stacked Oligo-p-phenylenes. *Organic Letters*. 2015.17(24), 6174–6177. ISSN 1523–7060.

234. YANG, P., *et al*. Science as Art: Self-Assembly of Hybrid SiO2-Coated Nanocrystals. *CrystEngComm*. 2011, 1814–1820. ISSN 1466−8033.

List of Publications

Publications in the Journals Included into the list of Web of Science (ISI):

1. **Keruckienė, Rasa;** Volyniuk, Dmytro; Ostrauskaitė, Jolita; Pečiulytė, Laura; Gražulevičius, Juozas Vidas; Kostjuk, Sergei V.; Lazauskas, Algirdas. Derivatives of 2-phenylindole and Carbazole as Host Materials for Phosphorescent Organic Light Emitting Diodes // *Dyes and Pigments*. Oxford: Elsevier. ISSN 0143–7208. 2017, vol. 137, p. 58–68.
2. **Keruckienė, Rasa;** Pečiulytė, Laura; Volyniuk, Dmytro; Gražulevičius, Juozas Vidas. Synthesis and Properties of Cross-Linkable Twin Derivatives of 2-phenylindole // *Synthetic Metals*. Lausanne: Elsevier. ISSN 0379–6779. 2016, vol. 212, p. 55–61.

Publications in International Conference Proceedings:

1. **Keruckienė, Rasa**; Mimaitė, Viktorija; Keruckas, Jonas; Volyniuk, Dmytro; Gražulevičius, Juozas Vidas. Derivatives of Indole and benzo[b]carbazole as Electroactive Materials // Open Readings 2017: 60th Scientific Conference for Students of Physics and Natural Sciences, March 14–17, 2017 Vilnius, Lithuania: programme and abstracts. Vilnius: Vilnius University. ISSN 2029-4425. 2017, p. 267. [M.kr. 03P].
2. **Keruckienė, Rasa**; Volyniuk, Dmytro; Gražulevičius, Juozas Vidas. 2-phenylindole and Carbazole Derivatives with Reactive Functional Groups as Host Materials for PHOLEDs // 6th EuCheMS Chemistry Congress, September 11–15, 2016, Seville, Spain. [S.l.: s.n, 2016]. p. [1].
3. **Keruckienė, Rasa**; Gražulevičius, Juozas Vidas; Kostjuk, Sergei V. 2-Phenylindolylcarbazole Derivatives with Reactive Functional Groups as Electroactive Materials // Chemistry and Chemical Technology : International Conference of Lithuanian Society of Chemistry : Lithuanian Academy of Science, Vilnius, Lithuania, April 28–29, 2016: Book of Abstracts / Fizinių ir technologijos mokslų centras, Vilniaus universitetas, Lietuvos mokslų akademija, Kauno technologijos universitetas. [S.l.: s.n, 2016], ISBN 9786099551135. p. 228.
4. **Laurinavičiūtė, Rasa**; Bagdžiūnas, Gintautas; Pečiulytė, Laura; Gražulevičius, Juozas Vidas. Polymerizable Derivatives of Indolyl-benzo[b]carbazole as Electroactive Materials // Baltic Polymer Symposium 2015: Sigulda, Latvia, September 16–18: programe and proceedings/ Riga Technical University Institute of Polymer Materials. Riga: Riga Technical University Institute of Polymer Materials, 2015, ISBN 9789934542121. p. 94.
5. **Laurinavičiūtė, Rasa**; Bagdžiūnas, Gintautas; Gražulevičius, Juozas Vidas. Derivatives of indolyl-benzo[b]carbazole as Electroactive Materials // ECME 2015: 13th European Conference on Molecular Electronics, September 1–5, 2015, Strasbourg, France. [S.l.: s.n, 2015]. p. 107.
6. **Laurinavičiūtė, Rasa**; Pečiulytė, Laura; Volyniuk, Dmytro; Gražulevičius, Juozas Vidas. Derivatives of Indole with Reactive Functional Groups as Electroactive Materials // Chemistry and Chemical Technology 2015: Programme

and Proceedings of the International Conference, Vilnius, Lithuania, January 23, 2015 / Vilnius University, Lithuanian Academy of Sciences, Kaunas University of Technology, Center for Physical Sciences and Technology. [S.l.: s.n, 2015], ISBN 9786094594618. p. 304–307.

Other publications:

1. **R. Keruckiene**, D. Peckus, T. Tamulevicius, S. Tamulevicius, M. Daniels, W. Dehaen, J. Simokaitiene & J. Grazulevicius. Indolyl-substituted Carbazole Derivatives: Electrochemical and Photophysical Properties and Computational Studies // *Molecular Crystals and Liquid Crystals*. 2016. Volume: 640, Issue: 01, pages 59–70.
2. Mimaitė, Viktorija; Gražulevičius, Juozas Vidas; **Laurinavičiūtė, Rasa**; Volyniuk, Dmytro; Jankauskas, Vygintas; Sini, Gjergji. Can Hydrogen Bonds Improve the Hole-Mobility in Amorphous Organic Semiconductors? Experimental and Theoretical Insights // *Journal of Materials Chemistry C*. London: Royal Society of Chemistry. ISSN 2050-7526. 2015, vol. 3, iss. 44, p. 11660–11674.
3. **Laurinavičiūtė, Rasa**; Ostrauskaitė, Jolita; Skuodis, Eigirdas; Gražulevičius, Juozas Vidas; Jankauskas, Vygintas. Hole-Transporting Phenothiazine-Based Hydrazones with Reactive Vinylbenzyl Groups // *Synthetic metals*. Lausanne: Elsevier. ISSN 0379-6779. 2014, vol. 192, p. 50–55.
4. **Laurinavičiūtė, Rasa**; Mimaitė, Viktorija; Ostrauskaitė, Jolita; Gražulevičius, Juozas Vidas; Jankauskas, Vygintas. Hole-Transporting Thiophene-Based Hydrazones with Reactive Vinyl Groups // *Synthetic Metals*. Lausanne: Elsevier. ISSN 0379–6779. 2014, vol. 197, p. 1–7.
5. **Laurinavičiūtė, Rasa**; Ostrauskaitė, Jolita; Gražulevičius, Juozas Vidas; Jankauskas, Vygintas. Synthesis, Properties, and Self-Polymerization of Hole-Transporting Carbazole- and Triphenylamine-Based Hydrazone Monomers // *Designed Monomers and Polymers*. Oxon: Taylor & Francis. ISSN 1385–772X. 2014, Vol. 17, No. 3, p. 255–265.

Acknowledgement

Prof. Juozas Vidas Gražulevičiusis greatly acknowledged for the opportunity to work in his research group.

Dr. Jolita Ostrauskaitė is thanked for the supervision of my first research attempts.

Prof. Wim Dehaen (KU Leuven, Belgium) is thanked for the supervision of my internship in his research group.

Dr. Pawel Wagner and dr. Klaudia Wagner (Intelligent Polymer Research Institute, Australia) are greatly thanked for the supervision of my internship and guidance during my visit to Wollongong, NSW, Australia.

Dr. Khrystyna Ivaniuk (Lviv Polytechnic National University, Ukraine) is greatly acknowledged for the production and characterization of electroluminescent devices as well as for the supervision during my visit to Lviv.

Dr. Gintautas Bagdžiūnas and dr. Viktorija Mimaitė are greatly thanked for introducing quantum mechanical modelings and for their assistance in interpreting the results of theoretical calculations.

Marytė Krenevičienė (Vilnius University) and dr. Greta Ragaitė (Department of Organic Chemistry, KTU) are thanked for the NMR spectroscopy measurements they conducted.

The specialists of the Department of Polymer Chemistry and Technology are acknowledged for conducting measurements of mass spectrometry, thermal, photoelectrical and electroluminescence properties and for all the scientific consultations they have provided.

I am very grateful to my family and friends for their cordial support and contribution to the successful completion of this thesis.

SL344. 2017-06-22, 14,75 leidyb. apsk. l. Tiražas 12 egz. Užsakymas 17-0199.
Išleido Kauno technologijos universitetas, K. Donelaičio g. 73, 44249 Kaunas
Spausdino leidyklos „Technologija“ spaustuvė, Studentų g. 54, 51424 Kaunas